# MULTIPLE SPACE OBJECT TRACKING USING A RANDOMIZED HYPOTHESIS GENERATION TECHNIQUE

A Dissertation

by

WESTON RYAN FABER

Submitted to the Office of Graduate and Professional Studies of
Texas A&M University
in partial fulfillment of the requirements for the degree of

DOCTOR OF PHILOSOPHY

| | |
|---|---|
| Chair of Committee, | Suman Chakravorty |
| Committee Members, | P.R. Kumar |
| | Raktim Bhattacharya |
| | Srinivas Rao Vadali |
| Head of Department, | Rodney Bowersox |

May 2018

Major Subject: Aerospace Engineering

# ABSTRACT

In order to protect assets and operations in space, it is critical to collect and maintain accurate information regarding Resident Space Objects (RSOs). This collection of information is typically known as Space Situational Awareness (SSA). Ground-based and space-based sensors provide information regarding the RSOs in the form of observations or measurement returns. However, the distance between RSO and sensor can, at times, be tens of thousands of kilometers. This and other factors lead to noisy measurements that, in turn, cause one to be uncertain about which RSO a measurement belongs to. These ambiguities are known as data association ambiguities. Coupled with uncertainty in RSO state and the vast number of objects in space, data association ambiguities can cause the multiple space object-tracking problem to become computationally intractable. Tracking the RSO can be framed as a recursive Bayesian multiple object tracking problem with state space containing both continuous and discrete random variables. Using a Finite Set Statistics (FISST) approach one can derive the Random Finite Set (RFS) based Bayesian multiple object tracking recursions. These equations, known as the FISST multiple object tracking equations, are computationally intractable when solved in full. This computational intractability provokes the idea of the newly developed alternative hypothesis dependent derivation of the FISST equations. This alternative derivation allows for a Markov Chain Monte Carlo (MCMC) based randomized sampling technique, termed Randomized FISST (R-FISST). R-FISST is found to provide an accurate approximation of the full FISST recursions while keeping the problem tractable. There are many other benefits to this new derivation. For example, it can be used to connect and compare the classical tracking methods to the modern FISST based approaches. This connection clearly defines the relationships between different approaches and shows that they result in the same formulation for scenarios with a fixed number of objects and are very similar in cases with a varying number of objects. Findings also show that the R-FISST technique is compatible with many powerful optimization tools and can be scaled to solve problems such as collisional cascading.

# DEDICATION

This dissertation is dedicated to my family and friends. To my mother and father, for supporting me on this journey and showing me that no dream is too big and no kindness is too small. To my grandparents, for teaching me to love life, to love others, and to see the beauty in everything.

# ACKNOWLEDGMENTS

To Professor Suman Chakravorty, thank you for giving me this opportunity. It has been an honor to be your student. To Dr. Islam Hussein, I am blessed to have met you in Albuquerque all those years ago. I truly appreciate everything you have done for me. To Rose Sauser and Gail Rowe, thank you for all your help and guidance over the years.

## CONTRIBUTORS AND FUNDING SOURCES

This work was funded by AFOSR grant number: FA9550-13-1-0074 under the Dynamic Data Driven Application Systems (DDDAS) program. This work was supported by a dissertation committee consisting of Professor Suman Chakravorty, Professor Raktim Bhattacharya, and Professor Srinivas R. Vadali of the Department of Aerospace Engineering and Professor P. R. Kumar of the Department of Electrical & Computer Engineering. Other support provided by Dr. Islam I. Hussein and others at Applied Defense Solutions. All other work conducted for the dissertation was completed by the student independently.

# NOMENCLATURE

| | |
|---|---|
| RSO | Resident Space Object |
| SSA | Space Situational Awareness |
| FISST | Finite Set Statistics |
| RFS | Random Finite Sets |
| MCMC | Markov Chain Monte Carlo |
| R-FISST | Randomized Finite Set Statistics |
| PDF, pdf(s) | Probability Density Function |
| DAP | Data Association Problem |
| EKF | Extended Kalman Filter |
| UKF | Unscented Kalman Filter |
| PGM | Particle Gaussian Mixture Filter |
| OTTA | Observation-To-Observation Association |
| TTTA | Track-To-Track Association |
| OTTA | Observation-To-Track Association |
| SSMCMC | Smart Sampling Markov Chain Monte Carlo |
| MHT | Multiple Hypothesis Tracking |
| HOMHT | Hypothesis Oriented Multiple Hypothesis Tracking |
| SMC | Sequential Monte Carlo |
| GM | Gaussian Mixture |
| UT | Unscented Transform |
| SIOD | Statistical Initial Orbit Determination |
| CAR | Constrained Admissible Region |

| | |
|---|---|
| PAR | Probabilistic Admissible Region |
| GNN | Global Nearest Neighbor |
| DDL | Differed Decision Logic |
| ECI | Earth Centered Inertial |
| ECEF | Earth Centered Earth Fixed |
| FOR | Field of Regard |
| FOV | Field of View |
| MT | Multi-Target |
| GEO | Geostationary Earth Orbit |
| MEO | Medium Earth Orbit |
| LEO | Low Earth Orbit |
| TLE | Two Line Element |

TABLE OF CONTENTS

Page

LIST OF FIGURES

FIGURE Page

# 1. INTRODUCTION

What does it mean to have perfect awareness of the space environment? Is perfect SSA achievable? If it is not, what are the limiting factors and how can they be improved upon? These questions are the driving force behind researchers in the SSA field and are the foundations for the research within this treatise. To be specific, there is an issue in multiple space object tracking that occurs when the number of possible hypotheses is computationally intractable. In approaching this problem, a framework was developed that allows for the support and analysis of many other aspects of SSA. That being said, this dissertation discusses, first and foremost, the rigorous development of randomized hypothesis generation within multiple space object tracking. This leads to the development of a new multi-object tracking technique called randomized Finite Set Statistics (R-FISST). Throughout this development, a number of related topics will be discussed. These topics include but are not limited to 1) Object Probability Density Function (PDF) initialization, 2) Object PDF representations, 3) the Data Association Problem (DAP), 4) hypothesis generation techniques, and 5) Bayesian inference and filtering techniques. In this section, these topics and their applications within SSA are introduced.

## 1.1 Multiple Space Object Tracking

Multiple space object tracking is the cornerstone of SSA. It is used to maintain accurate state information for RSOs. This is used in many aspects of SSA including but not limited to, catalog maintenance, catalog update, conjunction analysis, and sensor tasking. It is a probabilistic problem due to uncertainties in RSO dynamics and uncertainty in the observation caused by measurement noise. In the single space object-tracking case, the problem can be posed as a recursive Bayesian filtering problem. Space object tracking is an example of a multi-object tracking problem in a clutter-filled environment where closely spaced objects or noise related clutter can cause ambiguities in data association. This creates the necessity to maintain multiple hypotheses that include data association hypotheses or object birth, death, and maneuver hypotheses. There are many different

techniques to maintain the hypotheses and they will be discussed in the literary review.

### 1.1.1 RSO PDF Representation

Due to the uncertainty in object state and the process noise in RSO dynamics, the RSO state is a random vector distributed according to some PDF. This PDF is typically assumed to be Gaussian because of the unique nature of the Gaussian PDF that allows it to be completely characterized by its first two moments, mean and covariance. This is however just an approximation of the true uncertainty. Whether or not this is an accurate representation is of particular interest to the SSA community. It is known that the Gaussian assumption breaks down during propagation of the RSO. If the RSO PDF is not an accurate representation of the true uncertainty then it will increase the number of poor data association assignments, which in-turn leads to poor state estimation. Other representations are discussed in the literature review.

### 1.1.2 Measurement Types and PDF Initialization

Throughout the years that society has been interested in detecting space objects, many different types of sensors have been developed. These types range from Earth-based to space-based and radar to optical. The typical measurement return is a partial state measurement meaning that the measurement does not contain information about every element in the RSO state vector. For example, an RSO state vector might include the position and velocity but optical measurements may return just angles-only information. This poses the question of how to initialize a new RSO given radar or optical data. Specifically, can an RSO PDF be initialized given a single optical or radar observation? Can this be done in a way that takes account of the measurement noise?

### 1.1.3 Filtering Techniques

Depending on the type of PDF representation different techniques for object-measurement update may be necessary. Well-known methods for non-linear systems such as the Extended Kalman Filter (EKF) and the Unscented Kalman Filter (UKF) are typically used with Gaussian PDF assumptions. When particle representations are used, common techniques included the Particle Filter (PF) or the Ensemble Kalman Filter (EnKF). These techniques alongside newer techniques such

as the Particle Gaussian Mixture (PGM) Filter will be discussed below.

### 1.1.4 The Data Association Problem

One important topic addressed in this dissertation is an occurrence in multi-object tracking where the number of possible hypotheses becomes computationally intractable. This occurs when associations are highly ambiguous. In SSA there are three types of data association that are generally defined. These three types are Observation-to-Observation (OTOA), Track-to-Track (TTTA), and Observation-to-Track (OTTA). Although, each type of data association can cause scenarios where the number of possible hypotheses is computationally intractable the latter method is most easily described. OTTA is where one associates measurement returns to RSO. The number of resulting data association hypotheses, which has combinatorial growth, is a function of the number of returns and the number of associable objects. It is further complicated when considering birth or death hypotheses. Exhaustively generating all possible hypotheses can cause memory issues that lead to the computational intractability. On the other hand, not generating a statistically relevant set of hypotheses can lead to inaccurate estimation. These issues motivated the development of the randomized hypothesis generation technique within R-FISST. The technique uses a Markov Chain Monte Carlo (MCMC) based sampling technique, termed Smart Sampling MCMC (SSMCMC), which allows one to sample the highly probable hypotheses without having to generate all possible hypotheses.

## 1.2 Outline

The next chapter contains a discussion of the relevant previous literature and details areas where necessary improvements align with the research herein. Chapter 3, serves as an introduction to multi-object tracking. Chapter 4, takes a hypothesis perspective to the multi-object Bayesian filtering recursions. The insights provided by this development, pertaining to the relationship between classical and modern tracking techniques, are discussed in Chapter 5. An overview of hypothesis generation techniques, along with a breakdown of the randomized hypothesis generation technique within R-FISST, is discussed in Chapter 6. Then, Chapter 7 details applications of R-FISST tech-

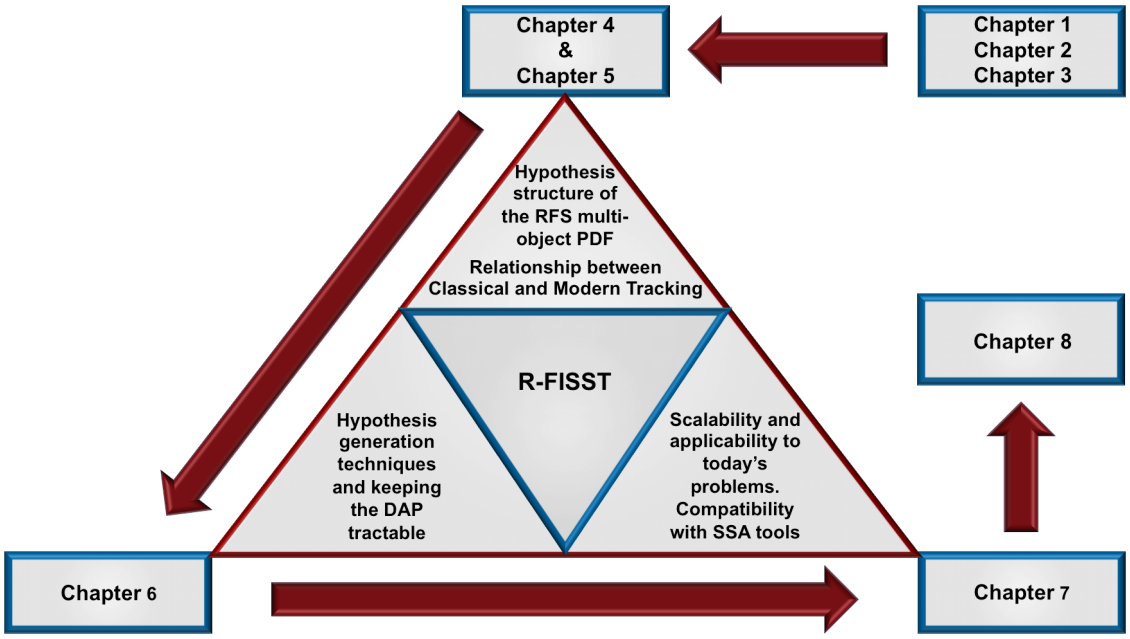


Figure 1.1: Description of the flow and the key points of the dissertation.

nique to SSA multi-object tracking scenarios. Lastly Chapter 8, summarizes the contributions of this research. The overall outline of the dissertation is illustrated in figure 1.1.

# 2. LITERATURE REVIEW

This section discusses relevant previous work and areas to be expounded upon within this research. In section 2.1, different multi-object tracking techniques are discussed. Section 2.2, summarizes the relevant filtering techniques. Section 2.3, describes object PDF initialization, otherwise known as Statistical Initial Orbit Determination (SIOD). Lastly, section 2.4 discusses work regarding the Data Association Problem (DAP) and relevant hypothesis generation techniques.

## 2.1 Multi-Object Tracking Techniques

The vast body of research on multi-object tracking contains variations in techniques that date back to the 70's. Starting with some of the notable figures of multi-object tracking such as Bar-Shalom, Reid, and Blackman, their classic techniques such as Probabilistic Data Association (PDA) and Multiple Hypothesis Tracking (MHT) [3, 4, 5] have influenced generations of SSA researchers in creating techniques such as Joint Probabilistic Data Association (JPDA), Track-Oriented MHT (TOMHT), and Hypothesis-Oriented MHT (HOMHT) [6, 7, 8]. In the last twenty years, the theory of Random Finite Set (RFS) based multi-object tracking has been developed based on theory of Finite Set Statistics (FISST) [9],[10]. The RFS based implementation of the multi-object Bayes filter provides a rigorous framework for approaching challenges in multi-object tracking. In these modern approaches a FISST PDF describes the state set in its entirety. The greatest challenge in implementing FISST based methods in real-time, which is critical to any viable SSA solution, is computational burden. Approximating the FISST PDF using its first-moment and cardinality, the Probability Hypothesis Density (PHD) approach and the Cardinalized PHD (CPHD) approach are computationally tractable approximations of the multi-object Bayes filter [11], [12]. The PHD filter essentially finds the density of the probability of an object being at a given location, and thus, can provide information about the number of objects (integral of the PHD over the region of interest) and likely location of the objects (the peaks of the PHD). Besides approximating the PDF using its first-moment, other techniques approximate the PDF using a type of PDF that can

be characterized by a finite set of definable parameters. These parameters are then propagated and updated over time. This can be seen in the multi-Bernoulli (MB) filters, which lead to the Labeled MB (LMB) filter and further to the generalized LMB (GLMB) [13, 14, 15, 16]. These techniques have been implemented in multiple ways including the incorporation of Gaussian Mixture (GM) or Sequential Monte Carlo (SMC) approximations [17, 18, 19, 20]. In other previous work, a GM approximation was applied to the full FISST multi-object Bayes recursions [21],[22]. These full PDF approximations eliminate any information loss associated with using the first-moment approximation; while at the same time increase the computational burden of the multi-object FISST recursions. A similar approach can be seen in the concept of the "para-Gaussian" PDF that was described in [23]. Other multiple hypothesis filters differentiate themselves by combining attributes from the above filtering techniques or by adding some functionality. Techniques that add functionality such as an SIOD technique or a randomized generation technique will be discussed in the following corresponding sections.

### 2.2 Filtering Techniques

One benefit of the R-FISST technique is that there are no assumptions of the form of the underlying object PDF. There are also no assumptions about the type of continuous filter that should be used to update the object PDF. However, the type of filter used in application must be compatible with the representation of the object PDF. It also must be capable of handling the dynamics of the problem. For the application of SSA the dynamics are non-linear. This means that the standard Kalman filter [24, 25], which provides the unbiased minimum variance for linear systems perturbed by Gaussian noise, would not be sufficient. Non-linear extensions of the Kalman filter such as the Extended Kalman filter (EKF) and Unscented Kalman filter (UKF) [26, 27, 28] are commonplace in multiple hypothesis filters. EKF can have issues caused by cumulative linearization errors, which lead to the development of the UKF and other sigma point filters. Both EKF and UKF produce a single Gaussian when approximating the posterior PDF. This tends to be more compatible when assuming the object PDF is Gaussian. However, the Gaussian object PDF assumption is known to fall apart during propagation, albeit at different rates in different coordinate

systems [29]. The breakdown of the Gaussian assumption lead to different object PDF representations such as the Gaussian Mixture Model (GMM) and the Sequential Monte Carlo (SMC) or particle ensemble representation [30, 31, 32, 33]. Particle ensemble representations are more compatible with particle updates such as the Particle Filter (PF) or the Ensemble Kalman Filter (EnKF) [34, 35, 36, 37, 38]. However, particle methods too have their drawbacks such as particle depletion with the PF or troubles with multi-modal PDFs as in the EnKF. Recent, work has been performed to combine the benefits of both methods without the drawbacks of either. The Particle Gaussian Mixture (PGM) filter uses a particle ensemble for object PDF representation during propagation [39]. Then, using an optimal clustering algorithm, converts the particle ensemble into a Gaussian Mixture (GM). With each cluster representing a different mixture component with, the components are updated using either an EKF or the Unscented Transform (UT). After update the posterior GMM is re-sampled and the process is repeated. The multi-object tracking technique presented in this paper will be used as a platform for comparative measures between the different methods.

### 2.3 Statistical Initial Orbit Determination (SIOD)

As discussed in the introduction, one of the challenges in SSA is to initialize an object PDF given partial state measurements. Typical Initial Orbit Determination (IOD) methods (Gauss, Laplace, Gooding, etc. [40],[41]) require multiple measurements and do not account for measurement noise. Admissible region approaches have been studied in depth and are used in SIOD for a number of SSA applications. For the near earth SSA application, the admissible region is defined as the region of space near earth that contain viable orbit solutions, i.e. the orbit is of the earth system with negative energy [42]. This region can be further constrained by setting bounds about the objects orbital parameters. The new region defined by the bounds has been termed the Constrained Admissible Region (CAR). The CAR has been developed for SIOD of both radar and optical type measurements [43, 44, 45, 46, 47, 48]. The Constrained Admissible Region Multiple Hypothesis Filter (CAR-MHF) is an example of a Multiple Hypothesis Filter that uses the CAR to initialize object PDF given a very short arc optical tracklet [49]. Using an optical tracklet (a group

of three or more optical angles-only observations) one can compress the tracklet to obtain angle and angle-rate information for the assumed RSO. This allows one to develop a CAR in range, range-rate space. For the applications discussed in this proposal, the measurements are highly ambiguous. The challenge of OTOA necessary for the CAR measurement compression may be computationally intractable. Also, a probabilistic representation of the CAR, termed Probabilistic Admissible Region (PAR), has been developed to provide faster convergence and less ambiguity in a multiple hypothesis framework [50, 51, 52].

### 2.4 The Data Association Problem (DAP)

The DAP occurs when observations can be associated to one or more objects or vice versa. This occurs when objects are closely spaced or when object state uncertainty is large. A new hypothesis must be created each time a data association is changed. This problem quickly becomes intractable as the number of ambiguous returns grows. It is further complicated when incorporating the idea that each measurement can also be associated with clutter or a new object, and even more so when objects can be associated to a miss detection, death, or a maneuver. These associations and their effect on the number of hypotheses will be further explained in Chapter 6. The first approach to solving the data association problem within a multi-object tracking framework was the Global Nearest Neighbor (GNN) technique [53]. GNN simply makes a hard decision and maintains only one hypothesis that corresponds to the data association combination that has the highest likelihood. This technique often fails in scenarios when objects are crossing, objects are closely spaced, or when the observations are highly cluttered. This failure occurs due to the fact that in these scenarios poor associations are made causing tracking inaccuracies. The cumulative tracking inaccuracies eventually lead to a complete breakdown of tracking accuracy. This issue motivated the development of Differed Decision Logic (DDL) approaches that are used by most tracking techniques today. In DDL, the possible hypotheses created by the DAP are generated exhaustively and maintained until the data disambiguates (i.e., multiple hypotheses are maintained and the decision on which to believe is true is differed until more information is received). MHT methods do this by maintaining a tree structure that is pruned when the probability of a branch

falls below a user-defined value. This method is generally called pruning and is used in both MHT methods and in RFS based techniques. Pruning is a method done after the hypotheses are generated and does not help when data association ambiguity causes the problem to be intractable in one step. There have been methods that help in such a scenario. For example, gating. Gating significantly reduces the number of possible data association hypotheses by setting a bound around the measurement. Only objects that fall within the measurement gate can be associated. However helpful, gating is still not sufficient in large cases and can at times truncate a true data association causing type 1 and type 2 errors. Other methods have been used to rank the top hypotheses, most notably Murty's algorithm also known as Murty's K-Best [54]. However, when considering a huge hypothesis space it is hard to determine how many hypotheses to keep. The true association may also be relatively low in weight and thus truncated prematurely. Algorithms that address the DAP using a randomized approach aim to sample from the posterior stationary distribution of hypotheses. MCMC techniques create a Markov Chain (MC) using the hypotheses as states. They then walk through these states according to a proposal distribution. A decision is made to stay at the current state or move to the next based on a defined MCMC criterion. After the burn in period, the remaining sampled states are taken as the stationary distribution. This alleviates the burden of having to exhaustively generate all the hypotheses but also maintains a distribution of likely hypotheses in case the true hypothesis is not highly probable at the time of sampling. The MCMC Data Association (MCMCDA) [55, 56] technique is an example of a randomized hypothesis generation technique used within a multi-object tracking framework. However, one must be aware that randomized techniques may too be computationally burdensome, potentially even more so than exhaustively generating the hypotheses, if the proposal distribution is uniform as in MCMCDA. In other words, using MCMC with a uniform proposal distribution on a large hypothesis space may take a very long time to "burn in". The randomized hypothesis generation technique developed in this proposal, called Smart Sampling Markov Chain Monte Carlo (SSMCMC), develops hypotheses by using an MCMC based technique that samples through association space and allows for biased non-uniform proposal distributions. This has been shown to sample a posterior stationary

distribution containing the true hypothesis in scenarios where the number of possible hypotheses $\mathcal{O}(10^{36})$ [57, 58, 59, 60, 61]. This technique will be explained in detail in Chapter 6.

**Remark 1.** *Pruning too can cause tracking errors when used incorrectly. Pruning can either be done by a threshold or by a sort. When using the threshold method, one must have a dynamic threshold bound that is dependent upon the number of hypotheses. If one uses a fixed value they will prune hypotheses prematurely. The sort method is a better approach to pruning. After each time step, the number of hypotheses can increase drastically. Since the weights of the hypotheses have to sum to one, the individual weights will naturally be lower in value. To avoid pruning prematurely, simply sort the hypotheses in descending order and truncate to keep the number of hypotheses within computational limits.*

# 3. MULTIPLE SPACE OBJECT TRACKING

This chapter has been provided as a review of the basic principles of multi-object tracking necessary for understanding the developments in later chapters. The multi-object tracking problem is most generally structured as a recursive Bayesian filtering problem. Models used to describe this problem and solutions techniques are discussed in the following sections. The chapter is organized as follows. Section 3.1 describes the typical state and measurement representations as well as the statistical motion and measurement models. Section 3.3 introduces some common approaches to solving the multi-object tracking problem. The concept of developing a multi-object Bayes filter using Random Finite Sets (RFS) or Finite Set Statistics (FISST) is described in section 3.4. In the last section of the chapter, section 3.5, the relationship between conventional methods and RFS based methods are discussed along with the advantages and disadvantages of the different methodologies.

## 3.1 Modeling The Space Object Tracking Problem

This section describes common models used for SSA applications. These models are based on the state-space model that represents space object dynamics and the statistical representations conform to the formal measurement and motion models found in most literature. The following subsections detail how the space object state space and measurement space is typically represented as well as the statistical models for object motion and object measurements.

### 3.1.1 Object States

The state space consists of all possible object states that describe the object's relevant physical attributes. These attributes are problem specific but for the application of SSA typical states may describe the position, velocity, orientation, and even discrete attributes such as an object identification number or an objects characteristic length. States are typically represented by vectors such as,

$$x_i = (a, e, i, \Omega, \omega, \nu, L_c)^T \tag{3.1}$$

where $x$ is a vector describing the states of object $i$, which in this case are the object's continuous states (orbital elements) and its discrete state (characteristic length). The state space is then a hybrid space consisting of the set of all possible continuous states and discrete states.

### 3.1.2 Object Measurements

Object measurements are collected by sensor resources that provide information about the object's state. The type of information that can be ascertained is typically defined by the sensor's capabilities. SSA sensor resources can be located on earth or in space. Two examples are optical and radar based sensors and often times these sensor can only provide partial state information. For example, optical sensors provide raw angles-only measurements. Common angles-only measurements are of the object's ECI J2000 right ascension and declination or a topocentric azimuth and elevation. Like states, measurements are represented using vectors such as the measurement, $z = (\alpha, \delta)^T$. Measurements are related to states through the measurement model. This is discussed in more detail in the following sections.

### 3.1.3 Motion Model

The statistical motion model for space object tracking accounts for the object's motion between measurement intervals and the uncertainty therein. Space object dynamic models describe how object states vary with time. A simplified version of these dynamics can be described by two-body motion and more accurate models can include perturbations, solar radiation pressure, atmospheric drag, etc. Space object dynamics in general are nonlinear and thus the statistical motion model is typically represented,

$$x_t = f_{t-1}(x) + W_{t-1}. \tag{3.2}$$

Where $f_{t-1}$ is a nonlinear transformation describing the deterministic object dynamics and $W_{t-1}$ is an additive noise term representing the uncertainty, which is typically assumed to be normally distributed with covariance $Q_{t-1}$.

### 3.1.4 Measurement Model

The measurement model is typically assumed to be a nonlinear additive model such as,

$$z_t = h_t(x) + V_t. \tag{3.3}$$

With $h_t(x)$ being the deterministic nonlinear transformation from the state space to the measurement space at time $t$ and $V_t$ being the sensor noise. The sensor noise is also typically assumed to be multi-variate zero-mean Gaussian with covariance $R_t$. The measurement model describes the information received by a sensor throughout time while accounting for measurement noise.

### 3.1.5 Markov Transitional Density

Markov processes signify that the current state is dependent only on the previous state. Markov transition densities are necessary to capture the statistical information contained within the motion model. The Markov density takes the following form for the above motion model,

$$p_{t|t-1}(x|x') = p(W_{t-1}) = p(x - f_{t-1}(x')). \tag{3.4}$$

In the case where $W_{t-1}$ is assumed normally distributed with covariance $Q_{t-1}$. The above equation reduces to,

$$p_{t|t-1}(x|x') = \mathcal{N}(f_{t-1}(x'), Q_{t-1}). \tag{3.5}$$

Where $\mathcal{N}(\mu, C)$ is a multivariate normal density with mean $\mu$ and covariance $C$

### 3.1.6 Likelihood Function

In a similar fashion to the previous section, the likelihood function describes the statistical information contained in the measurement model. As opposed to the previous section where the goal was to determine the chances of being at state $x$ given a previous state $x'$. The goal now is to determine the likelihood of a particular measurement $z$ given knowledge of the current state $x$.

The expression of the likelihood thus becomes,

$$p_t(z|x) = p(V_t) = p(z - h_t(x)). \tag{3.6}$$

In this case where $V_t$ is assumed multivariate normal with covariance $R_t$ the equation simplifies to,

$$p_t(z|x) = \mathcal{N}(h_t(x), R_t). \tag{3.7}$$

It is important to note the interpretation of the likelihood function when tracking multiple objects. In the case of multiple objects, one must consider a distinction between association to one object or another. The likelihood then takes the form,

$$l(z|x_i) = \int p(z|x_i)p^-(x_i)dx. \tag{3.8}$$

Where $p^-(x_i)$ is the predicted prior density of object $i$.

### 3.2 Single-Object Bayes Filtering

The Bayes filter recursively iterates through prediction and correction as measurements are received. Assume that some initial distribution that describes the possible states of an object has the probability density at a general time instance $t-1$,

$$p_{t-1}(x|Z^{t-1}) = p_{t-1}(x). \tag{3.9}$$

Where $Z^{t-1}$ contains all measurement information received up to and including time $t-1$. The next step in the recursion predicts the object PDF forward to the next time $t$. The prediction is as follows,

$$p_{t|t-1}(x|Z^{t-1}) = \int p_{t-1|t}(x|x')p_{t-1}(x')dx'. \tag{3.10}$$

Next the PDF is updated given a measurement $z_t$ using a form of Bayes rule.

$$p_{t|t}(x|Z^t) = \frac{p_t(z_t|x)p_{t|t-1}(x|Z^{T-1})}{p_t(z_t|Z^{t-1})}. \tag{3.11}$$

Dropping the subscripts on time and using over bar notation to represent prior information the Bayes filter update simplifies to,

$$p(x|Z) = \frac{p(z|x)p^-(x|\bar{Z})}{p(z|\bar{Z})}. \tag{3.12}$$

The denominator is a normalization ensuring that $p(x|z)$ is valid and can be expressed,

$$p(z|\bar{Z}) = \int p(z|x)p(x|\bar{Z})dx. \tag{3.13}$$

## 3.3 Conventional Multi-Object Tracking Methods

As mention in the literature review, early algorithms for multiple object tracking, including methods such as GNN, MHT, and JPDA, have become common place in SSA and Space Traffic Management (STM). These techniques are based off the conventional or standard approaches that are discussed in this section. The goal in multiple object tracking is to maintain accurate estimations of the objects' states and uncertainties. In the standard approaches this is typically done by maintaining lists of objects that are updated over time. It is also common to maintain a matrix of different data association hypotheses that were made over time. Some common approaches are described in the next few sections.

### 3.3.1 Problem Statement

The multiple space object tracking problem consists of multiple sensor resources tracking a varying number of unknown objects. Each sensor resource has a specified Field of Regard (FOR) and Field Of View (FOV) that determine the volume of measurement space that a sensor can detect. To clarify terminology, the FOR refers to the total volume of measurement space that can be seen

by a sensor. The FOR is applicable to sensors that can change their look direction. Once a look direction is fixed, the FOV refers to the total volume of measurement space that can be detected at that specified look direction. For sensors that have a fixed looked direction, the FOR at any given instance is the same as the FOV. Measurements can be generated by objects and false alarms. It is assumed that objects generate at most one measurement and no two objects can generate the same measurement. False alarm processes are typically modeled as Poisson in time and uniform in space and they are assumed to be independent of the object measurement process. Objects within the FOV of a sensor have a non-unity probability of detection, $p_D$, and it is typically modeled as either a constant or as a function of the object state. Object motion follows the model given in section 3.2 and is statistically independent of any other object's motion. Objects generate measurements according to section 3.1.4 where $h(x)$ and $V$ are sensor specific. The number of objects varies with time as new objects are born and as known objects die. Object birth is typically modeled as a Poisson process in time and uniform in space. Fragmentation events or spawn events do occur and can be model as Poisson processes with varied spatial representations that depend on the state of the fragmentation object. Object survival is modeled as a binomial process with probability of survival $p_S$.

To understand how classical methods maintain and update object beliefs consider the following example. At time $t-1$ there are assumed to be $n$ independent objects with corresponding PDFs $p^i(x)$ where $i = 1, ..., n$. Assuming that these $n$ objects represent the only possible hypothesis at time $t-1$ their state estimates can be stored in a track tree and/or the hypothesis itself can be stored in a hypothesis matrix. At time $t$ a measurement is taken consisting of $m$ returns, $Z_t = z_1, ...z_m$. To update the track tree and/or the hypothesis matrix each object is predicted forward to time $t$ at which point the measurements need to be assigned to the objects. Due to data association ambiguities it may be the case that the measurements $Z_t$ can be assigned to the objects in many different ways. Each valid set of measurement to object association (a.k.a OTTA or MTA) is called a data association hypothesis, $\sigma_j$, where $j$ can take values $j = 1, ..., A$ and $A$ is the total number of possible data association hypotheses. Track trees and the hypothesis matrix can be updated using

these data association hypotheses. The likelihood of a particular data association hypothesis, $\sigma_j$, can be expressed as a product the individual object to measurement associations within,

$$l_{\sigma_j} = \prod_i l(z_{\sigma_{j,i}}|x_i). \tag{3.14}$$

Defining the probability of the prior $n$ object hypothesis as $p_{t-1}(\Omega_{t-1}|Z^{t-1})$ where $\Omega$ the joint PDF for the $n$ object hypothesis. From Reid [3] an expression can be written for the probability of the updated hypothesis,

$$p_t(\Omega_{t-1}, \sigma_j|Z^t) = \eta l_{\sigma_j} p(\sigma_j|\Omega_{t-1}) p(\Omega_{t-1}) \tag{3.15}$$

In this case from left to right, $\eta$ is normalization factor, $p(Z|\sigma, \Omega_{t-1}) = l_{\sigma_j}$, $p(\sigma_j|\Omega_{t-1})$ is the probability of the data association hypothesis given the prior hypothesis, and $p(\Omega_{t-1})$ is the prior weight. The likelihood 3.14 and the hypothesis probability 3.15 are used in classical methods to update track trees and/or the hypothesis matrix.

### 3.3.2 Single Hypothesis Tracking

Some multiple object tracking methods maintain and update objects using only a single hypothesis at each time step. These methods are known as Single Hypothesis Tracking (SHT) or Single Hypothesis Correlation (SHC) methods. Examples include the Nearest Neighbor (NN) and the Global Nearest Neighbor techniques. In each of these cases, optimization is performed at each time step to determine the single hypothesis that satisfies particular cost function. NN approaches simply determine the optimal assignment that creates the minimal distance between measurements and predicted positions. A similar approach is used for the GNN method however the optimal association hypothesis is the hypothesis that minimizes the total Mahalanobis distance. The performance of these techniques typically degrades as observation ambiguity increases.

### 3.3.3 Multi-Hypothesis Correlation

As opposed to using a single hypothesis at every time step, Multiple Hypothesis Tracking (MHT) techniques keep record of all possible hypotheses at each step. This standard tracking

technique is known to perform better in highly ambiguous environments than SHC techniques. The main issue with MHT is the computational burden involved with data association problem. Problems with highly ambiguous associations the number of possible data association hypotheses at even a single step can be computationally intractable let alone maintaining large number of hypotheses throughout time steps. A number of heuristic techniques have been implemented to keep the computational burden tractable. These techniques include gating, track merging, pruning as well as a number of randomized sampling approaches that will be discussed in Chapter 6.

### 3.3.4 Joint Probabilistic Data Association

Another noteworthy filter commonly used in SSA is the JPDA filter. The nature of this filter is, in a sense, a hybrid of the previously discussed techniques. Although the JPDA is a multiple hypothesis filter, it maintains a single hypothesis on each object that is a weighted average of all the hypotheses pertaining to it. This approach intends to encapsulate the advantages of multiple hypothesis filters while keeping the problem tractable. These characteristics have made JPDA filters a "go-to" filter for industry and academia alike.

## 3.4 FISST Multi-Object Bayesian Filtering

In this section, the topic of multi-object Bayesian filtering is addressed with the use Random Finite Set (RFS) representations. Incorporating FISST techniques into the multi-object tracking problem was developed by Mahler [62] and has become increasingly popular in the SSA community. It was developed to provide a structured formulation in which handling the difficulties involved in multi-object tracking is done in a statistically rigorous fashion. The following sections discuss the outline of the RFS based formulation of the Bayes filtering recursions for the SSA application discussed in the previous section.

### 3.4.1 Introduction To RFS/FISST Based Approaches

Before getting into the multi-object Bayes formulation, this sections details necessary introductory concepts of FISST based approaches.

The multi-object state is represented as set of random vectors representing the individual object

states. For arbitrary number of objects $n$ the multi-object state is as follows,

$$X = \{x_1, ..., x_n\}. \tag{3.16}$$

This expression encapsulates every arbitrary possible combination of the object states. For example,

$$X = \{\} \quad \text{no objects present} \tag{3.17}$$

$$X = \{x_1\} \quad \text{one object present} \tag{3.18}$$

$$\vdots$$

$$X = \{x_1, ..., x_n\} \quad \text{n objects present } x_1 \neq ... \neq x_n \tag{3.19}$$

$$\vdots$$

This representation is an intuitively more accurate representation of the multi-object state since the true number of objects can be any arbitrary number and they have no implicit order. It is important to note that this representation comes at the cost of increased computational burden caused by implicit enumerations of the possibilities of $X$.

It is also important to note the multi-object distributions can be represented in both vector and set notations and they are related by,

$$p(\{x_1, ...x_n\}) = n!\, p(x_1, ..x_n). \tag{3.20}$$

Another important tool needed for determining expressions in the following sections is the set integral. The set integral is,

$$\int_S p(X)\delta X = \sum_0^\infty \frac{1}{n!} \int_{S^n} p(\{x_1, ..., x_n\}) dx_1 ... dx_n \tag{3.21}$$

### 3.4.2 Multi-Object Likelihoods

In this section the multi-object likelihood is shown for the SSA problem described in section 3.3.1, which includes association to objects born and existing alike, missed detections and false alarms. In accordance with [10] the development of the multi-object likelihood function for the measurement $Z_t = Z = \{z_1, ..., z_m\}$, provided the predicted multi-object state $X$ with $|X| = n$ is given by,

$$p_t(Z|X) = e^{\lambda} p_C(Z) p_t(\emptyset|X) \sum_{\sigma} \prod_{i:\sigma(i)>0} \frac{p_D p_t(z_{\sigma(i)}|x_i)}{(1-p_D)\frac{\lambda}{V}}. \tag{3.22}$$

In which, $\sigma$ is all possible data association hypotheses. The Poisson distributed clutter takes the form,

$$p_C(Z) = e^{-\lambda} \prod_{z \in Z} \frac{\lambda}{V} \tag{3.23}$$

where $\lambda$ is the average arrival rate for false alarm generated measurements and $V$ is the FOV volume. Also, the term that represents missed detections is,

$$p_t(\emptyset|X) = e^{-}\lambda \prod_{x \in X} (1 - p_D) \tag{3.24}$$

### 3.4.3 Multi-Object Markov Densities

This section presents the corresponding multi-object Markov transition density for the SSA problem described in section 3.3.1, which includes predicted birth, predicted death, and spawned fragments. In accordance to [62] the Markov density is as follows,

$$p_{t|t-1}(X|X') = e^{\lambda_{B(X')}} p_{B(X')}(X) p_{t|t-1}(\emptyset|X') \sum_{\theta} \prod_{i:\theta(i)>0} \frac{p_S p_{t|t-1}(x_{\theta(i)}|x'_i)}{(1-p_S)\lambda_{B(X')} B(x_{\theta(i)}|x'_i)}. \tag{3.25}$$

Where if $|X| = n$ and $|X'| = n'$ the summation is taken over all possible predicted hypotheses $\theta : \{1, ..n'\} \rightarrow \{1, ..n\}$ and the following is true,

$$p_{B(X')}(X) = e^{-\lambda_{B(X')}} \prod_{x' \in X'} \lambda_{B(X')} B(x|x'_i) \tag{3.26}$$

Where the Poisson arrival of the birthed objects and fragments has temporal arrival,

$$\lambda_{B(X')} = \lambda_0 + \lambda(x'_1) + ... + \lambda(x'_n), \tag{3.27}$$

with spatial distribution,

$$B(x|x'_i) = \frac{\lambda_0 B_(x) + \lambda(x'_1) B(x|x'_1) + ... + \lambda(x'_n) B(x|x'_n)}{\lambda_0 + \lambda(x'_1) + ... + \lambda(x'_n)}. \tag{3.28}$$

Lastly, the corresponding survival term is,

$$p_{t|t-1}(\emptyset|X') = e^{-\lambda_B(X')} \prod_{x' \in X'} (1 - p_S). \tag{3.29}$$

### 3.4.4 Multi-Object Bayes Filter

For some initialized distribution for a general time step $p_{t-1|t-1}(X|Z^{t-1})$ the multiple-object Bayes filter can be directly represented using Eq. 3.22 and Eq. 3.25 within the following expression,

$$p_{t|t}(X|Z^t) = \frac{p_t(Z|X) p_{t|t-1}(X|Z^{t-1})}{p_t(Z|Z^{t-1})}. \tag{3.30}$$

Where

$$p_{t|t-1}(X|Z^{t-1}) = \int p_{t|t-1}(X|X') p_{t-1|t-1}(X'|Z^{t-1}) \delta X', \tag{3.31}$$

and

$$p_t(Z|Z^{t-1}) = \int p_t(Z|X) p_{t|t-1}(X|Z^{t-1}) \delta X \tag{3.32}$$

## 3.5 Relationship Between The Approaches

The similarities and differences between the classical approaches to multi-object filtering and the more modern FISST approaches is a topic of much debate in the SSA community. This section has been included to provide a brief description of the main arguments made by practitioners on both sides of the spectrum. Understanding these arguments is crucial to properly ascertain any truth behind the claims.

Foundations of both the conventional and modern approaches are built within the Bayesian paradigm. The modern formulations follow a direct interpretation of the Bayes filter recursions through the use of RFS that leads to the multi-object Bayes filter. Conventional methods use Bayes rule to determine posterior probability densities of hypotheses. This brings about the first major criticisms of the conventional approaches. That is

> *Are the conventional methods to multiple-object tracking, such as MHT, rigorous within the Bayesian framework?*

The first argument suggesting they are not stems from the fact that conventional likelihood and posterior densities are conditioned on particular data association hypotheses, making it seem as though the hypotheses themselves are state variables. In [63] this topic is discussed and shown that mathematical representations of data associations are dependent on the parameters that are not state variables. It also shows an approach to remove such dependencies to construct a suitably Bayesian formulation; however, even taking this approach can causes the number of measurements to become a nonrandom variable and thus inconsistence with Bayesian statistics. This leads to the next major claim addressed in [63].

> *The RFS approach to multi-object tracking is a essentially a mathematical reinvention of MHT.*

RFS based approaches were developed, first and foremost, to provide a structured approach to solving the difficulties that arise in multi-object tracking. It is stated in [10] that the true multi-object likelihood arises from averaging over all association hypotheses and that hypotheses appear

as an additive term in the multi-object likelihood. On that note, differences in modeling Markov transitional densities can create inherent differences in the possible data associations. This can lead to improper handling of modeled parameters such as object birth. A structured approach helps to ensure the problem is modeled in a statistically rigorous fashion.

Lastly, practitioners debate about the overall tractability of each method. An inherent problem in multiple object tracking is the number of possible hypotheses caused by the DAP. It can be seen that both classical and modern methods can run into computational limitations in scenarios where the instantaneous number of possible data association hypotheses is intractable. This is the motivation for the developments in the following chapters.

It is the benefit of the hypothesis perspective taken in Chapter 4 that allows one to draw clear connections between classical and modern techniques. These connections are described in detail in Chapter 5.

# 4. A HYPOTHESIS PERSPECTIVE OF RFS BAYESIAN MULTIPLE OBJECT TRACKING

Multi-object tracking problems may encounter scenarios where the number of possible data association hypotheses is computationally intractable. This occurs when the number of observable objects is large and the objects themselves are closely spaced. One practical occurrence of such a scenario is the, not so uncommon, RSO fragmentation event. RSO fragmentation events (a.k.a RSO breakup events) can occur when RSO fail, explode, or collide with other objects. These fragmentations can cause thousands of debris fragments. In practice, tracking these events is often intractable and it forces practitioners to have to wait until data disambiguates, which can cause fragment loss. Providing timely, accurate tracking data is crucial in order to protect assets with close conjunctions to fragmented objects and prevent collisional cascading.

The intractability of these events can be seen in the formulations for both classical tracking methods and RFS based methods through the variable $\sigma$ in 3.15 and 3.22 respectively. MHT methods take a hypothesis dependent approach and even with techniques such as gating the DAP can still be computationally intractable. In RFS based methods the multi-object corrector is not dependent on $\sigma$ because it is marginalized out in the likelihood expression. However, even summing over all possible data association hypotheses is computationally intractable if done exhaustively. This can be avoided by approximating the summation in some fashion.

This chapter discusses the derivation of a hypothesis based representation of the FISST multi-object PDF. This was developed to appropriately address the intractability of the DAP. In the derivation, an RFS based approach is utilized in order to provide a systematic and rigorous development. The construction of the equations below are based upon the standard model discussed in the previous chapter, 3. The main contributions of the derivation are:

- The "hypothesis" based representation of the FISST multi-object PDF.
- The clarification of the relationship between the RFS based approaches and the classical methods such as HOMHT.

- The structure of the posterior PDF that plainly shows how to appropriately sample from the posterior when implementing hypothesis generation techniques.

The derivation is laid out in segments. First, the initialization of the FISST PDF is discussed. The next two sections discuss the multi-object Markov transition density and the multi-object likelihood according to the standard model assumptions presented in chapter 3. Lastly, a hypothesis based representation is derived and prediction and update steps are discussed.

## 4.1 Initialization

Initialization is the starting point to developing the multiple object tracker. How one initializes depends on the problem and the amount of information known about the environment. The next section discusses a general overview of initialization.

### 4.1.1 Initial Density

In this derivation, the initialization is shown using a general representation of which the terms can be chosen to model any specific problem. The initial distribution generally represented as a joint distribution of the objects' spacial distribution and a cardinality distribution. In SSA we often have some prior idea of the number of objects and their specific spatial density. Assuming there exists a set of objects $X = \{x_1, ..., x_n\}$ with an arbitrary number of objects, $n$. The initial distribution can be represented as follows:

$$p_0(X, n) = p_0(X)\rho_0(n), \tag{4.1}$$

where

$$p_0(X) = \sum_{\nu} \prod_{i} p_0^i(x_{\nu_i}). \tag{4.2}$$

Meaning the multi-object PDF, given that the cardinality is $n$, has independent object states with $p_0^i(.)$ denoting the PDF of the $i^{th}$ target. Note that the subscript notation above $p_0$ is reduced from subscript style $p_{0|0}$ for convenience.

## 4.2 Multi-Object Markov Transition Density Function

In this section, the multi-object motion model is discussed in three increasingly difficult cases. The first case, describes the motion of objects in the absence of birth and death. The second case increases complexity by including object birth. Lastly, the multi-object motion model including birth and death is described.

### 4.2.1 Fixed Number Of Objects

For a general time step $t-1$, the FISST multi-object transition density function, in the absence of birth or death, is given by the following:

$$p_{t|t-1}(X, n|X', n) = \sum_{\nu} \prod_{i=1}^{n} p_{t|t-1}(x_{\nu_i}|x'_i), \tag{4.3}$$

where $p_{t|t-1}(x_{\nu_i}|x'_i)$ denotes the corresponding single object transition density function, and $\nu = (\nu_1, \cdots \nu_n)$ represents all possible permutations of the numbers 1 through $n$.

### 4.2.2 With Object Birth

In the previous section, an $r$-object configuration could only result in another $r$-object configuration, however, now due to object birth an $r$-object model can result in an $n$-object model where $n > r$. Assume that one can encode a transition including any arbitrary number of births into a "birth hypothesis". The multi-object transition function, conditioned on the birth hypotheses and using the Law of Total Probability, is given by:

$$p(X, n|X', r) = \sum_{\sigma^b_{n-r}} p(X, n|\sigma^b_{n-r}, X', r)p(\sigma^b_{n-r}), \tag{4.4}$$

where transition subscripts $t|t-1$ are dropped for the sake of convenience and $\sigma^b_p$ represents a birth hypothesis that results in exactly $p$ births, $p(\sigma^b_p)$ is the probability of the birth hypothesis. In the case where a spatial binomial process is assumed for the birth model, $p(\sigma^b_p)$ is equal to $\alpha^p(1-\alpha)^{(M-p)}$ for all p-birth hypothesis $\sigma^b_p$. In this probability, $M$ is a measure of the number

of possible spatial birth PDF within the field of view. For example, this can be assumed to be the number of pixels in an photograph. Furthermore, the first factor in the summation of Eq. 4.4 is as follows:

$$p(X, n|\sigma^b_{n-r}, X', r) = \sum_{\nu} \prod_{i=1}^{r} p(x_{\nu_i}|x'_i) \prod_{i=r+1}^{n} p_{i-r}^{\sigma^b_{n-r}}(x_{\nu_i}), \tag{4.5}$$

where $p_j^{\sigma^b_p}(.)$ denotes the $j^{th}$ birth PDF under the p-birth hypothesis $\sigma^b_p$.

### 4.2.3 With Object Birth and Death

To incorporate death, first define a survival hypothesis as $\sigma^s_r$ that describes the $r$ surviving objects. The probability that an object survives can be modeled as a binomial process with the probability of survival equal to $p_s$ and the probability that an object does not survive equal to $1 - p_s$. The hypothesis $\sigma^s_r$ describes that exactly $r$ out of $n'$ objects survive and has probability $p(\sigma^s_s|n') = p^r_s(1 - p_s)^{n'-r}$. The survival process and birth process are independent. Thus, a new joint hypothesis, $\theta$, can be defined as the product of a birth hypothesis and a survival hypothesis, $\theta = \sigma^s_r \sigma^b_{n-r}$. Conditioning on $\theta$ and using the Law of Total Probability, the multi-object transition density including birth and death becomes,

$$p(X, n|X', n') = \sum_{\theta} p(X, n|\theta, X', n')p(\theta). \tag{4.6}$$

In this case the summation is take over all possible $\theta$. The first factor in the summation describes the underlying predicted and birth PDF,

$$p(X, n|\theta, X', n') = \sum_{\nu} \prod_{i=1}^{r} p(x_{\nu_i}|x'_{\sigma^s_i}) \prod_{i=r+1}^{n} p_{i-r}^{\sigma^b_{n-r}}(x_{\nu_i}). \tag{4.7}$$

There are never any underlying PDF corresponding to death, making $p^{\theta}_{i-r}(.) = p_{i-r}^{\sigma^b_{n-r}}(.)$. The second factor of Eq. 4.6 is the probability of a particular birth and death hypothesis. From the

independence of the birth and death process the probability of $\theta$ can be expressed,

$$p(\theta) = p(\sigma_r^s|n')p(\sigma_{n-r}^b) \tag{4.8}$$

This representation is an explicit way of writing the condensed version presented by Mahler [10] pg.472 for a binomial birth process. This can be seen if one makes the assumption that the birth arrival is Poisson, with arrival rate $\mu_0$. Note the differences in notation, Mahler's $\theta$ is an association hypothesis $\theta : (1, ..., n') \rightarrow (1, ..., n)$ and is equivalent to a specific $\theta$ hypothesis and $\nu$ permutation in the above development. Also, the probability density of new object appearance $b(x)$ in [10] is equivalent to a particular $p_{i-r}^{\theta}(x)$

### 4.3 Multi-Object Likelihood Function

This section discusses the multiple object measurement model. The multi-object measurement model, under certain assumptions, is analogous to the multi-object motion model and will be described using three cases of increasing complexity. The first case describes the scenario where there are no missed detections or false alarms. The second, describes what happens when objects can be missed detected. Lastly, the scenario with missed detections and false alarms is described.

#### 4.3.1 No Missed Detections Or False Alarms

Analogous to the multi-object Markov transition density function Eq. 4.3, for a general time step $t$, the multi-object likelihood function, in the absence of missed detections or false alarms, is given by the following:

$$p_t(Z|X, n) = \sum_{\nu} \prod_{i=1}^{n} p_t(z_i|x_{\nu_i}). \tag{4.9}$$

Provided a measurement set $Z = \{z_1, z_2, \cdots, z_n\}$ where $p_t(z_i|x_{\nu_i})$ denotes the single observation to object likelihood, and $\nu = (\nu_1, \cdots \nu_n)$ represents all possible permutations of the numbers 1 through $n$.

### 4.3.2 Missed Detections, No False Alarms

To include missed detections lets assume the measurement takes the form, $Z = \{z_1, z_2, \cdots, z_m\}$. Since, in this case, there a no false alarms $m \leq n$. Let the probability that a particular object, $i$, is detected be, $p_D(x_i)$. The probability that it is not detected is then, $1 - p_D(x_i)$. Next define a data association hypothesis, $\sigma^\phi : (1, \cdots, n) \rightarrow (0, 1, \cdots, m)$. Meaning that the data association hypothesis has length $n$ and each $\sigma_i^\phi$, where $i = 1, \cdots, n$, corresponds to a particular measurement, $z_{\sigma_i^\phi}$, or to nothing $\{\emptyset\}$. A data association hypothesis can assume up to $\phi \leq n$ missed detections. Conditioning on $\sigma^\phi$ and using the Law Of Total Probability,

$$p_t(Z|X, n) = \sum_{\sigma_\phi} p_t(Z|\sigma^\phi, X, n)p(\sigma^\phi). \tag{4.10}$$

The first factor in the summation, which describes the observation-to-object associations, can be expressed,

$$p_t(Z|\sigma^\phi, X, n) = \prod_{i:\sigma_i^\phi > 0} p(z_{\sigma_i^\phi}|x_i). \tag{4.11}$$

The second factor is the probability of the hypothesis $\sigma^\phi$ and can be expressed,

$$p(\sigma^\phi) = \prod_i^n (1 - p_D(x_i)) \prod_{i:\sigma_i^\phi > 0} \frac{p_D(x_i)}{(1 - p_D(x_i))}. \tag{4.12}$$

When the probability of detection is the same for all objects in the FOV the expression simplifies to,

$$p(\sigma^\phi) = p_D^{n-\phi}(1 - p_D)^\phi \tag{4.13}$$

### 4.3.3 Missed Detections and False Alarms

To incorporate both missed detections and false alarms, define a data association hypothesis for false alarms, $\sigma^f$, that contains information regarding the number of false alarms. Since the false alarm process and the missed detection process are independent the total association hypothesis can be described as a product of the false alarm hypothesis and the missed detection hypothesis,

$\sigma^{(n)} = \sigma^{\phi}\sigma^{f}$. The multi-object likelihood conditioning on all possible data associations $\sigma^{(n)}$ , and using the Law of Total Probability, is given by:

$$p(Z|X,n) = \sum_{\sigma^{(n)}} p(Z|\sigma^{(n)}, X, n)p(\sigma^{(n)}|X,n). \tag{4.14}$$

Above the subscript $t$ is dropped for the sake of simplicity and $\sigma^{(n)} = (\sigma_1^{(n)}, \sigma_2^{(n)}, ..\sigma_n^{(n)})$ denotes a data association hypothesis given that there are $n$ objects. The association hypothesis, $\sigma_i^{(n)} :\in \{z_1, z_2 \cdots z_m, \phi\}$, associates the $i^{th}$ object to one of $m$ measurements, $z_{\sigma_i^{(n)}}$, or to nothing, $\phi$. The term $p(\sigma^{(n)}|X,n)$ denotes the a priori probability of the data association $\sigma^{(n)}$ given that there are $n$ objects and can be shown to be:

$$p(\sigma^{(n)}|X,n) = p(\sigma^{(n)}|n) = p_D^{(m-k)}(1-p_D)^{n-(m-k)}p(\sigma^{f}), \tag{4.15}$$

where the data association $\sigma^{(n)}$ is assumed to assign exactly $k$ of the $m$ measurements to clutter. For notation convenience, $k$ is not explicitly represented within the hypothesis $\sigma^{(n)}$. If the clutter process is assumed to be a uniform Poisson process with intensity $\lambda$ in the total sensor volume $V$. The expression becomes,

$$p(\sigma^{(n)}|X,n) = p(\sigma^{(n)}|n) = p_D^{(m-k)}(1-p_D)^{n-(m-k)}\frac{e^{-\lambda V}(\lambda V)^k}{k!}, \tag{4.16}$$

For simplicity, we have assumed that the detection probability is uniformly $p_D$ in the FOV of the sensor, and 0 outside it, and therefore, $p(\sigma^{(n)}|X,n)$ does not depend on the multi-object state $X$, only on its size $|X| = n$. Further, the likelihood of the measurement $Z$ given the data association hypothesis $\sigma^{(n)}$ is given by:

$$p(Z|\sigma^{(n)}, X, n) = \prod_{i=1}^{n} p(z_{\sigma_i^{(n)}}|x_i)k! \prod_{z \notin \{z_{\sigma_i^{(n)}} \forall i\}} C(z), \tag{4.17}$$

where $C(z_{\sigma_i^{(n)}})$ is the clutter spatial distribution. In the case where clutter is uniformly distributed in the FOV, $C(.) = \frac{1}{V}$, Eq. 4.17 becomes,

$$p(Z|\sigma^{(n)}, X, n) = \frac{k!}{V^k} \prod_{i=1}^{n} p(z_{\sigma_i^{(n)}}|x_i), \tag{4.18}$$

## 4.4 Multi-Object Prediction and Update

In this section, the prediction and update steps for a general multi-object tracking problem are discussed. These steps will be described using cases of increasing complexity. The first case describes the recursion provided an initial multi-object PDF at $t = 0$ assuming the number of objects is fixed. This case is provided to show the development of the hypothesis structure under the RFS based Bayes filter. The next case describes the update step assuming the number of objects is fixed for a general time step $t$. For both cases the measurement models is assumed to include false alarms and missed detections. The last case describes the prediction step for the full multi-object PDF including birth and death.

**Remark 2.** *The methodology below can be adapted to incorporate spawn prediction and state dependent false alarms by incorporating dependence on state in both the birth model and false alarm model.*

### 4.4.1 Prediction and Update After Initialization For A Fixed Number Of Objects

**Assumption 1.** *Let the multi-object pdf at time $t = 0$ be as defined in Eq. 4.1*

$$p_0(X, n) = p_0(X)\rho_0(n),$$

*where*

$$p_0(X) = \sum_{\nu} \prod_{i} p_0^i(x_{\nu_i}).$$

Let the observation at time $t = 1$, be denoted as $Z_1 = \{z_1^1, z_2^1, \cdots z_m^1\}$. Let $p_1^-(X, n)$ denote the predicted MT-pdf just before receiving $Z_1$. Then, the following result holds:

**Proposition 1.** *Under Assumption 1, the predicted pdf $p_1^-(X,n)$ at time $t=1$ is given by:*

$$p_1^-(X,n) = p_1^-(X|n)\rho_0(n), \tag{4.19}$$

*where*

$$p_1^-(X|n) = \sum_{\nu} \prod_i p_1^{i-}(x_{\nu_i}),$$

$$p_1^{i-}(X_i) = \int p(x_i|x_i')p_0^i(x_i')dx_i',$$

*i.e., the predicted multi-object pdf , given cardinality $n$, is simply the product of the predicted PDFs of the individual targets.*

**Proposition 2.** *Under Assumption 1, the updated multi-object PDF at time $t=1$ is given by:*

$$p_1(X,n|Z_1) = \sum_{\sigma^{(n)}} p_1(X|n,\sigma^{(n)},Z_1)\omega_{\sigma^{(n)}}, \tag{4.20}$$

*where $\sigma^{(n)}$ is a data association "hypothesis" given that there are $n$ targets and the sum is over all such data associations, and*

$$p_1(X|n,\sigma^{(n)},Z_1) = \sum_{\nu} \prod_i p_1^i(x_{\nu_i}|z^1_{\sigma_i^{(n)}}), \tag{4.21}$$

$$p_1^i(x_i|z) = \begin{cases} \frac{p(z|x_i)p_1^{i-}(x_i)}{\int p(z|x_i')p_1^{i-}(x_i')dx_i'}, , & \text{if } z \neq \phi \\ p_1^{i-}(x_i), & \text{if } z = \phi \end{cases} \tag{4.22}$$

$$\omega_{\sigma^{(n)}} = \frac{l_{\sigma^{(n)}} p(\sigma^{(n)}|n)\rho_0(n)}{\sum_{q,\nu^{(q)}} l_{\nu^{(q)}} p(\nu^{(q)}|q)\rho_0(q)}, \tag{4.23}$$

*where $p(\sigma^{(n)}|n)$ is found from Eq. 4.16, and*

$$l_{\sigma^{(n)}} = \frac{k!}{V^k} \underbrace{\prod_i \int p(z^1_{\sigma_i^{(n)}}|x_i) p_1^{i-}(x_i|n) dX_i}_{\bar{l}_{\sigma^{(n)}}}, \tag{4.24}$$

*assuming that $\sigma^{(n)}$ assigns exactly $k$ measurements to clutter. Note that $\sigma^{(n)}$ implicitly assumes a sum over all $k$, again this is not shown explicitly purely for notational convenience.*

### 4.4.2 Update For A General Time Instance

Let the general multi-object PDF at time $t-1$ can be represented by,

$$p_{t-1}(X, n) = \sum_{q^{(n)}} p_{t-1}^{q^{(n)}}(X) \omega_{q^{(n)}}, \tag{4.25}$$

Where the sum is taken over all possible parent hypotheses $q^{(n)}$ containing $n$ objects and $\omega_{q^{(n)}}$ is the corresponding weight. The first factor of 4.25 corresponds to the underlying multi-object state given the particular set of $n$ objects, $q^{(n)}$, and is expressed,

$$p_{t-1}^{q^{(n)}}(X) = \sum_{\nu} \prod_i p_{t-1}^{q^{(n)},i}(X_{\nu_i}). \tag{4.26}$$

The predicted PDF at time $t$ is given by:

$$p_t^-(X, n) = \sum_{q^{(n)}} p_t^{q^{(n)}-}(X) \omega_{q^{(n)}}, \tag{4.27}$$

$$p_t^{q^{(n)}-}(X) = \sum_{\nu} \prod_i p_t^{q^{(n)},i-}(x'_{\nu_i}),$$

$$p_t^{q^{(n)},i-}(x_i) = \int p(x_i|x'_i) p_{t-1}^{q^{(n)},i}(x'_i) dx'_i.$$

**Proposition 3.** *Further, given a measurement $Z_t$, the updated multi-object PDF is given by:*

$$p_t(X,n|Z_t) = \sum_{q^{(n)}} \sum_{\sigma^{(n)}} p_t^{q^{(n)},\sigma^{(n)}}(X|Z_t) \frac{\omega_{q^{(n)}} p(\sigma^{(n)}|n) l_{q^{(n)}\sigma^{(n)}}}{\sum_q \sum_{r^{(q)}} \sum_{\nu^{(q)}} \omega_{r^{(q)}} p(\nu^{(q)}|q) l_{r^{(q)}\nu^{(q)}}}, \tag{4.28}$$

*where $\sigma^{(n)}$ represents an n-target data association hypothesis given measurement set $Z_t$, and*

$$l_{q^{(n)}\sigma^{(n)}} = \frac{k!}{V^k} \prod_i \int p(z^t_{\sigma_i^{(n)}}|x_i) p_t^{q^{(n)},i-}(x_i) dx_i, \tag{4.29}$$

$$p_t^{q^{(n)}\sigma^{(n)}}(X|Z) \equiv \sum_\nu \prod_i p^{q^{(n)}\sigma^{(n)},i}(x_{\nu_i}|z^t_{\sigma_i^{(n)}}),$$

$$p^{q^{(n)}\sigma^{(n)},i}(x_i|z^t_{\sigma_i^{(n)}}) = \frac{p(z^t_{\sigma_i^{(n)}}|x_i) p_t^{q^{(n)},i-}(x_i)}{\int p(z^t_{\sigma_i^{(n)}}|x'_i) p_t^{q^{(n)},i-}(x'_i) dx'_i} \tag{4.30}$$

**Remark 3.** *The hypothesis Based Structure of multi-object PDF: Propositions 1 through 3 clearly establish the hypothesis based structure of the multi-object pdf, in the absence of target birth and death. In particular, Propositions 2 and 3 show that the multi-object pdf has a hybrid structure consisting of a continuous multi-object pdf underlying a hypothesis $q^{(n)}$, and a weight corresponding to the $\omega^{q^{(n)}}$. Further, underlying any hypothesis $q^{(n)}$ is the FISST multi-object pdf whose components are the single object PDFs $p^{q^{(n)},i}(.)$, and hence, the FISST pdf for the hypothesis $q^{(n)}$ is completely specified by these component PDFs. Further, it may be seen that any hypothesis $q^{(n)}$ corresponds to a concatenation of a time sequence of data association maps $\sigma^{(n)}(t)$ till the current time, and thus, the pdf $p^{q^{(n)},i}(.)$ simply represents the pdf of the $i^{th}$ object under this sequence of maps.*

### 4.4.3 Prediction With Birth

The following proposition describes the prediction and update steps for a multi-object system with a varying number of objects caused by birth and death and includes a measurement model with both missed detections and false alarms.

**Assumption 2.** *Assume that the multi-object PDF $p(X, r)$ has the structure:*

$$p(X, r) = \sum_{q^{(r)}} \omega_{q^{(r)}} p^{q^{(r)}}(X), \tag{4.31}$$

$$p^{q^{(r)}}(X) = \sum_{\nu} \prod_{i=1}^{r} p^{q^{(r)},i}(x_{\nu_i}).$$

The predicted multi-object PDF under the above birth model is then given by (please see Appendix A.2 for the proof):

$$p^{-}(X, n) = \sum_{r} \sum_{\sigma^b_{n-r}} p(\sigma^b_{n-r}) \sum_{q^{(r)}} \omega_{q^{(r)}} p^{q^{(r)}-}_{\sigma^b_{n-r}}(X), \tag{4.32}$$

where

$$p^{q^{(r)}-}_{\sigma^b_{n-r}}(X) = \sum_{\nu} \prod_{i=1}^{r} p^{q^{(r)},i-}(x_{\nu_i}) \prod_{i=r+1}^{n} p^{\sigma^b_{n-r}}_{i-r}(x_{\nu_i}), \tag{4.33}$$

$$p^{q^{(r)},i-}(x_i) = \int p(x_i|x'_i) p^{q^{(r)},i}(x'_i) dx'_i,$$

i.e., the multi-object PDF $p^{q^{(n)}-}_{\sigma^b_{n-r}}(X)$ is simply the product of the $r$-target predicted PDF given the initial pdf is $p^{q^{(r)}}(.)$ and the birth hypothesis encoded in $\sigma^b_{n-r}$. It is clear from Eq. 4.32 that the following holds.

**Proposition 4.** *The predicted multi-object PDF, given that the prior multi-object PDF satisfies Assumption 2, may be expressed as:*

$$p^{-}(X, n) = \sum_{v^{(n)}} \omega_{v^{(n)}} p^{v^{(n)}}(X), \tag{4.34}$$

*where $v^{(n)} = (q^{(r)}, \sigma^b_{n-r})$, for all feasible $r$, i.e., each $v^{(n)}$ is a combination of some prior $r$-target*

*hypothesis $q^{(r)}$ and a corresponding birth hypothesis $\sigma^b_{n-r}$ with*

$$\omega_{v^{(n)}} = p(\sigma^b_{n-r})\omega_{q^{(r)}}, \tag{4.35}$$

$$p^{v^{(n)}}(X) = p^{q^{(r)}-}_{\sigma^b_{n-r}}(X).$$

*where $p^{q^{(r)}-}_{\sigma^b_{n-r}}(X)$ is given by Eq. 4.34.*

Given the predicted PDF $p^-(X, n)$ has the hypothesis based form above, with track independence inherent to the multi-object PDF underlying every hypothesis, it is clear that Proposition 3 can be used to perform the update step given a measurement $Z$.

**Remark 4.** *More on the hypothesis based Structure of the FISST PDF: Propositions 1-4 establish that under Assumption 1, the predicted and updated multi-object PDF at any time can be expressed as:*

$$p(X, n) = \sum_{q^{(n)}} \omega_{q^{(n)}} p^{q^{(n)}}(X),$$

*where each $q^{(n)}$ represents some particular sequence of birth and data association hypothesis till the current time, with $\omega_{q^{(n)}}$ representing the weight of the hypothesis and $p^{q^{(n)}}(.)$ representing the underlying multi-object PDF. Note that this is entirely equivalent to tracing all the descendants of an initial hypothesis, conditioned on all possible birth and data association hypotheses: precisely the goal of the MHT approach. In order to keep track of object identity, a unique label can be given to a birth hypothesis in a particular pixel at a particular time, for instance, using the 2-tuple $(t, p)$ which denotes a birth in the $p^{th}$ pixel at time $t$. With some bookkeeping, this allows us to associate the component PDFs under any hypothesis to a unique object.*

### 4.4.4 Hypothesis Weight Update Equation

Let $q^{(r)}$ denote an initial $r$-object hypothesis, $\sigma^b_{n-r}$ denote a subsequent birth hypothesis, and $\sigma^{(n)}_a$ denote a subsequent data association hypothesis. From Propositions 3 and 4, it follows that the weight of the grandchild hypothesis (birth followed by data association) of $q^{(r)}$ is given by the weight update equation:

$$\omega_{q^{(r)}\sigma^b_{n-r}\sigma^{(n)}_a} = \eta l_{q^{(r)}\sigma^b_{n-r},\sigma^{(n)}_a} p(\sigma^{(n)}_a|n) p(\sigma^b_{n-r}) \omega_{q^{(r)}}, \tag{4.36}$$

where $\eta$ is a suitable normalization constant found by summing the numerator over all possible grandchild hypotheses. In the above equation, $p(\sigma^b_{n-r})$ represents the probability of the birth hypothesis, $p(\sigma^{(n)}_a|n)$ represents the a priori probability of the data association hypothesis, and $l_{q^{(r)}\sigma^b_{n-r},\sigma^{(n)}_a}$ represents the likelihood of the data association hypothesis $\sigma^{(n)}_a$ given the predicted MT-pdf of $q^{(r)}$ under the birth hypothesis $\sigma^b_{n-r}$, $v^{(n)} = (q^{(r)}, \sigma^b_{n-r})$. The predicted MT-pdf underlying $v^{(n)} = (q^{(r)}, \sigma^b_{n-r})$ is specified by Proposition 4, and the likelihood is specified by Proposition 3, given the predicted multi-object PDF. In fact, the entire multi-object tracking problem is captured by the above equation, which is similar to the discrete MHT hypothesis weight update equation in [3], however, see Chapter 5 for more on this aspect.

**Remark 5.** *Incorporating Target Death: Given an $r$-object hypothesis $q^{(r)}$, the probability that a target survives can be modeled as a binomial process with the probability that a target survives equal to $\beta$, independent of any other target. Thus, the probability of the hypothesis that exactly $p$ of the targets out of $r$ survive, say $p(\sigma^d_p|r) = \beta^p(1-\beta)^{r-p}$. Even with target death, the multi-object tracking problem remains that of tracking all possible descendants of the parent hypotheses, and thus, the primary difference with Eq. 4.37 for the hypothesis update is that the survival probability $p(\sigma^d_p|r)$ is now multiplied to the right of Eq. 4.37, for all possible combinations of birth, survival and data association hypothesis:*

$$\omega_{q^{(r)}\sigma^b_{n-r}\sigma^d_p\sigma^{(n-p)}_a} = \eta l_{q^{(r)}\sigma^b_{n-r}\sigma^d_p\sigma^{(n-p)}_a} p(\sigma^{(n-p)}_a|n-p) p(\sigma^d_p) p(\sigma^b_{n-r}) \omega_{q^{(r)}}, \tag{4.37}$$

*where note that the number of targets due to the $p$ deaths reduces to $n-p$, and therefore the data association hypotheses are for $n-p$ targets. The MT-pdf underlying the hypothesis is simply that of the birth hypothesis minus the PDFs of the targets that do not survive according to the hypothesis $\sigma_p^d$. Note change in notation from Section 4.4.3 such that: $\sigma_p^d = \sigma_p^s$ and $\beta = p_s$. This is also illustrated in Fig. 4.1.*

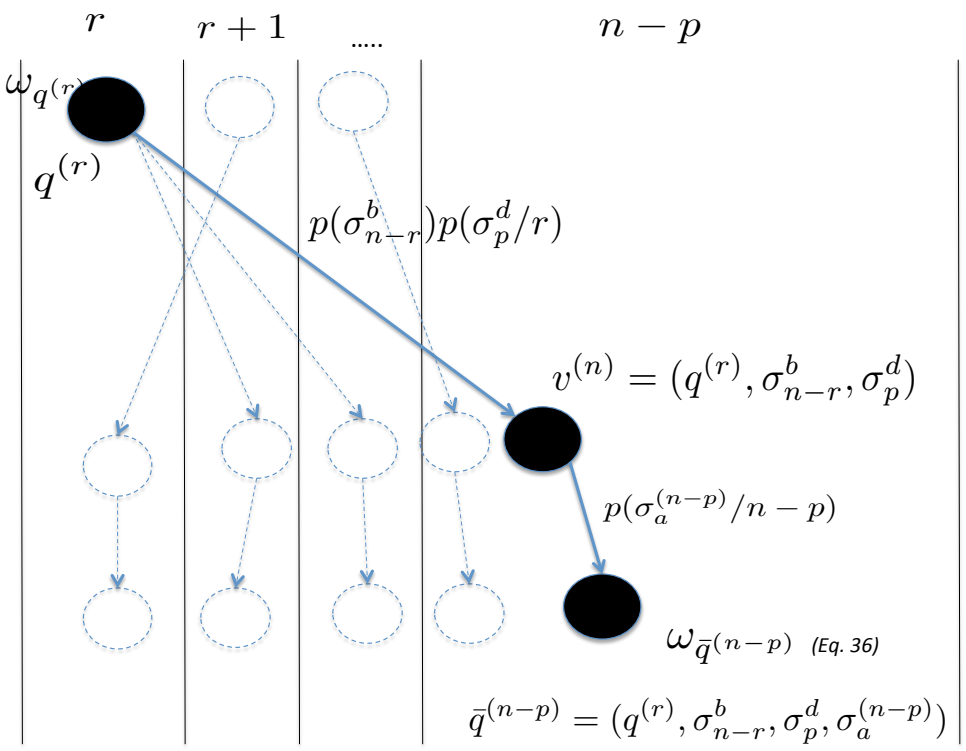


Figure 4.1: A schematic of the splitting of the hypothesis due to birth/ death of objects and data associations. Underlying each blob is a continuous multi-object pdf. A particular child and grand-child of a parent hypothesis, along with the transition probabilities, is outlined in bold, pictorially representing Eq. 4.37.

# 5. RELATIONSHIP BETWEEN CLASSICAL AND MODERN MULTI-OBJECT TRACKING TECHNIQUES

In the previous chapter, a hypothesis perspective was taken on the development of the RFS based multi-object Bayes filter. This approach was initially performed in order to develop a systematic approach to the inherent data association problem within multi-object tracking. In taking this hypothesis perspective, clear relationships between classical and modern techniques are illuminated. It is the intention of this chapter to highlight some of the insights and put to rest some of the issues discussed in 3.5.

The hypothesis perspective allows one to define a hypothesis structure of the RFS based multi-object Bayes filter. Under this hypothesis structure, as shown in Eqs. 4.25 - 4.34, the full RFS based multi-object PDF can be represented as a summation over all possible hypotheses. These hypotheses can be related to the MHC (specifically HOMHT) concept of a hypotheses in order to draw conclusive evidence about the relationship between the methods. There are two sections to this chapter. The first section discusses similarities between the approaches by considering the case where there is a fixed number of objects. The following section expands the discussion to include birth and death.

## 5.1 Relationship When The Number Of Objects Is Fixed

In this section, the connection of the modern RFS multi-object recursions to the classical MHT recursions is explored, as well as the structure of the respective multi-object PDFs In particular, Reid's HOMHT structure [3] is compared to the developments of Chapter 4. This is done using a simple written example and then described in general form.

### 5.1.1 Relationship Through A Simple Example

Consider a very simple situation with two objects, and only one measurement return, that illustrates Proposition 3, and the MHT-FISST relationship clearly. Let the prior multi-object PDF

be given according to Eq. 4.25:

$$p(\{x_1, x_2\}) = p_1(x_1)p_2(x_2) + p_1(x_2)p_2(x_1). \tag{5.1}$$

The predicted prior FISST PDF is given by Eq. 4.27:

$$p^-(\{x_1, x_2\}) = p_1^-(x_1)p_2^-(x_2) + p_1^-(x_2)p_2^-(x_1), \tag{5.2}$$

where

$$p_1^-(x) = \int p(x|x')p_1(x')dx',\ p_2^-(x) = \int p(x|x')p_2(x')dx'.$$

Given that there is a single observation $z$, there are three possible data associations: 1) $object_1 \rightarrow z$, 2) $object_2 \rightarrow z$, and 3) $clutter \rightarrow z$. The posterior FISST pdf is then (Proposition 3):

$$p(\{x_1, x_2\}) = \sum_{i=1}^{3} \omega_{(i)}[p_1^{(i)}(x_1)p_2^{(i)}(x_2) + p_1^{(i)}(x_2)p_2^{(i)}(x_1)]. \tag{5.3}$$

In the above, $p_1^{(1)}$ is obtained by updating $p_1^-(.)$ with $z$, and $p_2^{(1)} = p_2^-(.)$, i.e., the component PDFs of objects 1 and 2 under data association 1. The same observation holds for the multi-object pdf components under data associations 2 and 3 as well. The $\omega_{(i)}$ are the weights of the individual hypotheses calculated according to Proposition 2. For instance,

$$\omega_{(1)} \propto p_D[\frac{\int p(z|x)p_1^-(x)dx}{\lambda}](1 - p_D). \tag{5.4}$$

Hence, the FISST recursions are completely determined by the prediction of the component PDFs, and their update, according to the different data associations, along with the (data association) hypothesis weight update. In this case, HOMHT follows the exact same procedure for the prediction, and update, of the component PDFs under the exact same data associations (please see pg. 846-848 of [3]). In HOMHT, the individual PDFs $p_1(.)$ and $p_2(.)$ are assumed to be Gaussian

and the prediction and update of the PDFs, using the measurement $z$, is carried out using a Kalman filter, under the different data associations 1 through 3 above. Aside from those assumptions, the update equation is exactly the same, for instance,

$$\omega_{(1)} \propto p_D[\frac{p(z|x_1)}{\lambda}](1-p_D), \tag{5.5}$$

However, the HOMHT never explicitly represents the continuous multi-object pdf underlying the different hypotheses. Implicitly, the MHT seems to represent the multi-object pdf as:

$$p(x_1, x_2) = p_1(x_1)p_2(x_2), \tag{5.6}$$

where the co-ordinate $x_1$ is used to describe object 1 and $x_2$ is used to describe object 2 only. However, such a representation, in general, is heuristic. Suppose the supports of $p_1(.)$ and $p_2(.)$ overlap and consider states $(x_1, x_2)$ in the intersection of the supports as shown in Fig. 5.1. Due to the indistinguishability of the targets, the probability (density) that object 1 is at $x_1$ and object 2 is at $x_2$ can not be specified, albeit they are statistically independent. Instead, the basic event that can be specified is that object 1 and 2 occupy states $x_1$ and $x_2$. The probability (density) of the event is equal to the probability of the union of the two disjoint events, $E_1 : \{$ object 1 is at $x_1$ and object 2 is at $x_2\}$, and $E_2 : \{$ object 1 is at $x_2$ and object 2 is at $x_1\}$:

$$p(\{x_1, x_2\}) = p_1(x_1)p_2(x_2) + p_1(x_2)p_2(x_1). \tag{5.7}$$

However, if the supports of the pdf are disjoint (see Fig. 5.1), then it is indeed possible to write the multi-object pdf in the MHT form since event $E_2$ above has probability (density) zero. However, even if two PDFs have disjoint supports, there is no guarantee that after prediction they still have disjoint supports. Hence, the RFS representation of the multi-object pdf is better as it does not entail any assumptions and is a faithful representation of the “physics" of the problem. Nonetheless, the following observation regarding the connection between the FISST and MHT recursions can

be made: Modulo the multi-object PDF representation in FISST, the MHT technique and the RFS based technique result in the exact same set $q$ hypotheses, with identical weights and underlying PDF.

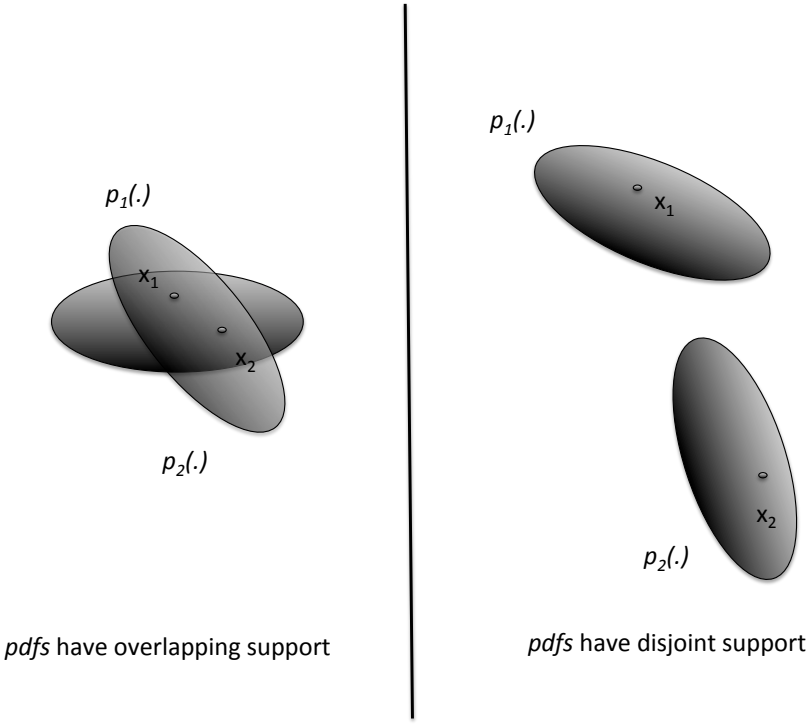


Figure 5.1: The FISST multi-object PDF: when the supports overlap, it is impossible to distinguish between the events $E_1$ and $E_2$ necessitating the use of the "symmetrized" form of the FISST pdf. However, when the supports do not intersect, it is possible to use the "heuristic" MHT representation of the multi-object pdf.

### 5.1.2 Relationship between FISST and MHT Hypothesis Weight Update

In this section, it is shown that in the case of no birth and death, that the probability of a particular hypothesis, in the MHT sense, is equivalent the posterior weight developed in Chapter 4 and thereby directly connected to the RFS multi-object derivation. Consider a prior n-object hypothesis $q^{(n)}$, and assuming no birth or death of objects, and the standard measurement model

including missed detections and Poisson false alarms. The MHT hypothesis probability pulled from [3, pg. 847 Eq. 8] also in full form [3, pg. 848 Eq. 16] and expressed in Eq. 3.15 as,

$$p_t(\Omega_{t-1}, \sigma_j | Z^t) = \omega_{MHT} = \eta l_{\sigma_j} p(\sigma_j | \Omega_{t-1}) p(\Omega_{t-1}) \tag{5.8}$$

where the likelihood $l_{\sigma_j}$ can be expressed using Eq. 3.8,

$$l_{\sigma_j} = \prod_i l(z_{\sigma_j,i} | x_i) = \prod_i \int p(z_{\sigma_{j,i}} | x_i) p^-(x_i) dx_i. \tag{5.9}$$

In the case where the data association hypothesis, $\sigma_j$, associates exactly $k$ measurements to clutter and assuming a uniform $p_D$, the last two factors of Eq.5.8 can be seen as follows,

$$p(\sigma_j | \Omega_{t-1}) p(\Omega_{t-1}) = p_D^{m-k} (1 - p_D)^{n-(m-k)} \lambda^k \omega_{\Omega_{t-1}} \tag{5.10}$$

Using Eqs. 5.9 and 5.10 in Eq. 5.8 the expression becomes

$$\omega_{MHT} = \eta p_D^{m-k} (1 - p_D)^{n-(m-k)} \lambda^k \omega_{\Omega_{t-1}} \prod_i \int p(z_{\sigma_{j,i}} | x_i) p^-(x_i) dx_i. \tag{5.11}$$

This expression for the MHT probability $\omega_{MHT}$ is exactly the same as the updated weight presented in Proposition 3.

## 5.2 Relationship Between HOMHT and FISST With Object Birth

The primary difference in the update equation 4.36 from the MHT update in [3] is the way new births are handled. In MHT, the new objects are treated the same as clutter as a part of the measurement update, but with a different arrival rate from clutter. However, in the RFS based recursions, the new objects are treated as part of the prediction equations, and thereby the likelihoods corresponding to a measurement to birth is treated the same as that done for existing objects (see Eq. 4.18). In particular, following HOMHT, the heuristic representation of Bayes rule for the

multi-object state with birth may be expressed as follows:

$$p(X,n|Z) = \eta p(Z|X,n)p^{-}(X,n)$$

$$= \eta \sum_{\sigma^b,\sigma^a} p(Z|\sigma^b,\sigma^a,X,n)p(\sigma^b)p(\sigma^a|\sigma^b,X,n)p^{-}(X,n),$$

however, due to the birth hypotheses $\sigma^b$, an n-target state on the right hand side does not remain an n-target state, thereby making the left hand side of the above equation inconsistent. If treated as part of the prediction step, as done in FISST, the birth hypotheses do not create the same inconsistency.

Consider now the weight update equation with birth, Eq. 4.36. The following development will show how this equation relates to that of [3]. Assuming a binomial process for birth, consider a particular birth hypothesis $\sigma^b_{n-r}$ that associated $n-r$ births at the specified pixel locations $(\sigma^b_{n-r,1},\cdots,\sigma^b_{n-r,n-r})$. Each spatial density is unique with pdf $p(x_{\sigma^b_{n-r,i}}) = \frac{1}{\bar{V}}$ where $\bar{V}$ is the volume of the pixel. Furthermore, consider a data association hypothesis $\sigma^{(n)}_a$ that associates exactly $s$ of these birth pdf to measurements, and $k$ to clutter. Then, let $\sigma^{(n)}_{a,i}$ such that $i = 1,...,m-(s+k)$ denotes the association to existing objects, and $\sigma^{(n)}_{a,i}$ such that $i = m-(s+k)+1,...,m-k$. Then by Eq. 4.36,

$$\omega_{q^{(n)}\sigma^b_{n-r}\sigma^{(n)}_a} = (1-p_D)^{n-(m-k)} \prod_{i=1}^{r} p_D \int p(z_{\sigma^{(n)}_{a,i}}|x_i)p^{q(r),i-}(x_i)dx_i \tag{5.12}$$

$$\prod_{i=r+1}^{n} p_D \int p(z_{\sigma^{(n)}_{a,i}}|x_i)\frac{1}{\bar{V}}dx_i \; \frac{k!}{V^k}\alpha^{n-r}(1-\alpha)^{M-(n-r)}e^{-\lambda_C V}\frac{(\lambda_C V)^k}{k!}\omega_{q^{(r)}}$$

Rearranging terms,

$$\omega_{q^{(n)}\sigma^b_{n-r}\sigma^{(n)}_a} = (1-p_D)^{n-(m-k)}p_D^{m-k} \prod_{i=1}^{r} \int p(z_{\sigma^{(n)}_{a,i}}|x_i)p^{q(r),i-}(x_i)dx_i \tag{5.13}$$

$$\prod_{i=r+1}^{n} \int p(z_{\sigma_{a,i}^{(n)}}|x_i)\frac{1}{\bar{V}}dx_i \; \frac{k!}{V^k}\alpha^{n-r}(1-\alpha)^{M-(n-r)}e^{-\lambda_C V}\frac{(\lambda_C V)^k}{k!}\omega_{q^{(r)}}$$

Note that $\alpha = \lambda_B V$ and due to Poisson's theorem:

**Theorem 1.** *As* $M \to \inf$ *and* $\alpha \to$ *such that* $M\alpha = \lambda_B V$

$$\binom{M}{(n-r)}\alpha^{n-r}(1-\alpha)^{M-(n-r)} = \frac{e^{-\lambda_B V}(\lambda_B V)^{(n-r)}}{(n-r)!} \tag{5.14}$$

which can be simplified to,

$$e^{-\lambda_B V}(\lambda_B)^{(n-r)}\bar{V}^{(n-r)} = \alpha^{(n-r)}(1-\alpha)^{M-(n-r)} \tag{5.15}$$

Now consider the factor:

$$\int p(z_{\sigma_{a,i}^{(n)}}|x_i)\frac{1}{\bar{V}}dx_i \tag{5.16}$$

If we assume that $z = x + v$, i.e., a full state measurement the integral is,

$$\int p(z_{\sigma_{a,i}^{(n)}}|x_i)dx_i = 1.$$

Thus,

$$\int p(z_{\sigma_{a,i}^{(n)}}|x_i)\frac{1}{\bar{V}}dx_i = \frac{1}{\bar{V}}. \tag{5.17}$$

Substituting Eq. 5.17 and Eq. 5.15 into Eq. 5.13,

$$\omega_{q^{(n)}\sigma_{n-r}^{b}\sigma_a^{(n)}} = (1-p_D)^{n-(m-k)}p_D^{m-k}\prod_{i=1}^{r}\int p(z_{\sigma_{a,i}^{(n)}}|x_i)p^{q(r),i-}(x_i)dx_i \tag{5.18}$$

$$(\frac{1}{\bar{V}})^s e^{-\lambda_B V}(\lambda_B)^{(n-r)}\bar{V}^{(n-r)}e^{-\lambda_C V}(\lambda_C)^k\omega_{q^{(r)}}.$$

This equation further simplifies to,

$$\omega_{q^{(n)}\sigma_{n-r}^{b}\sigma_a^{(n)}} = (1-p_D)^{r-(m-k)}p_D^{(m-k)}\prod_{i=1}^{r}\int p(z_{\sigma_{a,i}^{(n)}}|x_i)p^{q(r),i-}(x_i)dx_i$$

$$((1-p_D)\lambda_B)^{(n-r)}\bar{V}^{(n-r)-s}(\lambda_C)^k\omega_{q^{(r)}}. \tag{5.19}$$

Note that constant terms $e^{-\lambda_C V}$ and $e^{-\lambda_B V}$ are removed for the sake of clarity. Equation 5.19 is the "key" formula allows one to see the contrast between the FISST based approach and HOMHT. It can be seen from [3, pg. 848 Eq. 16] that, under the same hypothesis assumptions, the unnormalized probability is,

$$\omega_{HOMHT} \approx (1-p_D)^{r-(m-k)}p_D^{(m-k)}\prod_{i=1}^{r}\int p(z_{\sigma_{a,i}^{(n)}}|x_i)p^{q(r),i-}(x_i)dx_i\ (\lambda_B)^s(\lambda_C)^k\omega_{q^{(r)}}. \tag{5.20}$$

Equation 5.19 plainly shows that the FISST approach treats object birth as part of the prediction, and thus, there may be more births than detected. Moreover, the predicted births are carried forward in time, i.e., note the multi-object PDF underlying Eq. 5.19 contains the updated existing object PDFs and those birth PDFs associated to observations, as well as, the undetected birth PDFs. On the other hand, in Eq. 5.20 the number of births can not be more than the number of observations assigned to birth, i.e., $s$. In other words, every birth has an observation assigned to it. Suppose now that in Eq. 5.19, exactly $s = n - r$, stating that all new births are detected. Then Eq. 5.19 becomes,

$$\omega_{q^{(r)}\sigma_{n-r}^{b}\sigma_a^{(n)}} = (1-p_D)^{r-(m-k)}p_D^{(m-k)}\prod_{i=1}^{r}\int p(z_{\sigma_{a,i}^{(n)}}|x_i)p^{q(r),i-}(x_i)dx_i$$

$$((1-p_D)\lambda_B)^{(n-r)}(\lambda_C)^k\omega_{q^{(r)}}. \tag{5.21}$$

The only difference between Eq. 5.21 and Eq. 5.20 is the factor $((1-p_D)\lambda_B)^{(n-r)}$. Since the HOMHT approach handles birth in the update step the factor is different than as in the FISST based approach. This shows that for the exact same hypothesis the FISST approach will have inherently lower weight. Making it less probable to birth new objects. Besides that factor, everything else, including the underlying continuous multi-object PDF, is the same. Lastly, it is important to note the practicality issue with handling birth in the prediction. Doing so means that all predicted birth PDFs are carried forward in time. This adds computational burden with no added information gain,

and thus, is inherently wasteful. The HOMHT approach of handling birth in the update, be it may an approximation of the true update, only initializes PDF given an observation, which all together avoids the extraneous birth PDF prediction.

# 6. HYPOTHESIS GENERATION TECHNIQUES

This chapter presents a technique for performing randomized hypothesis generation. Such techniques are needed due to the combinatorial explosion caused by the DAP that, in turn, makes the multiple object tracking problem computationally intractable. This problem does not occur often, and only does occur when objects are highly ambiguous, i.e., large numbers of objects are closely spaced relative to the single-to-noise ratio. However, if the objects are highly ambiguous the use of exhaustive hypothesis generation techniques, even when combined with gating and pruning techniques, often can not sufficiently characterize all the data association hypotheses within computational limits. Randomized hypothesis generation techniques take advantage of the fact that the vast majority of the data association hypotheses are very unlikely and aim to accurately characterize the problem using a set of highly probable hypotheses without having to generate all possible hypotheses. This chapter discusses the details of randomized hypothesis generation by introducing the basic DAP with no false alarms or missed detections then expanding to more difficult scenarios including birth, death, false alarm, and missed detections. Standard hypothesis generation techniques are discussed as well as a newly developed technique called Smart Sampling Markov Chain Monte Carlo (SSMCMC).

## 6.1 Fixed Number Of Objects and No False Alarms

This section discusses the basic data association problem where there exists a fixed number of objects that are always detected without any false alarms. It is assumed that the objects are close enough to where all objects can be associated to all measurements. In other words, all objects lie within the association gates for all measurements. Consider a set of objects with states $X = \{x_1, ..., x_n\}$ and a corresponding measurement set $Z = \{z_1, ..., z_n\}$. Due to uncertainty in both the object states and observations one can never be certain which object a particular measurement corresponds to. The following subsections outline the challenges and common approaches to solving this data association problem.

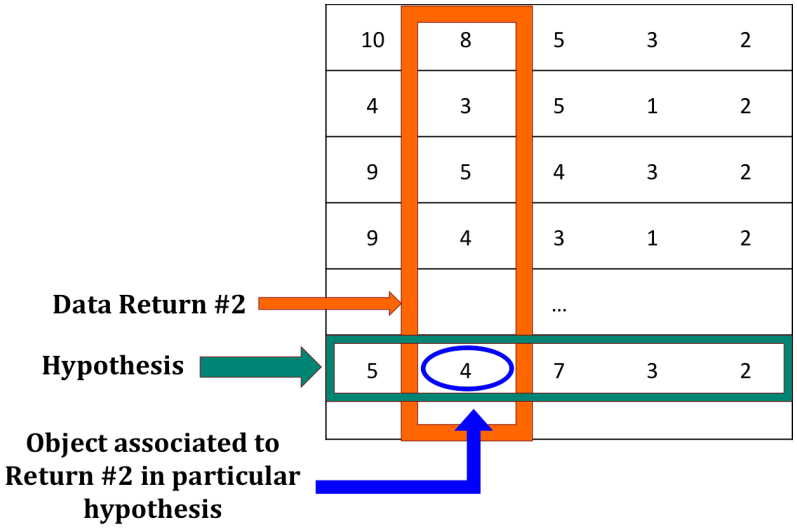


Figure 6.1: Hypothesis matrix used in hypothesis generation. Each row corresponds to a different data association hypothesis. Each column represents a measurement return while each element is the corresponding object association.

### 6.1.1 Computational Complexity

The data association problem for the scenario above increases in complexity with the number of objects. The number of possible hypotheses $A(n)$ as a function of the number of objects $n$ has the form,

$$A(n) = n!. \tag{6.1}$$

This accounts for all possible permutations of the numbers $1, ..., n$. If the number of objects is sufficiently large exhaustively generating all possible hypotheses can consume platform allocated memory and cause the intractability. This can be explained through illustration by looking at the hypothesis matrix 6.1. The hypothesis matrix is generated to store data association hypotheses. There is a different hypothesis matrix for every prior hypothesis at every measurement instance. Each column represents a particular measurement return and each element represents the corresponding object association. Every row of the hypothesis matrix corresponds to a different data association hypothesis. It can be seen from 6.1 that as the number of objects increases the size of this matrix will become extremely large. Generating this matrix is the root of the computational

complexity. It is also important to reiterate that there is a matrix like 6.1 for every prior hypothesis at every measurement step. This causes significant computational burden.

### 6.1.2 Linear Assignment Problem and Score Matrix

The data association problem discussed in this section can be seen as a linear assignment problem for which an optimization problem may be solved to find the most probable association. The formulation of this problem involves an $n \times n$ score matrix containing elements that represent scores of certain data association assignments. This matrix can be constructed using the *data association matrix* that contains the measurement to objects association probabilities. The optimal assignment can be determined by finding a permutation matrix that maximizes the following,

$$\begin{aligned} \text{maximize} \quad & J = \sum_{z}^{n} \sum_{x}^{n} M_{zx} D_{zx} \\ \text{subject to} \quad & \forall \sum_{z}^{n} M_{zx} = 1 \\ & \forall \sum_{x}^{n} M_{zx} = 1 \\ & M_{zx} \in \{0, 1\}. \end{aligned} \tag{6.2}$$

Where $M_{zx}$ is the permutation matrix and $D_{zx}$ is the score matrix.

### 6.1.3 Global Optimal Assignment

Through the field of combinatorial optimization a solution to the linear assignment problem can be found in polynomial time using the Munkres assignment algorithm [64, 65]. Using Munkres algorithm one can find the global optimal association. This technique is used in single hypothesis tracking methods such as GNN and in multi-object tracking methods to seed randomized techniques.

### 6.1.4 Multiple Hypothesis Generation Techniques

As mentioned in 3, methods that maintain only one hypothesis throughout time perform poorly in scenarios where objects are closely spaced or when objects are crossing paths. This is caused

by the fact that in these situations maximum association probabilities may not correspond to the correct or true association. It may be that during these times the correct association actually has relatively low probability. Using only the global maximum association can lead to type I and type II errors. Maintaining multiple hypotheses is of particular importance in these scenarios. Some common techniques that are used to provide multiple hypotheses are exhaustive generation, Murty's K-best, and Markov Chain Monte Carlo.

### 6.1.5 K-Best Assignment or Murty's Algorithm

The $K$-Best assignment algorithm or Murty's Algorithm [54] is a way to find the top $K$ association hypotheses. The algorithm is first seeded with the global optimal association. The association hypothesis is then systematically tweaked to determine the next most probable association. This is performed user defined number of times until the top $K$ hypotheses are determined.

### 6.1.6 Markov Chain Monte Carlo

Randomization techniques sample through the possible hypotheses and can be beneficial in both determining the global association hypothesis and a set of highly likely hypotheses without having to generate all possible hypotheses. This is of particular importance when the number of possible hypotheses is computationally intractable. Markov Chain Monte Carlo (MCMC) [66] is an example of a randomized hypothesis generation technique from the field of combinatorial optimization that can be used to determine a set of highly probable hypotheses. MCMC is beneficial because one does not have to determine the top association before using it and one can find a set of highly probable hypotheses without having to generate all possible hypotheses. It is performed by creating a Markov Chain using the association hypotheses as states of the chain. A random walk is performed on the chain favoring states with higher probability. After sufficient exploring of the chain the states sampled will be from the chain's stationary distribution. The states belonging to stationary distribution can be taken and used as a set of highly probable hypotheses.

## 6.2 Incorporating Birth, Death, False Alarms, and Missed Detections

In SSA tracking scenarios the number of objects varies with time due to birth, death, and spawn events. The number of observations also varies due to missed detections and false alarms. Hypotheses must be created to include such associations. This section illustrates how to handle these associations within a single data association framework. The development within the following section is performed in a manner that is compatible with all standard methods such as the Munkres algorithm, Murty's $K$-best, and MCMC.

### 6.2.1 Computational Complexity

To incorporate multiple-birth, multiple-death, false alarm, and missed detection into a randomized hypothesis generation technique one must account for all transition hypotheses, $\theta$ and all data association hypotheses $\sigma^{(n)}$. Assume that at time $t-1$ there exist a set of objects $X' = \{x'_1, ..., x'_r\}$ where $|X'| = r$. Taking into account birth and death the states $X'$ can be represented at time $t$ using $X = \{x_1, ...x_n\}$ where $|X| = n$. Due to birth and death the number of predicted objects $n$ can be greater than or equal to the previous number of objects $r$ and by set notation be countably infinite. However, an upper bound on $n$ is usually set by limiting the number of possible births. Furthermore, at time $t$ a measurement is received with $Z = \{z_1, ..., z_m\}$. These measurements include observations generated by false alarms and those from objects with high enough probability of detection. Having to deal with the different types of associations increases the computational complexity and exponentially increases the DAP discussed in the previous section. Figures 6.2 and 6.3 provide an illustration to clarify the difference in number of possible hypotheses. In figure 6.2, the parent hypothesis corresponds to a single prior hypotheses represented by $q^{(n)}$ in the chapter 4. The child hypotheses refer to those hypotheses generated by the data association problem or, in other words, the $\sigma^{(n)}$ hypotheses. In figure 6.3, the parent hypothesis is a single $q^{(n)}$ hypothesis however the child hypotheses are those brought about by birth and death and correlate to the $\theta$ hypotheses in chapter 4. The grandchild hypotheses are those correlating to the $\sigma$ hypotheses.

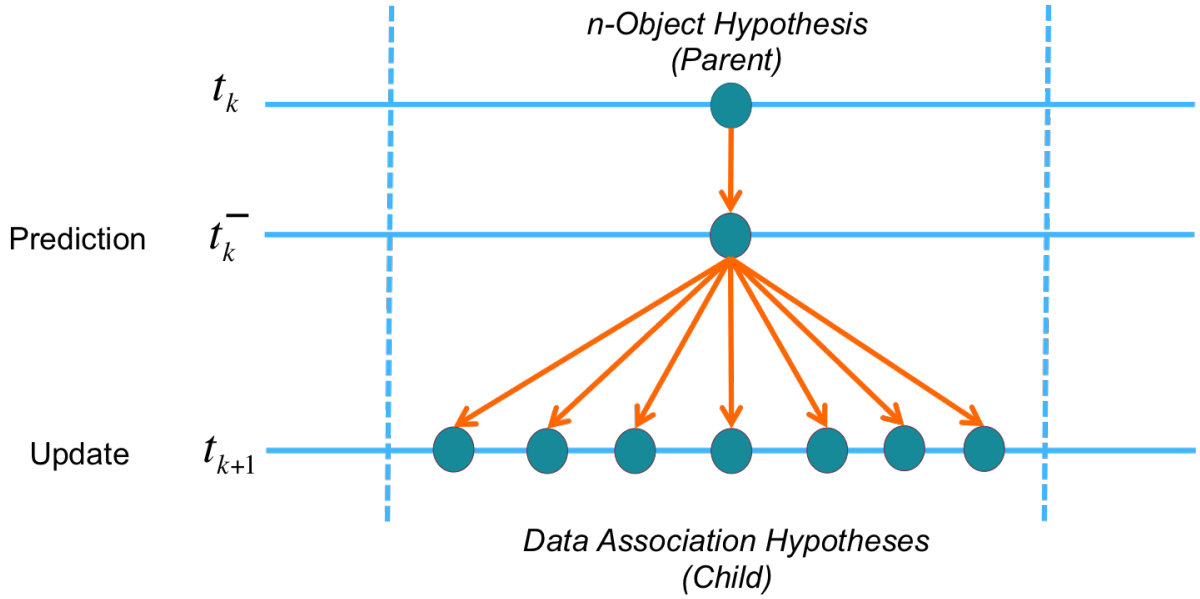


Figure 6.2: Transition of parent hypothesis to child hypotheses assuming the number of objects is fixed.

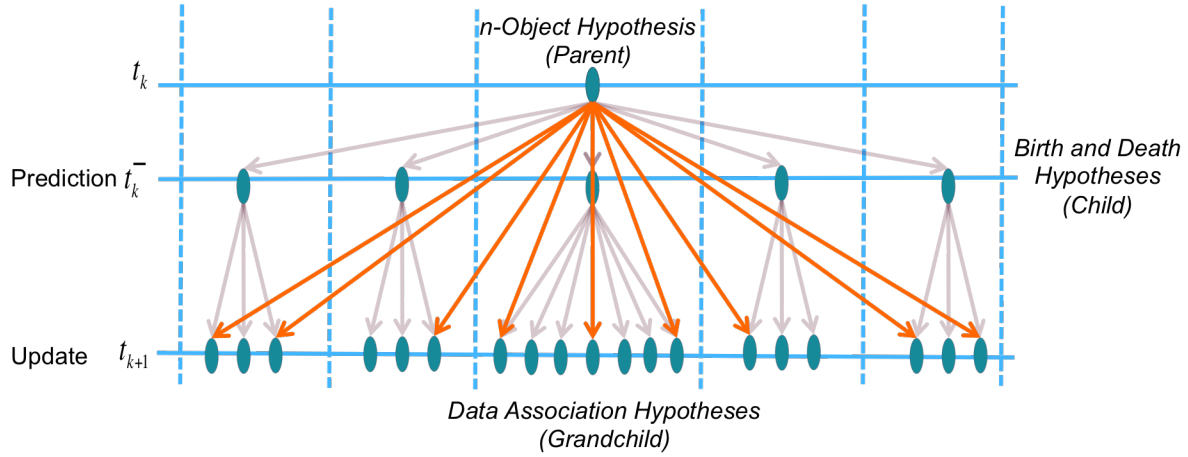


Figure 6.3: Transition of parent hypothesis to grandchild hypotheses with birth and death.

### 6.2.2 Data Association Matrix and Score Matrix

As in section 6.1, in order to determine the optimal assignment or perform randomized hypothesis generation a score matrix is needed. In this case, the number of measurements and the number of objects may be different. Also, the score matrix must include scores for the more complex types of data association such as observation to birth or object to death as well as the standard observation to object associations. This can be done by carefully constructing a data association matrix that contains assignment scores for all relevant types of association. Construction of such a data association matrix will be shown in detail in section 6.3. Careful construction of the data association matrix can allow for the use of the Munkres algorithm to find the global optimal assignment. The data association matrix can also incorporate multiple dynamic models, spawn type associations, and maneuver type associations.

### 6.2.3 Constraining The Data Association Matrix

When considering hypotheses on object motion as well as hypotheses on data associations the dimensions of the data association matrix may become large. In fact, if a limit is not set on the number of possible predicted births then the dimensions necessarily become countably infinite. Taking advantage of the fact that a majority of the possible hypotheses have probabilities near zero one can constrain the data association matrix to include only practical associations. Typical constraints include limiting the number of possible births to the number of measurements or, as in gating, constraining the number of observation to object associations based on a user defined minimum probability.

## 6.3 Smart Sampling Markov Chain Monte Carlo

This section introduces a new MCMC based technique called Smart Sampling Markov Chain Monte Carlo (SSMCMC) that can be used for hypothesis generation. In scenarios where generating all possible association hypotheses is computationally intractable, SSMCMC determines a set of hypotheses that can be used to approximate the multi-object posterior. It does this by creating a Markov chain using the particular association hypotheses as states of the chain. It then uses a biased

random walk to explore the states of the chain. While exploring the chain, the technique uses an MCMC decision making criterion that favors the states with higher posterior probability and by doing so generates samples from the multi-object posterior distribution. The walk is performed until the assumed burn in period is reached. After the burn in period the stationary distribution of the chain is sampled and the resulting states are taken as the highly probable hypotheses. The algorithm for these steps is presented in algorithm 1.

**Algorithm 1** SSMCMC Hypothesis Generation

1: Create data association matrix $D$
2: Generate child hypothesis $\Sigma_k$,
3: set $k = 0$.
4: Generate $\Sigma_{k+1} = \pi(\Sigma_k)$ where $\pi(.)$ is the proposal distribution
5: MCMC Criterion: If $\omega_{\Sigma_{k+1}} > \omega_{\Sigma_k}$
6: $\Sigma_k := \Sigma_{k+1}$;
7: else $\Sigma_k := \Sigma_{k+1}$ with probability proportional to $\frac{\omega_{\Sigma_{k+1}}}{\omega_{\Sigma_k}}$;
8: end
9: set $k = k + 1$.
10: repeat steps 2-8 until assumed burn in is reached
11: after burn in keep repeated $\Sigma_k$

**Remark 6.** *The mixing time or burn in period of a Markov Chain can not be proven. There are some common practices that can be beneficial in determining when the assumed burn in is reached. For instance, checking the rate at which proposed states are accepted. Note that the time spent at a particular state in the Markov Chain is proportional to the probability of the state as the number of steps goes to infinity. One can also seed multiple MCMC runs for the same problem with different initial conditions to see if the set of states at assumed convergence are similar between runs.*

### 6.3.1 Implementing SSMCMC

In the section, the process used to perform the SSMCMC sampling is revealed. This is done by using a small SSA example. Figure 6.4 shows an instance of a possible SSA optical measurement return. The return contains a set of two observations $Z = \{z_1, z_2\}$. At this instance assume there

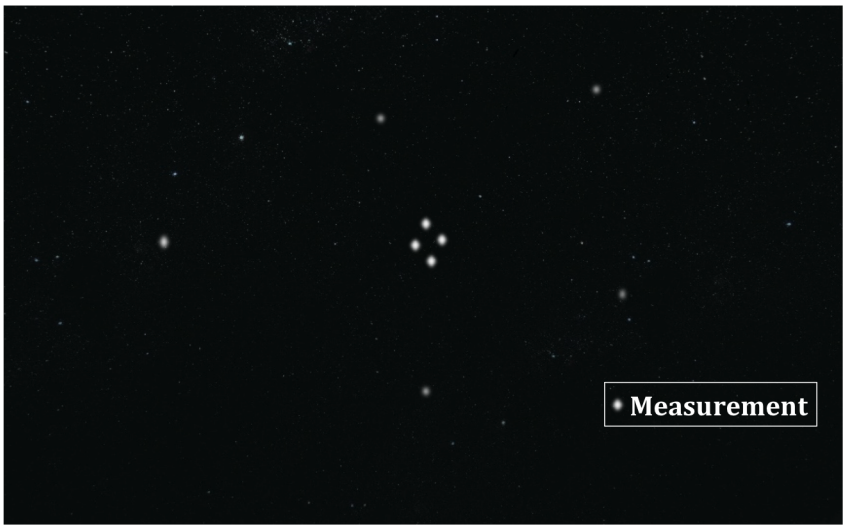


Figure 6.4: A possible SSA optical measurement return.

exist one prior hypothesis $q$ that contains one object $X = x_1$. The first step in the SSMCMC process is to create the data association matrix $D$. The following construction is performed in a manner such that it is compatible with the Munkres algorithm, i.e., it can be converted to a score matrix and the global optimal assignment can be determined. When constructed in this manner $D$ will have dimensions $n + m \times 2n + 2m$ and it will contain elements that represent all relevant association types including those that correspond to object birth, object death, object missed detection, observation to object, and false alarm associations. Construction of the data association matrix is most easily described using eight sub matrices.

$$D = \begin{bmatrix} D_1 & D_2 & D_3 & D_4 \\ D_5 & D_6 & D_7 & D_8 \end{bmatrix}. \tag{6.3}$$

The first sub matrix $D_1$ is an $m \times n$ matrix that contains the information pertaining to observation-to-object association. Assuming the object has a probability of survival $p_s$ and probability of detection $p_D$, then $D_1$ can be expressed as follows.

$$D_1 = [d_{ij} = \frac{p_s p_D p(z_i|x_j)}{(1 - p_D)}] \tag{6.4}$$

where $d_{ij}$ are elements of $D_1$ with $i = 1, .., m$ and $j = 1, ..., n$ being the row and column indexes respectively.

**Remark 7.** *In Eq. 6.4, the denominator* $(1 - p_D)$ *is not a common factor of the individual observation-to-object association probability. However, it is a necessary factor due to this particular construction of the data association.*

Sub matrix $D_2$ has dimensions $m \times m$ and contains the information for association to false alarm. In order to avoid breaking row and column rules $D_2$ is a diagonal matrix. Assuming that false alarm arrival is Poisson with average arrival rate $\lambda_C$ then $D_2$ is constructed as follows,

$$D_2 = diag(\lambda_C C(z_i)). \tag{6.5}$$

Where $i = 1, ...m$. $D_3$ is also an diagonal matrix where each element of the diagonal corresponds to a different birth association. Assuming birth arrival is Poisson with average arrival rate $\lambda_B$ and limiting the number of births to the number of measurement returns the sub matrix $D_3$ is an $m \times m$ matrix and can be expressed as,

$$D_3 = diag(\lambda_B p_D p_B(z_i|x_i)). \tag{6.6}$$

Limiting the number of births to the number of observations makes $i = 1, ..., m$. Also, assuming the birth PDF spatial distribution is uniform in the FOV allows for the convenient simplification $p_B(z_i|x_i) = \frac{1}{V}$. Another common assumption is to assume a spatial distribution that is normal centered around the observation. Matrices $D_4$, $D_6$, and $D_7$ are all zero matrices used as place holders in order to prevent breaking row and column rules. In large scenarios, these sub matrices cause the data association matrix to be sparse, but issues can be avoided by using sparse matrix tools that reduce extraneous computation and memory usage. $D_5$ is an $n \times n$ diagonal matrix that accounts for the probability of associating the objects to death. The expression for $D_5$ can be

written as,

$$D_5 = diag((1 - p_s(x_i))). \tag{6.7}$$

In which, $i$ takes values $1, ..., n$. Lastly, $D_8$ is an $n \times n$ diagonal matrix that accounts for missed detections and can be expressed by,

$$D_8 = diag(p_s(x_i)(1 - p_D)). \tag{6.8}$$

Where $i$ goes from $1, ..., n$. This construction of the $D$ allows for the simple conversion into a score matrix that can be used in Munkres algorithm. It is also set up so that when any valid selection of $n + m$ elements creates a particular grand child hypothesis that correlates to a specific selection $q$, $\theta$, and $\sigma$. The product of these elements then becomes the numerator of the discrete weight of the posterior PDF as in 4. Averaging over all possible $\theta$ and $\sigma$ hypotheses provides the posterior weight for the given parent hypothesis $q$. This ensures that when SSMCMC is performed samples are taken from the posterior distribution and the corresponding set of highly probable hypotheses $q^*$ accurately quantifies the grandchild hypothesis population. Using Eqs. 6.3-6.8 and assuming that the prior parent hypothesis $q$ contains one object $X = x_1$ the data association matrix for sample problem illustrated in 6.4 is as follows,

$$D = \begin{bmatrix} \frac{p_D p_s p(z_1|x_1)}{1-p_D} & \lambda_C C(z_1) & 0 & p_D \lambda_B B(x) & 0 & 0 \\ \frac{p_D p_s p(z_2|x_1)}{1-p_D} & 0 & \lambda_C C(z_2) & 0 & p_D \lambda_B B(x) & 0 \\ (1 - p_s) & 0 & 0 & 0 & 0 & (1 - p_d) \end{bmatrix}. \tag{6.9}$$

Creating the data association matrix has no added computational cost because each element of the matrix is necessary in calculating hypothesis probability and is used in every hypothesis generation technique. Also, the dimensions of the data association matrix are much smaller than those of the hypothesis matrix. This makes it much more practical to explore using MCMC.

After creating the data association one can begin the MCMC procedure. In the MCMC procedure one iterates through different values of a $2n + 2m \times n + m$ permutation matrix $M$. Each

different $M$ corresponds to a different grandchild hypothesis. To start the derivation, one must choose an initial $M = M_0$. This can be done randomly or for faster convergence can be initialized with the global maximum likelihood. An example of such a matrix is as follows,

$$M_0 = \begin{bmatrix} 1 & 0 & 0 \\ 0 & 0 & 0 \\ 0 & 0 & 0 \\ 0 & 0 & 0 \\ 0 & 1 & 0 \\ 0 & 0 & 1 \end{bmatrix}. \tag{6.10}$$

To be a valid permutation matrix that represents a grandchild hypothesis an $M$ matrix must have the following properties.

- matrix elements must be either zero or one:

$$m_{ij} \in \{0, 1\}.$$

- The sum of any particular column $j$ must be unity:

$$\sum_{i=1}^{n+m} m_{ij} = 1.$$

- The sum of any particular row $i$ must be less than or equal to one:

$$\sum_{j=1}^{2n+2m} m_{ij} = 1.$$

- It must not contain any non-zero elements corresponding to zeros in the data association matrix:

$$m_{ij} \neq 1 \text{ if } D_{ji} = 0.$$

Equation 6.10 has all properties for a valid permutation matrix and pertains to a particular grandchild hypothesis in which, one observation is associated to a previously known object and another observation is associated to a predicted birth hypothesis.

The next step is to begin the random walk by setting the initial permutation matrix to the current permutation matrix $M_k$ and determining the probability of the corresponding hypothesis. This can be done by taking the product of $M_k$ and $D$ creating a matrix where the nonzero elements correspond to the factors within the posterior weight. The weight is then the product of the nonzero elements. An example is shown using Eq. 6.10,

$$M_0 D = M_k D = \begin{bmatrix} \frac{p_D p_s p(z_1|x_1)}{1-p_D} & 0 & 0 & 0 & 0 & 0 \\ 0 & 0 & 0 & 0 & 0 & 0 \\ 0 & 0 & 0 & 0 & 0 & 0 \\ 0 & 0 & 0 & 0 & 0 & 0 \\ 0 & 0 & 0 & 0 & p_D \lambda_B B(x) & 0 \\ 0 & 0 & 0 & 0 & 0 & (1-p_d) \end{bmatrix}. \tag{6.11}$$

The nonzero elements are,

$$M_k D > 0 => [\frac{p_D p_s p(z_1|x_1)}{1-p_D} \quad p_D \lambda_B B(x) \quad (1-p_d)]. \tag{6.12}$$

Taking the product of the nonzero elements we get the discrete weight,

$$\omega_k = p_D^2 p_s p(z_1|x_1) \lambda_B B(x). \tag{6.13}$$

By including factors, like those from Poisson process models, that are missing from the data association matrix the numerator of the posterior weight from 4 can be recovered exactly to ensure the hypotheses are being sampled according to the posterior distribution. Including the missing fac-

tors is done on a hypothesis by hypothesis basis to ensure correct weight is used in the MCMC and is one reason why SSMCMC is advantageous over other methods. For this example, the weight becomes,

$$\overline{\omega}_k = e^{-\lambda} p_D^2 p_s p(z_1|x_1) \lambda_B B(x). \tag{6.14}$$

After the current weight is determined, the next step is to determine a proposed state $M_{k+1}$ to walk to. Typical randomized hypothesis generation techniques determine the proposed hypothesis by switching a single data association within the current hypothesis according to uniform proposal distribution. SSMCMC instead biases the proposal distribution to generate a smart data association switch. This is extremely important when handling large matrices because the probability of uniformly sampling a highly likely hypothesis is vanishingly small. The smart switch is done by randomly sampling a row $i$ and sampling the association $j$ to switch to according the distribution of the row $i$. For the example shown, randomly sample a row $i$ of $D$ then sample $j$ from $i$ according to the PMF for the row $i$. After the switch is chosen, make the corresponding switch in $M_k$ to create $M_{k+1}$. Assume the proposed switch was $i = 2$ and $j = 3$. The proposed hypothesis $M_{k+1}$ is then,

$$M_{k+1} = \begin{bmatrix} 1 & 0 & 0 \\ 0 & 0 & 0 \\ 0 & 1 & 0 \\ 0 & 0 & 0 \\ 0 & 0 & 0 \\ 0 & 0 & 1 \end{bmatrix}. \tag{6.15}$$

Next determine the weight of the proposed hypothesis $\overline{\omega}_{k+1}$ and compare it to the weight of current hypothesis $\overline{\omega}_k$ using an MCMC criterion that favors the more probable hypothesis. The expression for the MCMC criterion is,

$$M_k = \begin{cases} M_{k+1}, & \text{if } \frac{\overline{\omega}_{k+1}}{\overline{\omega}_k} \geq U([0,1]) \\ M_k, & \text{otherwise} \end{cases}. \tag{6.16}$$

In words, if the probability of the proposed hypothesis is greater than the probability of the current hypothesis then keep the proposed hypothesis and use it as the new current hypothesis and continue the random walk. If not, keep the current hypothesis.

Continue the random walk until the assumed burn in period is reached. After it is reached, continue walking and take the set of repeated hypotheses as the set of highly probable hypotheses $q^*$. The data association matrix can be modified to include any type of association including but not limited to multiple maneuver, multiple model, and spawn type associations. It is also compatible with different Markov motion models and different measurement models.

### 6.3.2 SSMCMC Advantages and Caveats

SSMCMC has some important advantages over other hypothesis generation techniques. The first is that SSMCMC uses a different proposal distribution than other MCMC techniques. Changing the proposal distribution allows the MCMC to mix well in scenarios where very low probability associations may be sampled. In fact, in applications with very large numbers of possible hypotheses, if the random walk is performed using a uniform proposal distribution the computational benefits of MCMC may not be substantial. As mentioned previously, a vast majority of the possible hypotheses have very low weight. The probability of sampling a highly probable hypothesis using a uniform distribution is vanishingly small. This causes the MCMC to have a very long burn in period. If the burn in period is underestimated one can end up with a set of hypotheses that poorly represent the highly probably population of possible hypotheses.

Another reason why the SSMCMC is advantageous is because of the inherent diversity of the sampled hypotheses. When using techniques such as Murty's $k$-best, $k$ is a user defined value that specifies how many of the top hypotheses are kept. This can lead to a lack of diversity in the representative set of hypotheses. In other words, hypotheses will be very similar minus a few data associations. MCMC based techniques differ because the number of kept hypotheses is not user defined, instead it is defined by the properties of the Markov Chain itself. This allows for more diversity in the sampled hypotheses and this diversity can be influenced by the number of steps used in the MCMC. Scenarios where the associations are highly ambiguous tend to return

more hypotheses than those with less ambiguities. This diversity comes with the caveat of having to determine the burn in period as well as higher computational burden for more ambiguous scenarios.

SSMCMC does have its caveats that practitioners should be wary of. The first of which was mentioned in Remark 6 and pertains to determining the number of steps until the assumed burn in period is reached. In short, convergence can not be proved. One must be cautious and take measures to avoid prematurely assuming that burn in has been reached. Another caveat occurs when the number of associable objects is large but the association probabilities are small. Since the probability of independent associations is the product of each individual association, one can encounter situations where the hypothesis probabilities are so small that they are assumed to be zero in computing platforms. For example, the smallest positive normalized floating-point double that the Matlab environment can store on most platforms is $2.2251e-308$. Any number smaller will be assumed zero. A common work around for this scenario is to use log likelihood values. To implement log likelihood values in the SSMCMC algorithm above, one must change the MCMC criterion to support negative values. Also, due to the nature of the logarithm simple ratios of the current and proposed probability may cause chains to mix poorly requiring more steps until assumed convergence.

# 7. APPLICATIONS

In this chapter, SSA examples are used to display the fact that randomized hypothesis generation techniques are sine qua non in multi-object tracking. As mentioned previously, events in SSA that cause the multi-object tracking DAP to become intractable are rare. The most well known precipitates are large debris events. Internal explosions, satellite failures, and RSO collisions are the root causes for RSO debris events. As more objects are launched into space, the potential for breakup events and space object collisions is ever increasing. These events create large clouds of debris that are extremely hazardous to space operations. Providing timely, accurate, and statistically meaningful SSA data is crucial in order to protect assets and operations in space and prevent subsequent events as in the Kessler syndrome [67]. NASA Orbital Debris Program Office reported that within the first seven years of the 21st century there had been over 10 confirmed debris events such as a breakups, collisions, or intercepts. They also estimate that 94% of the GEO population is debris [68]. Just in the year 2017, there have been at least two GEO breakup events (AMC-9, Telkom 1), debris of which not tracked or cataloged [69]. It is for these types of events that R-FISST is particularly suited. The Chapter is outlined as follows:

- Section 7.1 shows proof of concept examples and highlights the need for hypothesis generation techniques in SSA.
- In Section 7.2, the realism of the simulations begins to increase. For example, the NASA Standard Breakup Model [70] is used for more accurate simulation of RSO fragmentation. A variety of other techniques are considered and are discussed in Appendix B. Section 7.2 also discusses the sensitivity to birth model selection by showing three SSA cases.
- Section 7.3 shows the scalability of the R-FISST technique to large scale problems.

## 7.1 Proof Of Concept

This section contains applications of the R-FISST technique to some introductory SSA examples. These examples are used as a proof of concept and to show the need for randomized hypothesis generation techniques in SSA.

The first application is an example of the R-FISST technique's ability to keep the multi-object tracking problem computationally tractable that was presented at the AAS/AIAA Astrodynamics Specialist Conference 2016 [58]. A simulation was created where the number of possible hypotheses is too large to generate exhaustively. Gating, which is a heuristic technique used to reduce the number of hypotheses, will not be sufficient in these situations because a large number of ambiguous measurements and objects will be within the gating tolerance. GNN techniques will also fail in these situations because the highest likely hypothesis is often not the correct data association hypothesis creating the need to maintain multiple hypotheses throughout the simulation.

In the second example, the R-FISST technique was tested using Two Line Elements (TLE)[1] from the public catalog available at space-track.org [71]. The SSA example was used to show that the number of RSOs is not the limiting factor in space object tracking. Also, aspects of the simulation were created to show a simulated fragmentation scenario. This is used as a preliminary example to the more realistic fragmentation events shown later on.

### 7.1.1 2-D Planar Model

Using a planar SSA example a simulation was created that demonstrates the previously mentioned scenario. There are two goals to this experiment. The first is to show that the example simulation creates a situation where techniques like gating, Global Nearest Neighbor, and exhaustive hypothesis generation will fail. The second goal is to show that under these circumstances the randomized hypothesis generation technique developed above will sample the most likely hypotheses as well as the correct hypothesis and maintain correct cardinality and accurate tracking data throughout the simulation. RSOs were simulated in either Lower Earth Orbit (LEO) or low Medium Earth Orbit (MEO). Figure 7.1, depicts the true objects (squares) in their initial positions

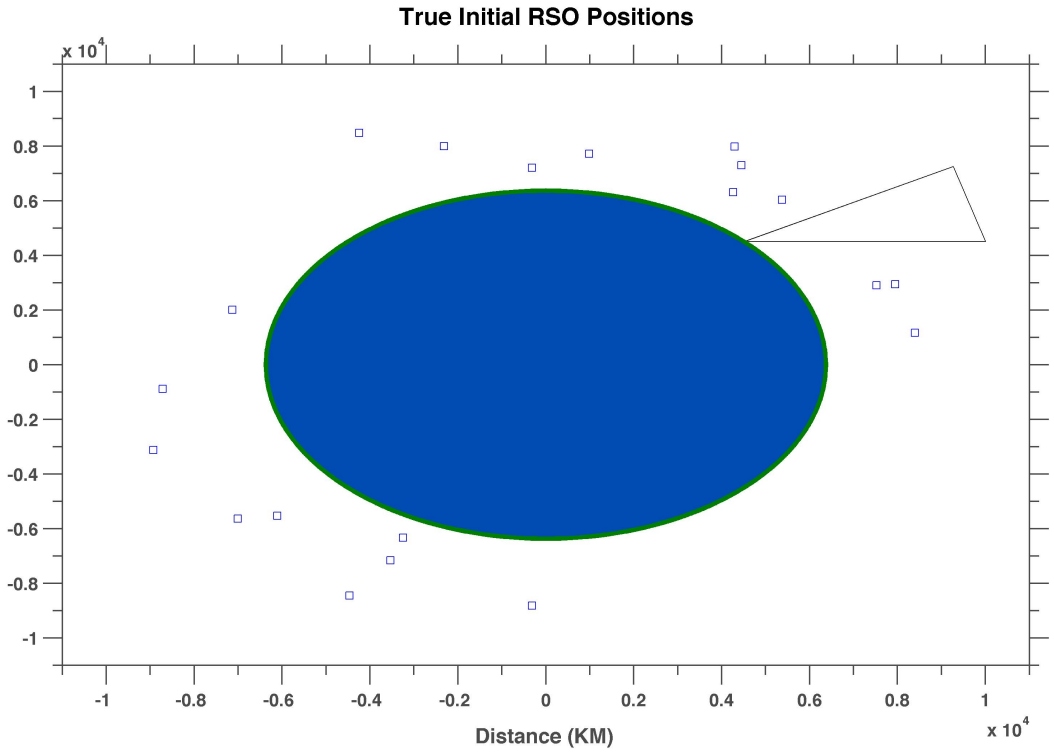


Figure 7.1: The true initial mean positions of the RSOs (squares) relative to the earth. Reprinted with permission from [1].

around the earth. This simulation was set up to incorporate multiple birth, multiple death, spawn, and clutter type events that resulted in a total of $30$ RSOs being simulated that remained at the end of the simulation. The simulation was run long enough such that each object passed through the field of view a minimum of one time. The state vector for each object contained the objects position and velocity in the Cartesian $x$ and $y$ frame. Clutter was added and assumed to be Poisson distributed with an average arrival rate $\lambda_C = 10$. The R-FISST technique was applied and given only an imperfect initial hypothesis and noisy sensor readings throughout the simulation. The initial hypothesis contained the initial means and covariances for some but not all of the RSOs. A single noisy sensor was positioned at $45\,\mathrm{deg}$ above the $x$-axis and had a Field of View (FOV) of $30\,\mathrm{deg}$. The sensor model measured $x$ and $y$ position of the objects with added Gaussian zero mean noise that allowed for an error in position of up to $20$ km. For simplicity, each assumed birth was initialized with a full state measurement and objects outside the field of view were con-

sidered to have zero probability of detection. The probability of detection inside the FOV was, $p_D = 0.9$. Measurements were taken at a standard interval that resulted in a total number of $200$ scans throughout the simulation. Once measurements were received hypotheses were generated using the randomized technique of R-FISST. The MCMC in the R-FISST technique was assumed to converge after a maximum of one million steps and one thousand steps were used to generate the likely hypotheses after convergence. Underlying continuous states were updated using an Extended Kalman Filter (EKF).

For the majority of the simulation time, techniques like GNN, gating, and exhaustive generation will work. However, Fig. 7.2 shows a particular instance in the simulation where GNN fails and gating with exhaustive generation is intractable. In Fig. 7.2, the number of possible hypotheses before gating is $\mathcal{O}(10^{11})$. After using a standard gating technique and keeping gated likelihood values of $p(z|x) = 10^{-7}$ or larger the number of possible hypotheses was still $\mathcal{O}(10^{9})$. Generating this amount of hypotheses exhaustively would call for the creation of a hypothesis matrix that will require more memory than is available on most standard platforms. Causing a system error created by Random Access Memory (RAM) availability constraints. Therefore, gating and exhaustively generating the hypotheses is intractable. Also, assuming the most likely association is the correct association, as in GNN, will cause poor associations leading to inaccurate tracking data. When applying R-FISST to the scenario in Fig. 7.2. The technique is able to keep the problem computationally tractable while sampling the correct hypothesis. Figure 7.3 shows snapshots as the RSOs in the scenario pass through the FOV. True object positions are depicted as squares while the estimated positions from the top hypothesis are shown as circles. The first snapshot shows that the imperfect initial hypothesis provides a belief that four objects exist. In actuality, there are fourteen true objects. These true objects are the result of spawn, birth, and death events.

Specifically, there are two objects that do not undergo any birth, death, or spawns, five-birth events, two death events, and one spawn event that results in seven new objects. As measurements are received, in snapshots two and three, the number of possible hypotheses is on the order $\mathcal{O}(10^{9})$. Even with a computationally intractable number of hypotheses, the estimations of the R-FISST

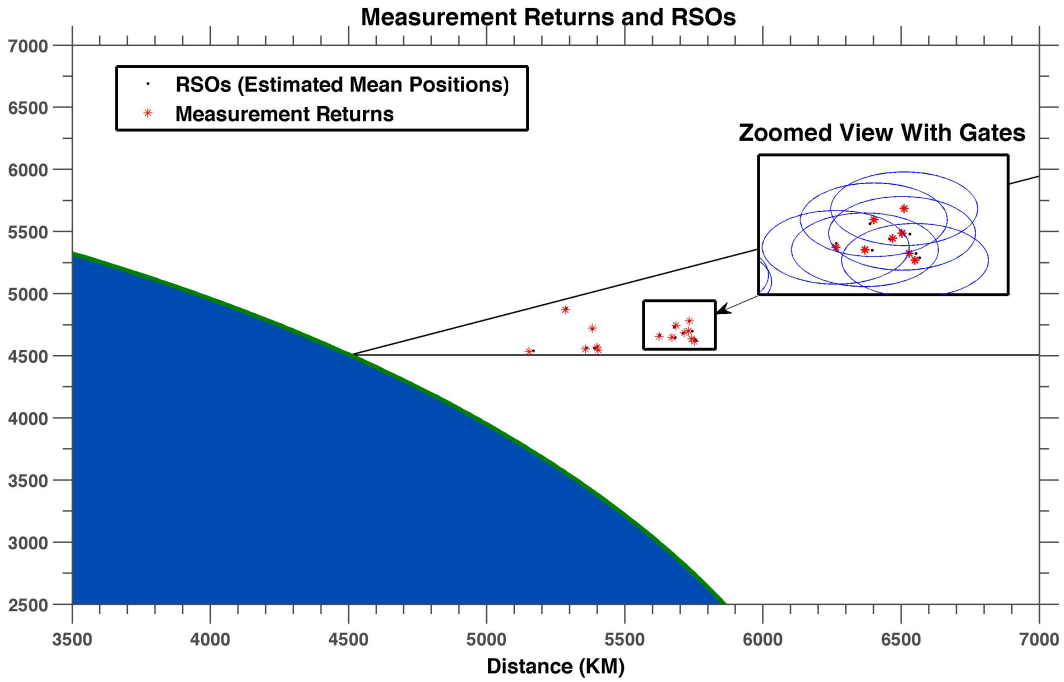


Figure 7.2: An instance in the simulation where GNN fails, and gating is not sufficient in reducing the number of possible hypotheses. Reprinted with permission from [1].

method begin to and eventually completely match that of the true RSOs. This shows that the R-FISST technique is able to sample the correct hypotheses as each measurement occurs. This is due to the fact that if the R-FISST technique were unable to sample the correct hypothesis then it would estimate the incorrect number of RSOs and/or have poor accuracy when estimating the positions of the RSOs.

### 7.1.2 Catalog Maintenance With RSO Fragmentation

The goal of this particular simulation is to create a truth model based on real RSO TLE and generate measurement data to be used in the R-FISST implementation. In this simulation, TLE data from the public catalog was used to generate true RSO state as well as measurement data from various sensors globally. The RSO in this particular simulation consisted of all the RSO residing in Medium Earth Orbit (MEO) known by the public catalog. Also, selected at random, one of the objects experiences a simulated spawn event creating a total of nine new objects caus-

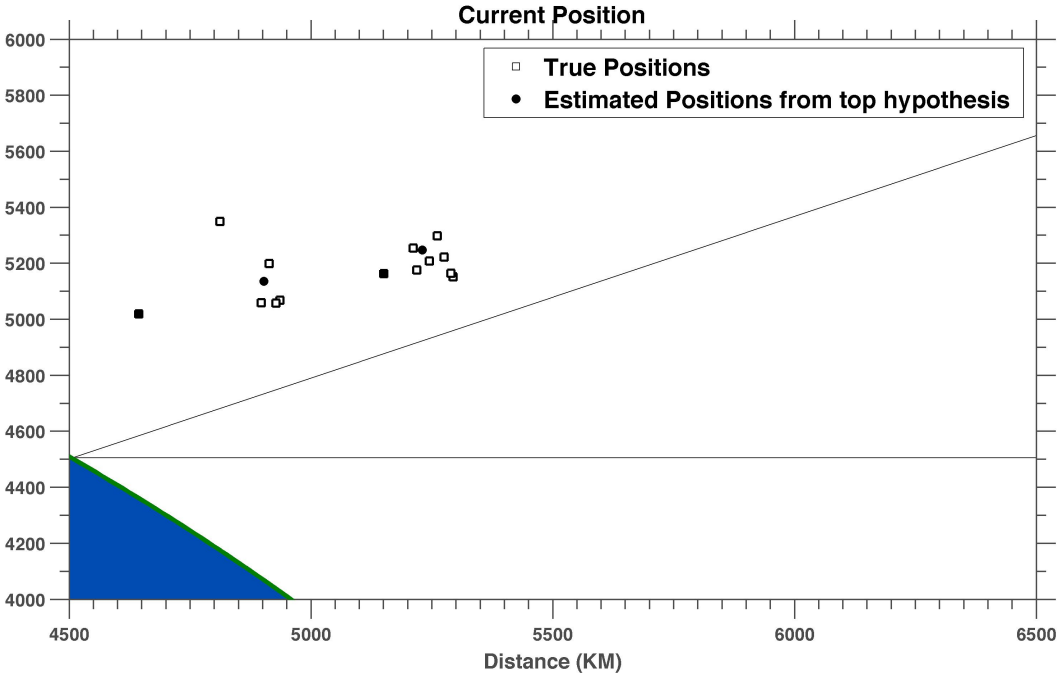


Figure 7.3: Belief before the Field of View. Reprinted with permission from [1].

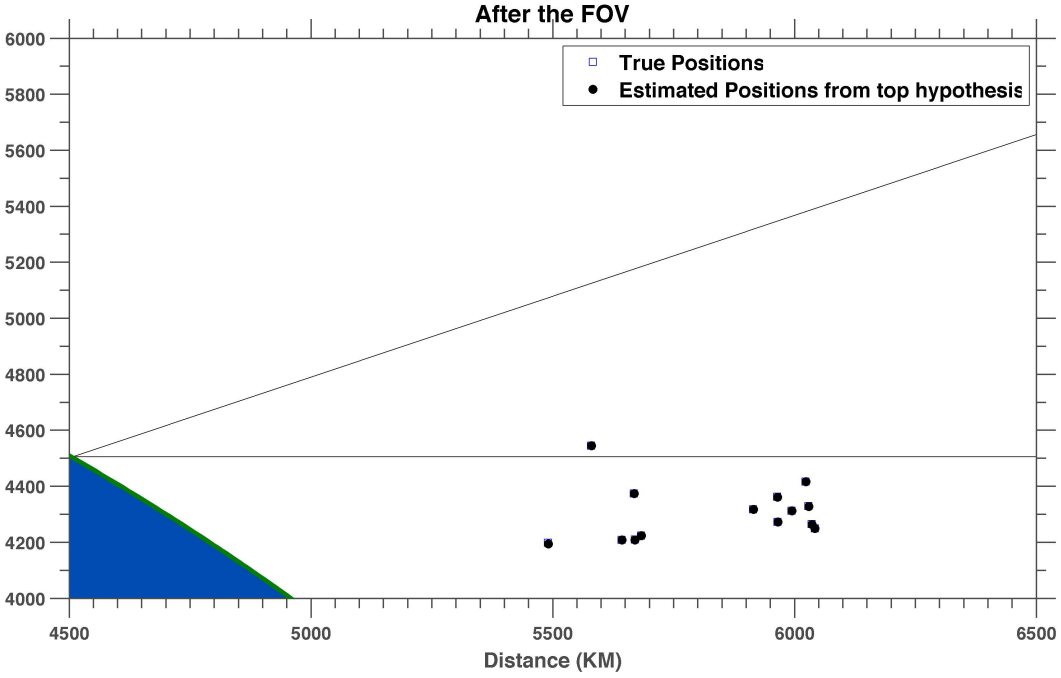


Figure 7.4: Belief after the Field of View. Reprinted with permission from [1].

ing the true total number of objects to be $221$. Multiple sensors were used to track these objects however, for this particular example; only one sensor is used to track the breakup event. The focus of the application will be on this occurrence do to the fact that the breakup event creates the scenario were the number of possible hypotheses is computationally intractable. The RSO orbits were generated using the General Mission Analysis Toolkit (GMAT) for a total simulation time of two days from the most recent epoch given in the TLE data. A Matlab script was required to read the TLE text file and convert the given orbital parameters to those required by GMAT. GMAT propagated the orbits using the RungeKutta$89$ integrator with accuracy $10E-12$ and a high-fidelity force model which included JGM-$2$ Earth potential with twenty-first degree and order. Sun, Jupiter, and lunar Point-mass gravity affect, solar radiation pressure, and atmospheric drag were also included. The random spawn scenario was generated early in the simulation by modeling an RSO breakup. The RSO breakup was simulated by randomly selecting an RSO and simulating fragments that accelerate away from the initial RSO with change in velocity sampled according to a Gaussian distribution with mean of $30$ meters per second and a unity standard deviation. The direction of the change in velocity was sampled uniformly from $[-1, 1]$ in the x, y, and z directions. GMAT's preferred measurement model provides radar range and range rate measurements. Further sensor design was done in Matlab to incorporate different measurement types including angles only models and Cartesian position models. The measurement error was ground station dependent and some assumptions were made to make incorporating multiple data types seamless. For tracking the spawn event an Electro-Optical (E-O) surveillance system located $GS_p = [4849.52 \quad -360.641653 \quad 4114.50459]$ km in the Cartesian Earth Centered Earth Fixed (ECEF) frame. The field of view (FOV) used was $5$ degrees to ensure desirable ambiguity in measurement returns. The look direction of the sensor varied to track the spawn event and did so using estimated position data propagated from the predicted orbital elements. A Gaussian measurement noise was used with values that varied dependent on the particular measurement model used. Measurements were received regardless of day or night environment and the rotation of the Earth was accounted for. No sensor biases were considered. The probability of detection was set to a high

value of $p_D = .95$ for this proof of concept simulation.

As mentioned previously, taking advantage of the derivation used in R-FISST allows for the development of the randomized sampling approach that keeps R-FISST tractable. However problems such as this, where the number of objects is in the hundreds or even thousands, can become computationally intractable do to having to generate the objects' PDF and store the values at every time step. The multi-object PDF is a joint PDF that consists of some product of the individual object PDFs. To represent an object's PDF in implementation, the first and most common way is to make an assumption that the PDF is Gaussian. This assumption is made because a Gaussian PDF can be completely characterized by its first two moments. This means that by making this assumption all the user would need at every time step is the mean and covariance of the object's PDF. However, this would be different for every object and every hypothesis making it still increasingly more burdensome as the number of objects grows. Complexity increases with the number of dimensions. One way of avoiding the Gaussian assumption is to represent the object's PDF by using an ensemble of particles. The particles can be predicted forward in time and the PDF can be reformed after prediction. This increases computational burden by the number of particle necessary to accurately represent the PDF. These numerical methods can be accurate but can cause crippling computational burden. In this R-FISST implementation, using an analytical approach to predict the objects PDF forward in time mitigates the computational burden. The analytical approach was presented by Mahajan, et. al. [72]. Also, in this R-FISST implementation the measurement data received can be of right ascension and declination or Cartesian position coordinates. The measurements received from this particular simulation were of the RSO's position in Cartesian ECI frame. Also any compatible filter could be used to update the object PDF. In this example, the Unscented Kalman Filter (UKF) is used to update the PDF. In the interest of time, in case of a birthed RSO the object is initialized using a full state measurement. The R-FISST technique is given initial hypotheses containing the orbital elements of all $212$ initial objects provided by the catalog data at the initial time of the simulation. PDFs were created for these objects using the TLE parameters as the mean and a generic covariance value adjusted for each RSO according to the epoch of last

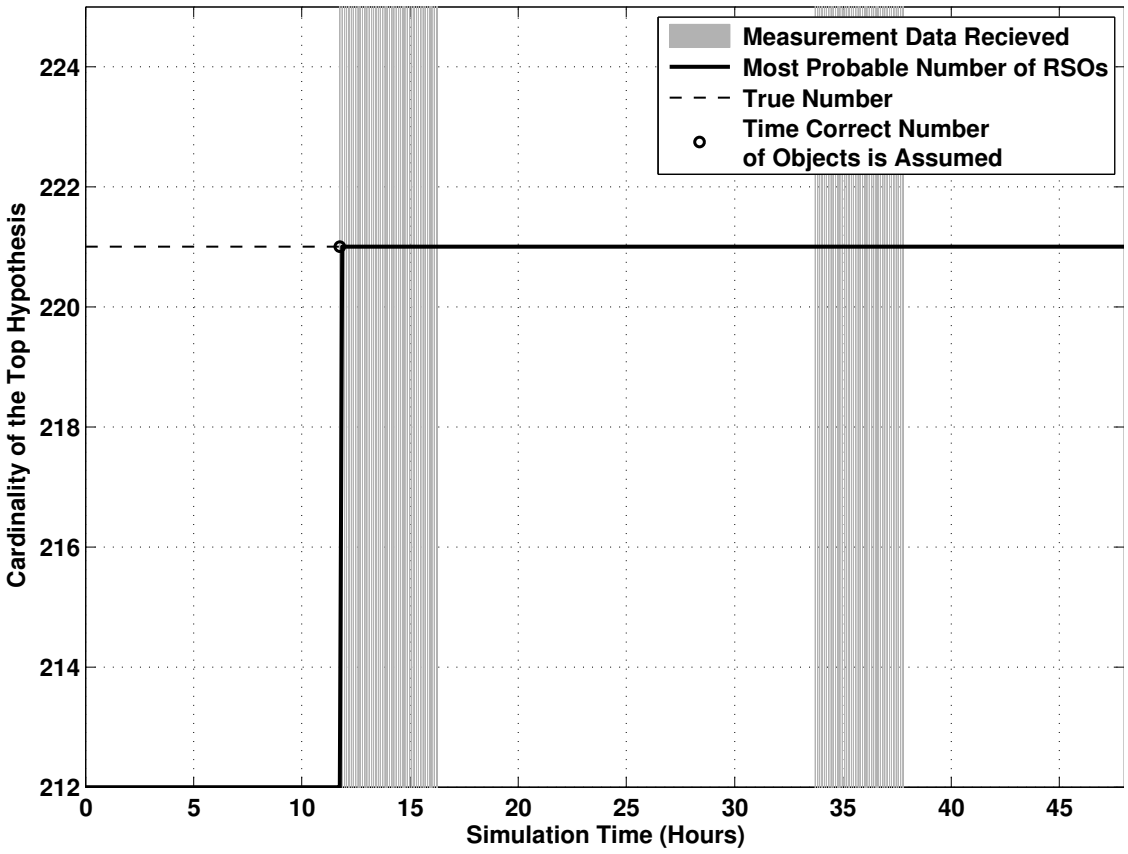


Figure 7.5: Estimated number of objects within the most probable hypothesis throughout time. Gray bars show when estimated RSOs are within the field of view and measurements are received. Reprinted with permission from [1].

entry. The overall goal is to accurately track and maintain the orbital elements of all $212$ original objects while correctly estimating the true number of objects using simulated measurement data. The false alarm rate, for this problem was assumed to be Poisson distributed with values $\lambda_C = 2$ uniformly distributed in the FOV. Birth was assumed to be a spatial binomial process with probability of birth $\alpha$. Birth and the Death probabilities $\beta = 1 - p_s$ were tuned heuristically to provide accurate representation based on the measurement returns and estimated number of objects in the field of view. To show the results of the R-FISST approach two figures are shown Figure 7.5 and 7.6. Figure 7.5, illustrates the estimated number objects within the top hypotheses throughout time.

One can see that, in the beginning of the simulation, the R-FISST technique assumed that the number of objects was still $212$. After the first, measurement is received the assumed number of

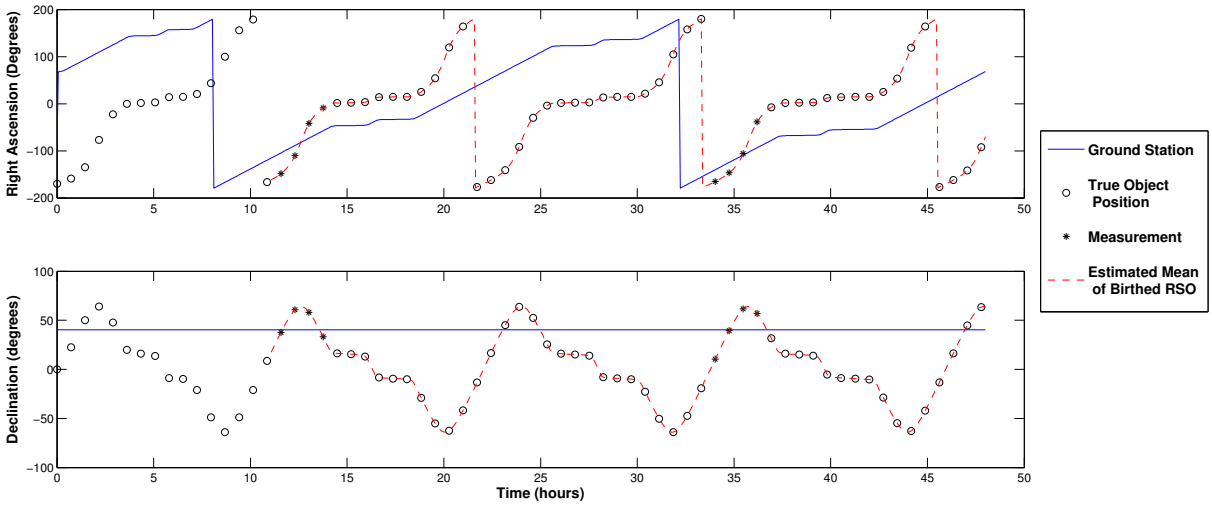


Figure 7.6: Position versus time in Cartesian ECI frame. Showing Ground Station (solid line), True Position of RSO (circle), Measurement (asterisk), and the Estimated Mean of the Birthed RSO (dotted line). Reprinted with permission from [1].

begins to change to the correct estimation of the number of object and settles to the correct estimation after a few measurement instances. This provides evidence that the number of objects is being correctly estimated by the R-FISST approach. Figure 7.6, is provided to give an idea of tracking accuracy and to show sensor returns are simulated correctly. From figure 7.6, ECI Cartesian position is given for the True Object (circles), the Ground Station (solid line), the Measurement Times (asterisk), and the estimated ECI position of the Birthed RSO (dotted line). From this plot one can see that measurements are only received when the sign of the position in every coordinate correlates between the Ground Station and the True RSO. Also note that the estimated mean data from the birthed RSO only begins after the measurements are received. After birth, the estimated mean of the RSO aligns with the true object position throughout time, suggesting two things: 1) that the measurement returns for the RSO are being correctly associated to the hypothesized birth RSO. 2) that the update for the estimated RSO is being performed correctly.

## 7.2 Increased Realism and Sensitivity To The Birth Model

In this section, a single fragmentation event is used to illustrate the influence of user defined parameters on the performance of the R-FISST technique. The goal of this section is to develop a high level understanding of how sensitive the R-FISST tracking technique is to deviations in the model parameters. The first section discusses parameters of interest and why they are the focus of this analysis. The following section discusses the simulation used to test the parameters and illustrates the results.

### 7.2.1 Model Parameters

Performance of multi-object tracking techniques deteriorate as modeled parameters deviate from the truth. Thus, it is important to understand how the R-FISST technique is affected by these deviations. The parameters that are studied in this section are part of the standard motion and measurement models presented in Chapters 3 and 4. The motion model considered includes birth and death with a non-unity probability of survival $p_s$ and the birth process as Poisson in time with average arrival rate $\lambda_B$. The measurement model includes false alarms and missed detections. False alarms are modeled as Poisson in time with arrival rate $\lambda_C$. The objects also have a non-unity probability of detection $p_D$. These four parameters are of particular importance for the simulations considered below. They also appear explicitly in the SSMCMC randomized hypothesis generation technique inherent to the R-FISST application. Parameters associated with the measurement model $\lambda_C$ and $p_D$ are well studied for most sensors and thus of less interest to the discussion below. Along with these parameters, the heuristic approaches to limiting the number of birthed objects is also investigated. Other parameters such as those associated with fragment initialization and propagation are considered well modeled due to the full state measurement initialization and the short time windows of the simulations. Sensor parameters such as measurement noise and biases are also considered well modeled. The next section discuses how parameters $\lambda_B$, $p_s$ and the selection of the birth model itself, affect the tracking performance.

### 7.2.2 Analysis Using Small Fragmentation

This section describes the affect of model parameter selection on R-FISST tracking performance. In particular, the selection of the parameters motion model, $\lambda_B$ and $p_s$.

The analysis is performed using a single simulated GEO RSO that undergoes a fragmentation event. The fragmentation was simulated as an explosion using the NASA standard breakup model (see Appendix B for details) and resulted in eleven fragments. Clutter was generated using a Poisson model with an average arrival rate of $\lambda = 1$ arrivals per scan. No other objects are detectable within the FOV. Measurements were generated using a single sensor. The sensor was operated in constant stare mode and returned observations in $30$ second intervals. Fragments remained within the FOV throughout the simulation each with a uniform probability of detection $p_D = 0.85$. Observation noise and process noise were considered to be well modeled.

In the following cases, R-FISST assumes states consisting of objects' ECI J2000 position and velocity. The R-FISST technique is initialized with the belief that one object exists with a Gaussian spatial distribution centered around the initial RSO with standard deviation in position and velocity of $10$ km and $10e-2$ km/s respectively. In each case, multiple Monte Carlo runs are performed and analyzed.

**Case 1:** Figure 7.7 shows the estimated number of objects versus the true number of objects for an hour long simulation period. The modeled parameters for false alarm rate, $\lambda_C$, and the probability of detection, $p_D$, match the true parameters. However, model choices for probability of survival $p_s = 0.05$ and birth average arrival rate $\lambda_B = 1$ do not match the true scenario. Also, within the data association matrix (see chapter 6) the number of births is limited to only the number of uncorrelated observations. In other words, observations are only associated to birth objects when the likelihood of association to any other object is a low value or zero. As a result the R-FISST methodology does not converge to the true number of objects within the simulation time. This can be attributed to two factors. The first is that a Poisson spontaneous birth model is not an accurate approximation for situations involving fragmentation events since the birth rate $\lambda_B$ can be interpreted to varying throughout time. A more accurate model would incorporate spawning as

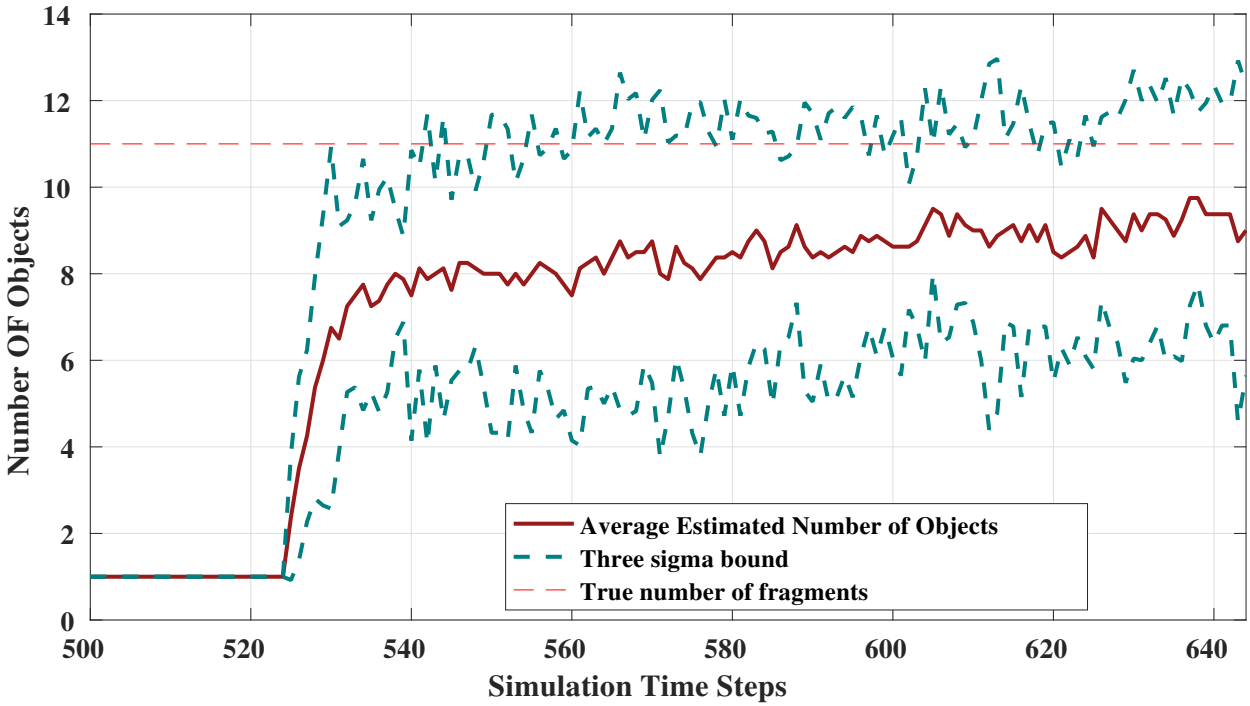


Figure 7.7: Case 1: The mean estimated number of objects for 10 Monte Carlo simulations with inaccurate model parameters. Inaccuracies in model parameters can be interpreted as delays in approximating truth.

well as spontaneous birth and death. The second factor stems from the heuristic of limiting the number of births to the number of uncorrelated measurements. In fragmentation events it is likely that the initial observations after fragmentation are all correlated. Using this heuristic actually prevents fragments from being captured and tracked.

**Remark 8.** *Even though the Poisson spontaneous birth model assumed here is not a very accurate model for tracking fragmentation events the R-FISST methodology provided enough information will converge to the true number of objects, albeit with a delay. The more significant the deviation in model parameter from truth the more significant the delay.*

**Case 2:** Figure 7.8 shows a situation with the same parameters as in figure 7.7 however, the heuristic on the number of possible births is lifted. As a result, the R-FISST algorithm is able to accurately estimate the correct number of objects within the allotted simulation time. As a measure of filter performance figures 7.9 and 7.10 show the Optimal Sub-Pattern Assignment

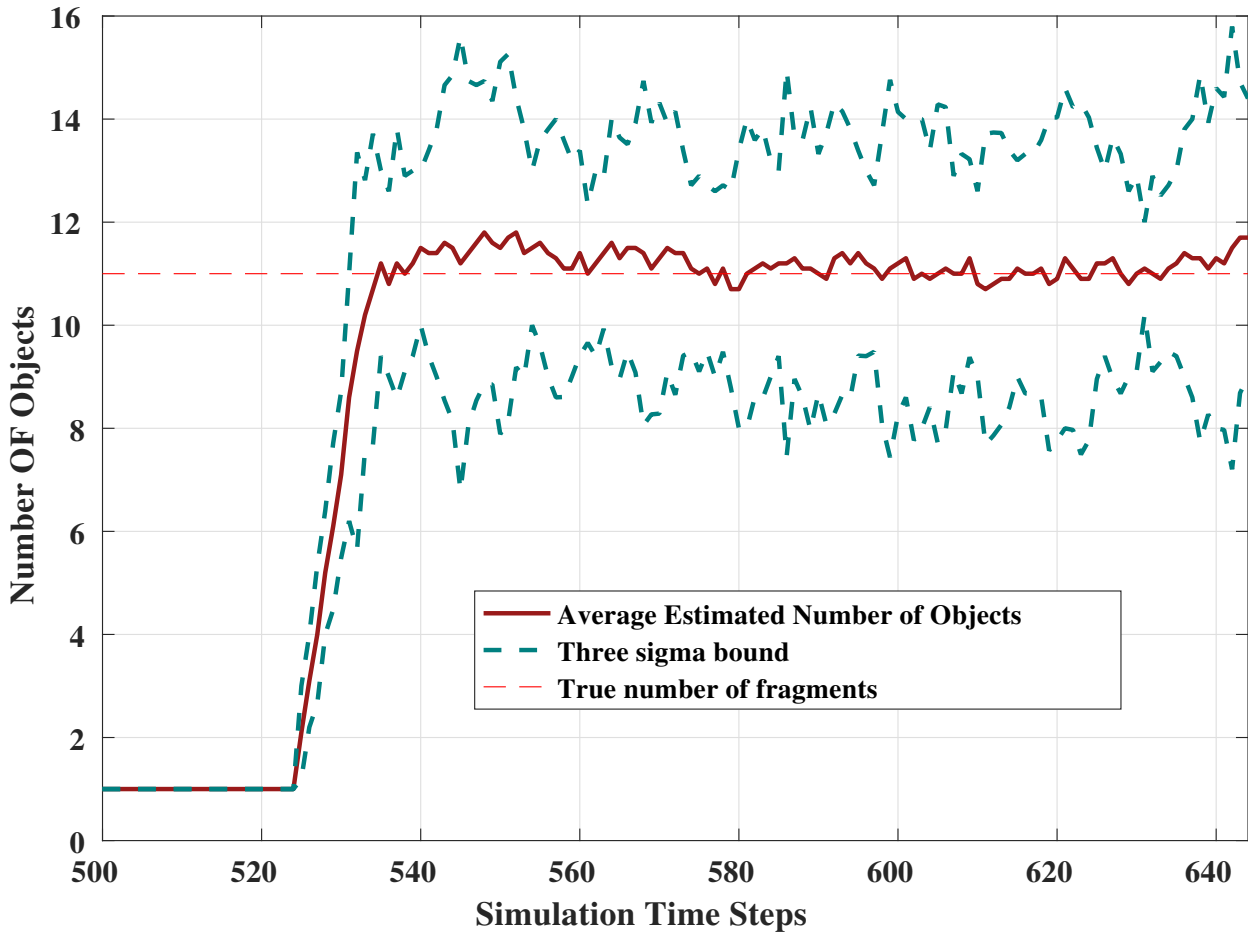


Figure 7.8: Case 2: The mean estimated number of objects for 10 Monte Carlo simulations with tuned model parameters.

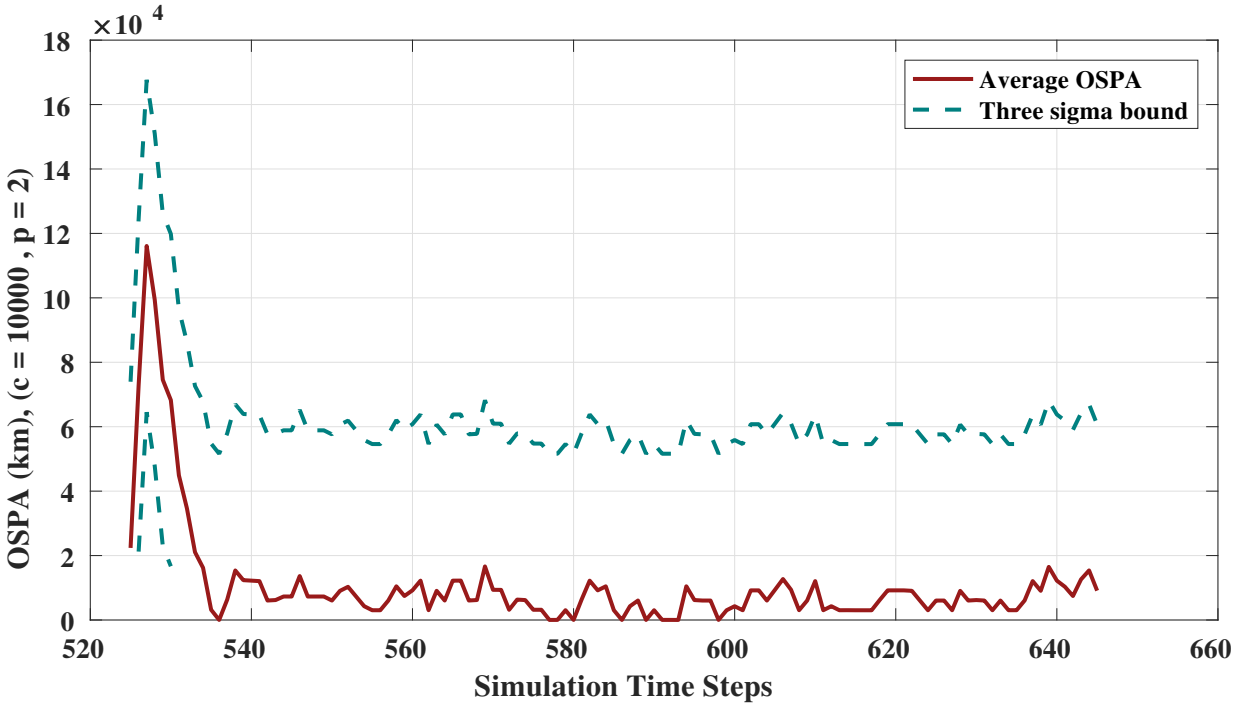


Figure 7.9: Case 2: The "per-object" average OSPA distance versus time. Cut-off value $c = 10,000$km to emphasize cardinality errors (averaged over 10 Monte Carlo simulations).

(OSPA) metrics with two separate cut-off values to emphasize cardinality errors and localization errors respectively. Refer to appendix B for more information about the OSPA metric. Figure 7.9 confirms cardinality results shown in figure 7.8 while figure 7.10 shows that, on average, fragment localization errors remain around $4$ km after the fragmentation event. Note that the specific value of $4$km is of relatively little interest since localization errors are mainly based on factors such as propagation errors, underlying continuous filter performance, and the choice of initialization method that are not directly analyzed in this example. What is of interest however is the trend of figure 7.10. Overtime the localization errors remain level, showing that the techniques accuracy is stable overtime and not diverging as associations become more ambiguous.

The delay can be further reduced, even eliminated, by incorporating fragmentation or spawn in the motion model. Figure 7.11 illustrates the use of such a model when applied to the sample RSO fragmentation event. Problem parameters include a new assumption that fragmentations are Poisson in time but average arrival rate and spatial distributions are dependent on the fragmenting

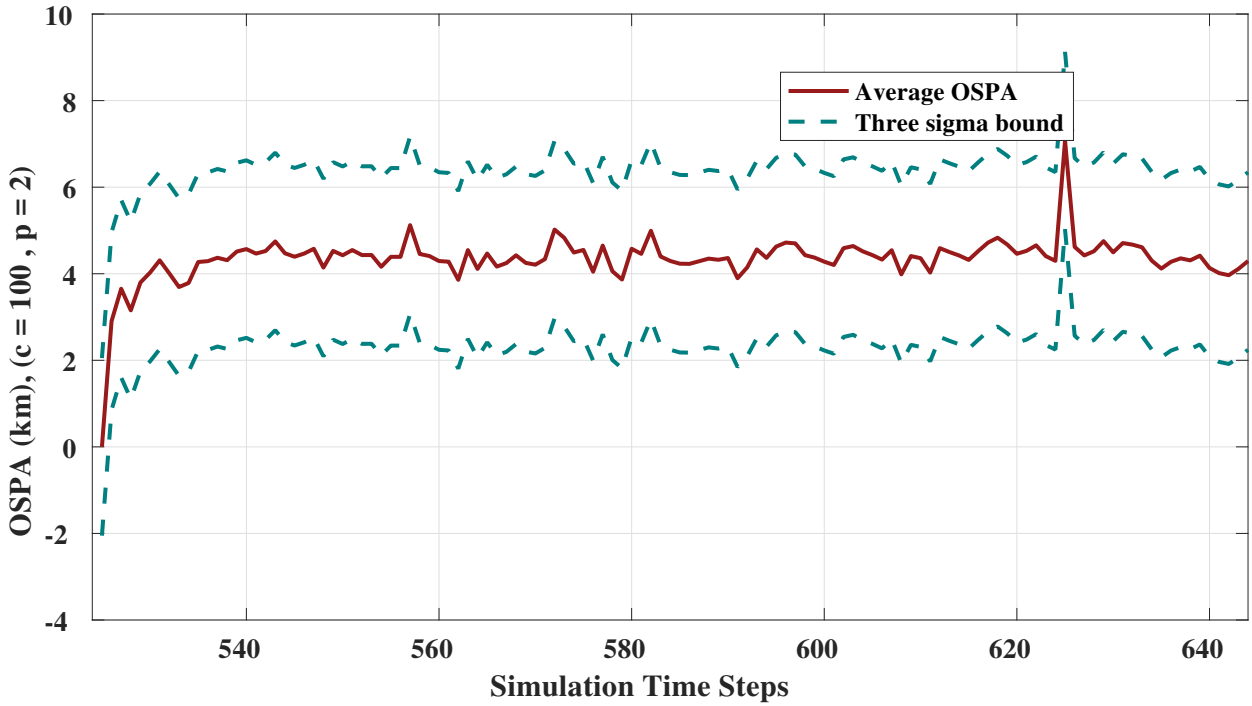


Figure 7.10: Case 2: The "per-object" average OSPA distance versus time. Cut-off value, $c = 100$ km to emphasize localization errors (averaged over 10 Monte Carlo simulations).

object state. In this case fragments were assumed to have an expected arrival rate of $\lambda(x_1) = 11$ for the initial object and $\lambda(x) = 0$ for all other objects. Results show that the estimated number of objects converges to the true number of objects more rapidly than in the other cases. This behavior is reflected in the cardinality focused OSPA metric, provided in figure 7.12, with lower OSPA distances immediately following breakup. Localization errors remain consistent with other cases and can be seen in figure 7.13.

## 7.3 Scalability

In this section, two SSA applications with increasing complexity are discussed. The first application considers a fragmentation within a high density region of objects. The second application is a simulation of Collisional Cascading (a.k.a the Kessler Syndrome). The goal of these simulations is to show that the R-FISST technique can be scaled to "worst case" scenarios that the space-object tracking industry is not fully prepared for.

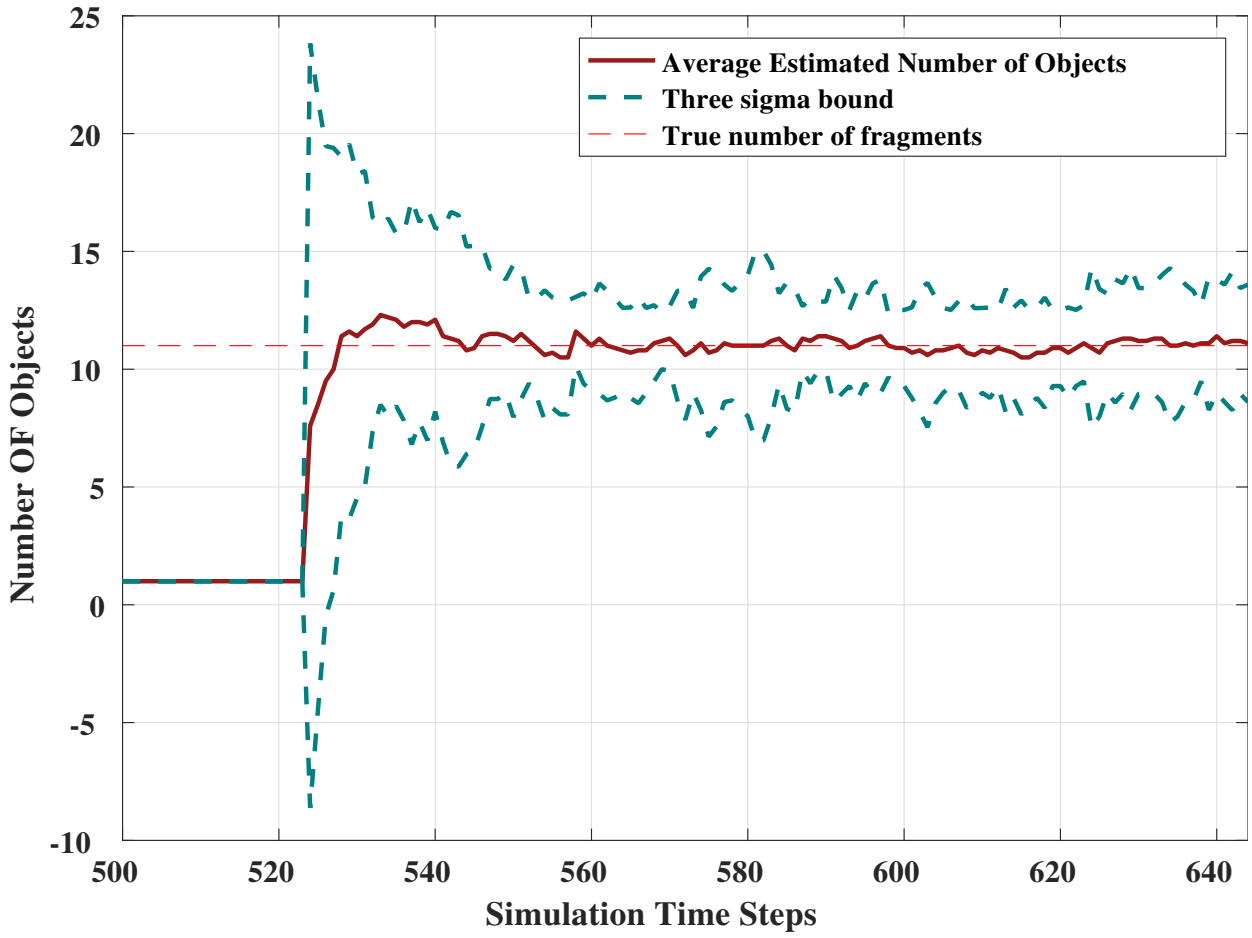


Figure 7.11: Case 3: The mean estimated number of objects throughout time averaged over values for 10 Monte Carlo runs.

### 7.3.1 Fragmentation With Background Objects

In this section, a simulation is performed to begin to scale the R-FISST technique to larger more ambiguous scenarios. This is done by adapting the previous fragmentation example to include closely spaced background objects. The simulation parameters are as follows:

- Twenty-one initial GEO RSOs.
- RSOs were closely space with closest approach distance to the nearest neighbor on the order of tens of kilometers
- During tracking, a single fragmentation event occurs resulting in 11 fragments and was sim-

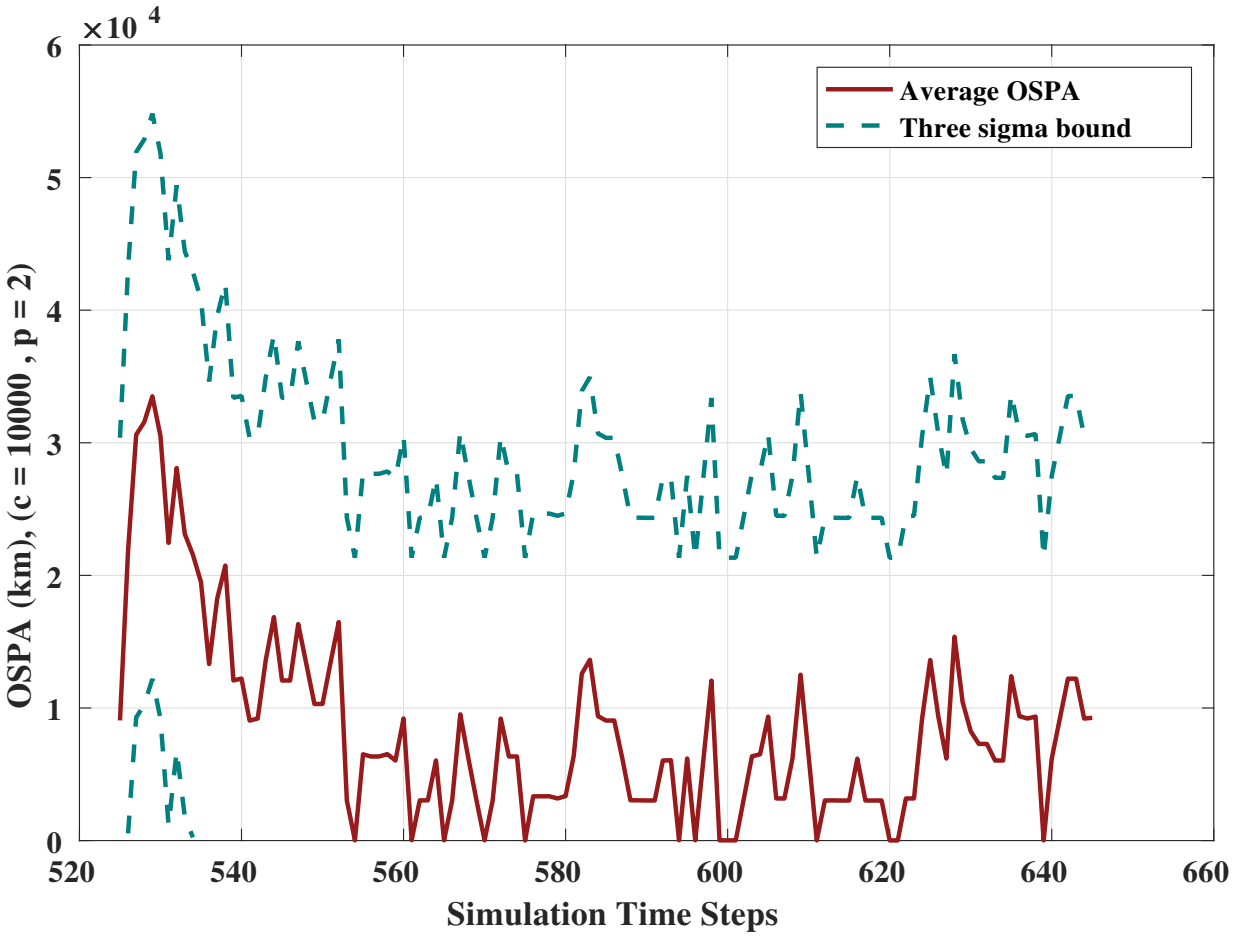


Figure 7.12: Case 3: The "per-object" average OSPA distance versus time. Cut-off value $c = 10,000$km to emphasize cardinality errors (averaged over 10 Monte Carlo simulations).

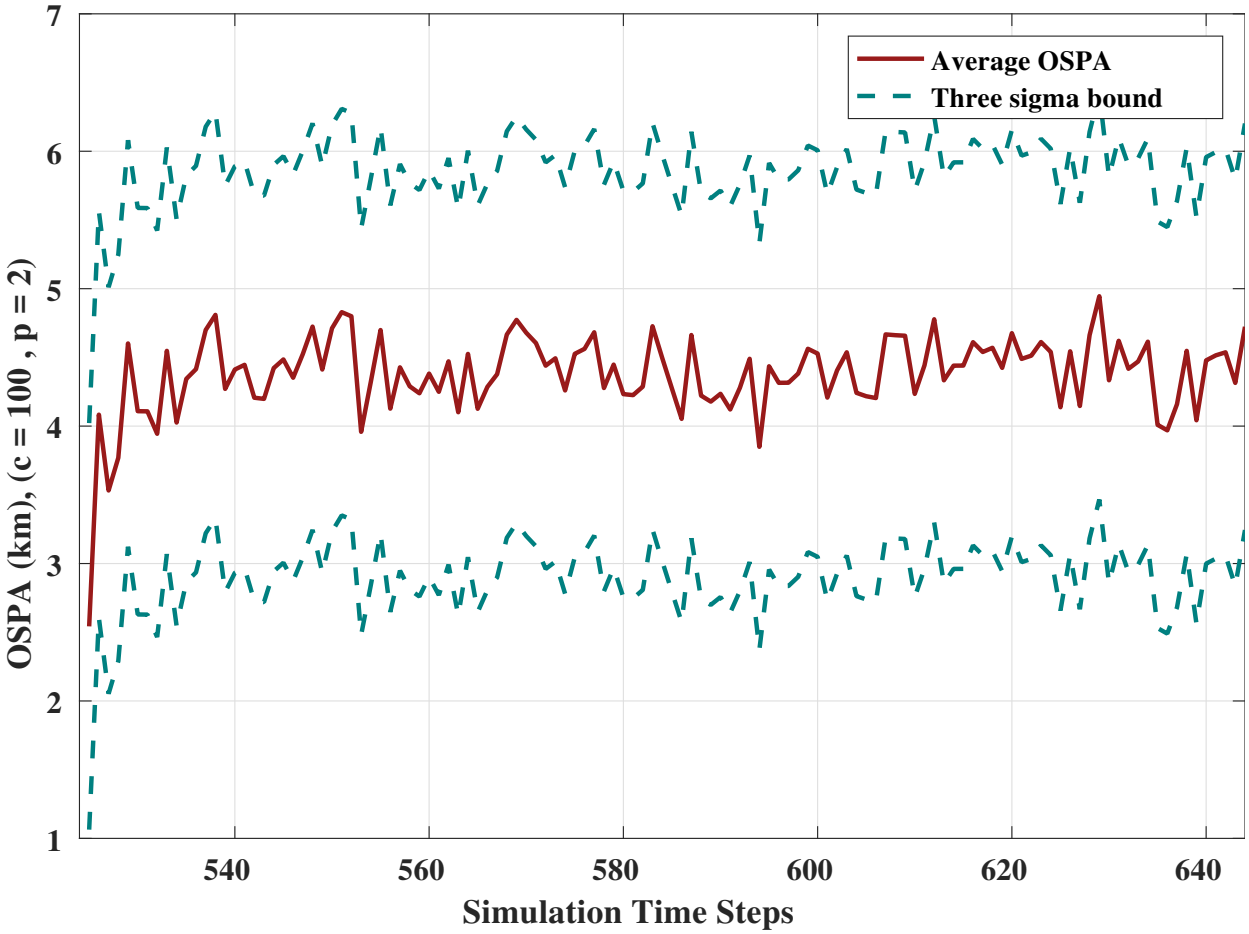


Figure 7.13: Case 3: The "per-object" average OSPA distance versus time. Cut-off value, $c = 100$ km to emphasize localization errors (averaged over 10 Monte Carlo simulations).

ulated using NASA's standard breakup model.

- Object states included object's position and velocity in J2000 ECI.
- A single sensor, located near Maui, HI, is used and assumed to have a twelve degree FOV centered at the mean position of the fragmentation event.
- Fragment PDFs are initialized assuming a full state measurement.
- Observations are received in 30 second intervals containing ECI J2000 right ascension, declination, and range information. With assumed zero-mean Gaussian noise with standard deviation of 2 arc seconds in right ascension and declination and 2 km in range.

- R-FISST is initialized with a single hypothesis with Gaussian spatial beliefs on all twenty-one objects. Each spatial distribution was initialized with mean equal to the RSO true initial state with uncertainty represented by $10$ km in position standard deviation and $0.1$ km/s standard deviation in velocity.

- the simulation is stopped after one hour's worth of measurements are received.

- Assumed model parameters $\lambda_B = 1, p_s = 0.9, \lambda_C = 1$, and $p_D = 0.85$.

- No fragmentation model was assumed in the motion model.

Including the twenty background objects increases the total number of associable objects and, in turn, increases the size of the inherent data association problem. In this example, the fragmentation occurs at time step $525$. Figure 7.14 shows the estimated number of objects versus time. The true number of objects before the fragmentation is twenty-one and after the fragmentation is thirty-one. Even with the larger inherent data association problem the R-FISST technique provides an accurate representation of the number of objects present. Most importantly it does this within an hour of event. This is important for providing timely tracking data that can prevent collisional cascading. Some other tracking techniques must wait hours for data to disambiguate before they can be applied [49]. Figure 7.15 shows the same information using a condensed box and whiskers plot at every time step.

Figure 7.16 shows the average total entropy throughout time. After breakup the entropy of the system is high due to the uncertainty in the initial birth PDF. After the first update the entropy reduces and remains low. The entropy however has a slight upward trend. This is due to the fact that as the time from breakup increases some objects escape from the field of view. The corresponding PDFs of the objects no longer being detected slowly increase in uncertainty due to process noise. For more information regarding the entropy please see Appendix B.

One of the Monte Carlo simulations was used to show how estimated tracks develop over time, Figures 7.17-7.19 show a subset of the estimated tracks plotted against the corresponding true tracks at $15$, $35$, and $60$ minutes respectively. At each segment, the currently observed objects

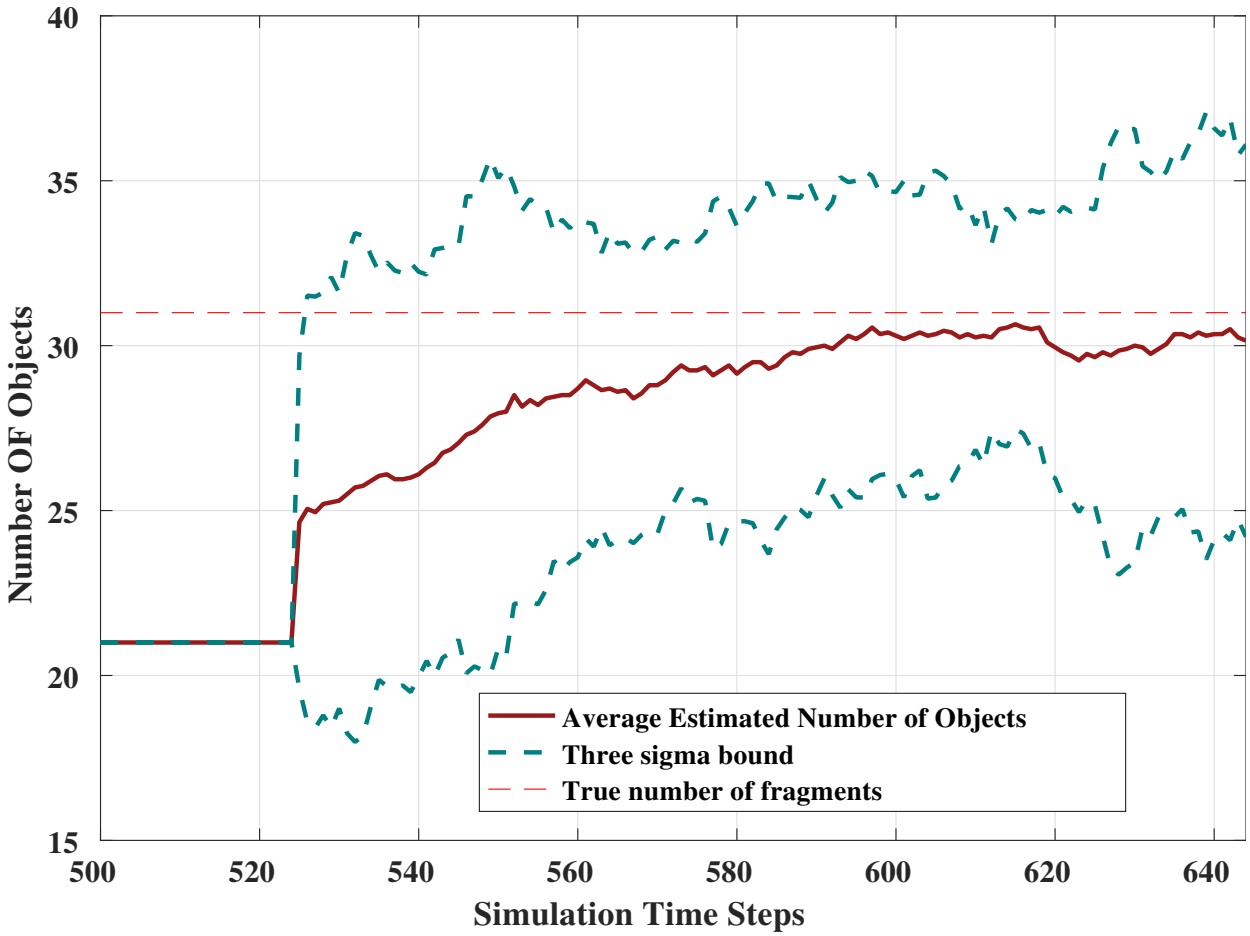


Figure 7.14: The estimated number of objects throughout time averaged over 55 Monte Carlo runs.

are shown using red diamonds. It can be seen in 7.17 that some of the true objects are yet to be estimated. As time passes, more and more of the true objects are estimated. It can be seen in figure 7.19 that objects that receive frequent measurements lie directly over their corresponding true track. However, those objects that are not updated frequently may drift away from the truth until update. These deviations can cause the localization errors seen in 7.22. Figure 7.20 shows the full set of estimated tracks and observations over the entire simulation time. In this figure true tracks are also shown, but they are completely covered by estimated tracks.

Figures 7.14-7.22 are included to show that, even with the larger problem, tracking performance remains comparable to the other cases.

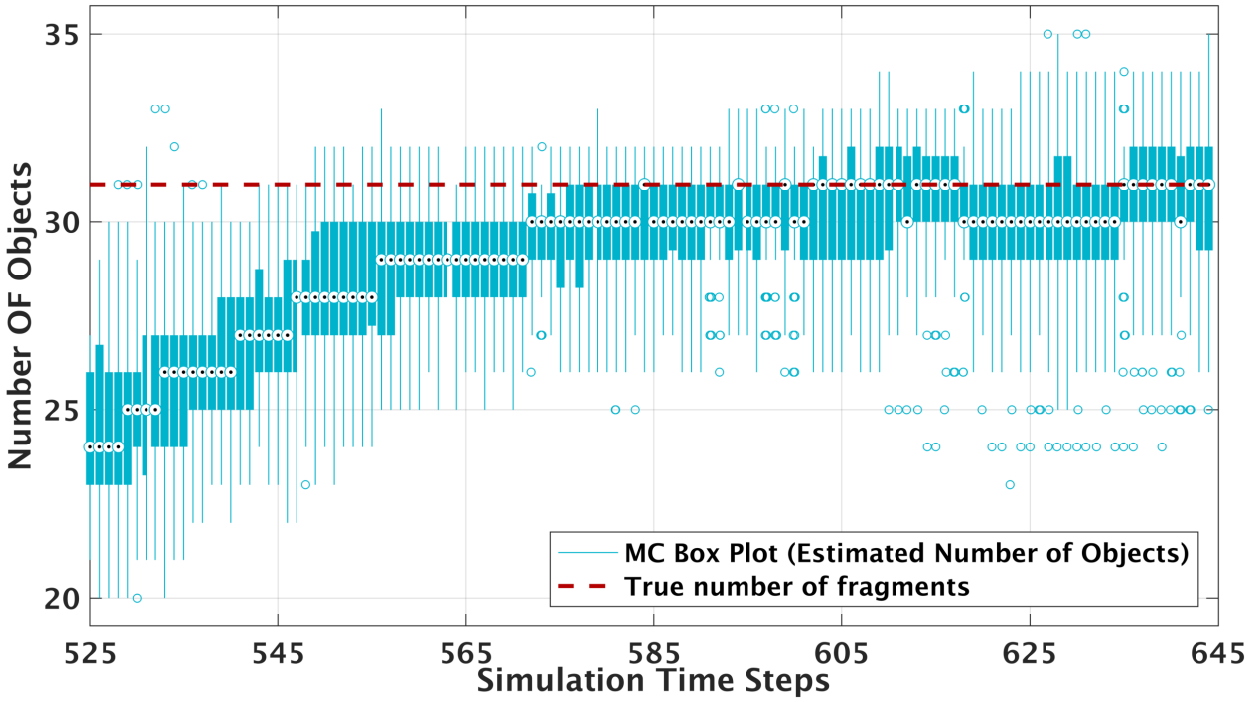


Figure 7.15: Estimated number of objects throughout the simulation using a condensed box plot at each time step for the 55 Monte Carlo runs.

### 7.3.2 Collisional Cascading

To show full scalability of the R-FISST technique an SSA example scenario was simulated of the feared Collisional Cascading event, otherwise known as the Kessler Syndrome. In this simulation, all of the current unclassified GEO objects were taken from the GEO catalog [71] and propagated to a time in the near future. Then, over a period of ten hours, ten adjacent RSOs undergo a simulated fragmentation. The simulation parameters are listed below.

- Initially the entire current GEO population was taken from the GEO public catalog. Ten fragmentations occur resulting in a new population of $952$ objects. Signifying over $100$ fragments were created from the collisional cascading.
- Objects were tracked for up to $37.33$ hours using the R-FISST technique.
- Object states included object's position and velocity in J2000 ECI.

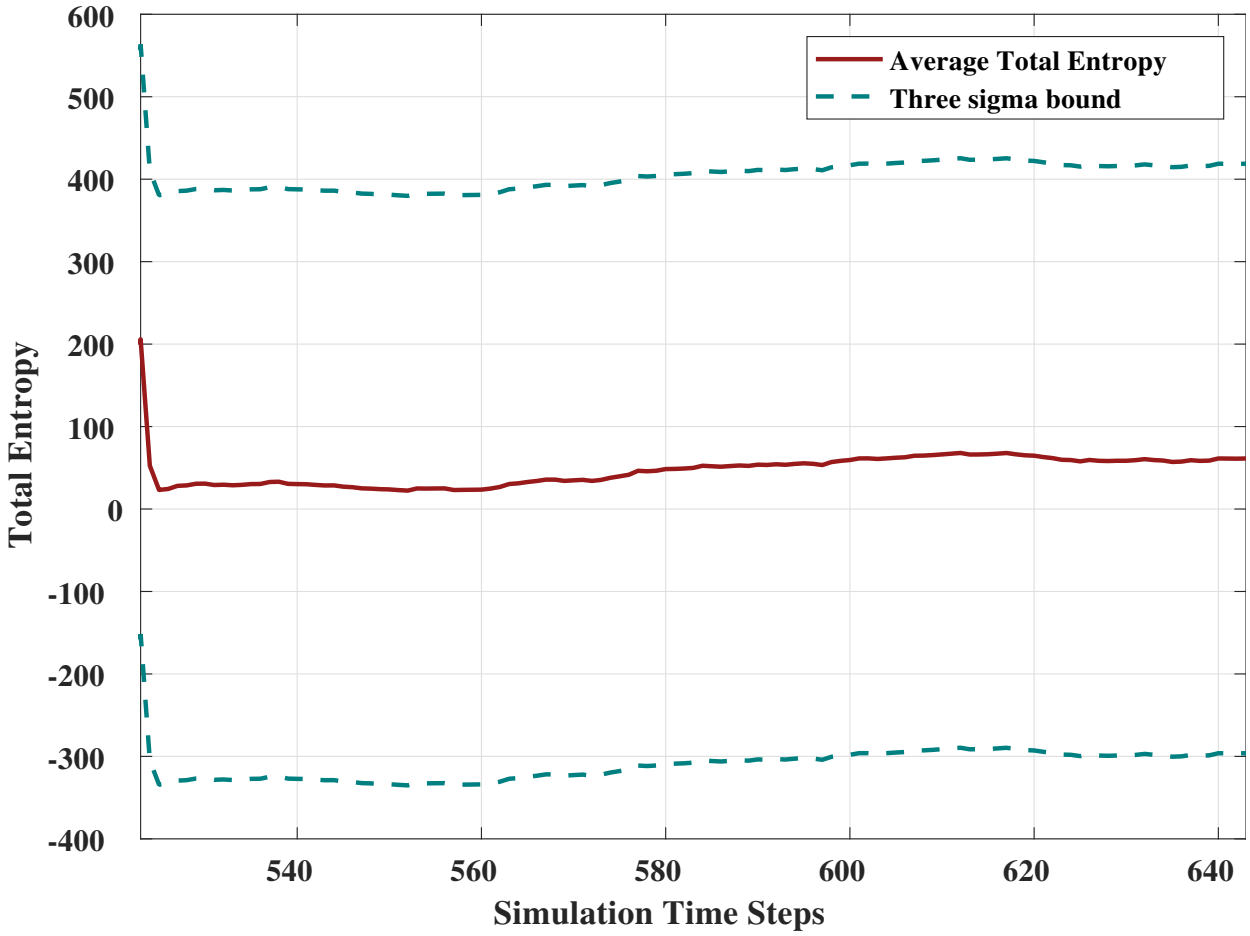


Figure 7.16: The total entropy averaged over 55 Monte Carlo runs.

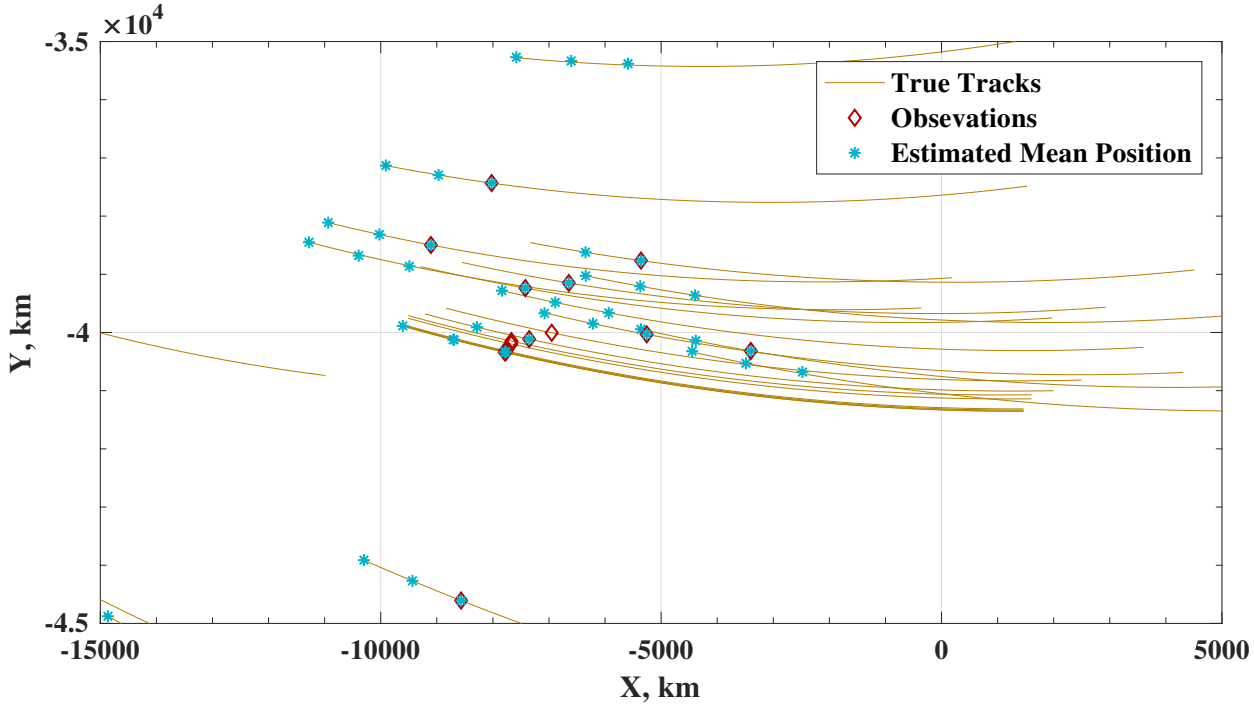


Figure 7.17: Estimated $x$,$y$ positions 15 minutes after breakup represented as blue stars. Estimated states are overlaid on top of true tracks.

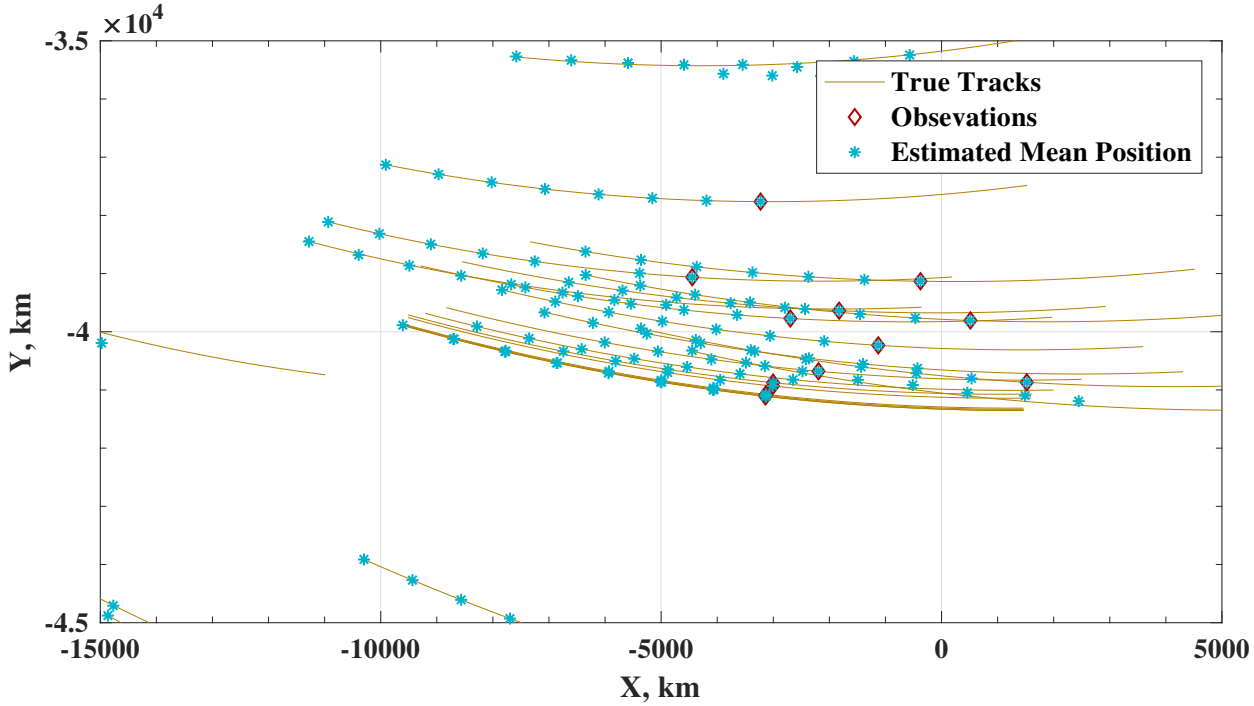


Figure 7.18: Estimated $x$,$y$ positions 35 minutes after breakup represented as blue stars. Estimated states are overlaid on top of true tracks.

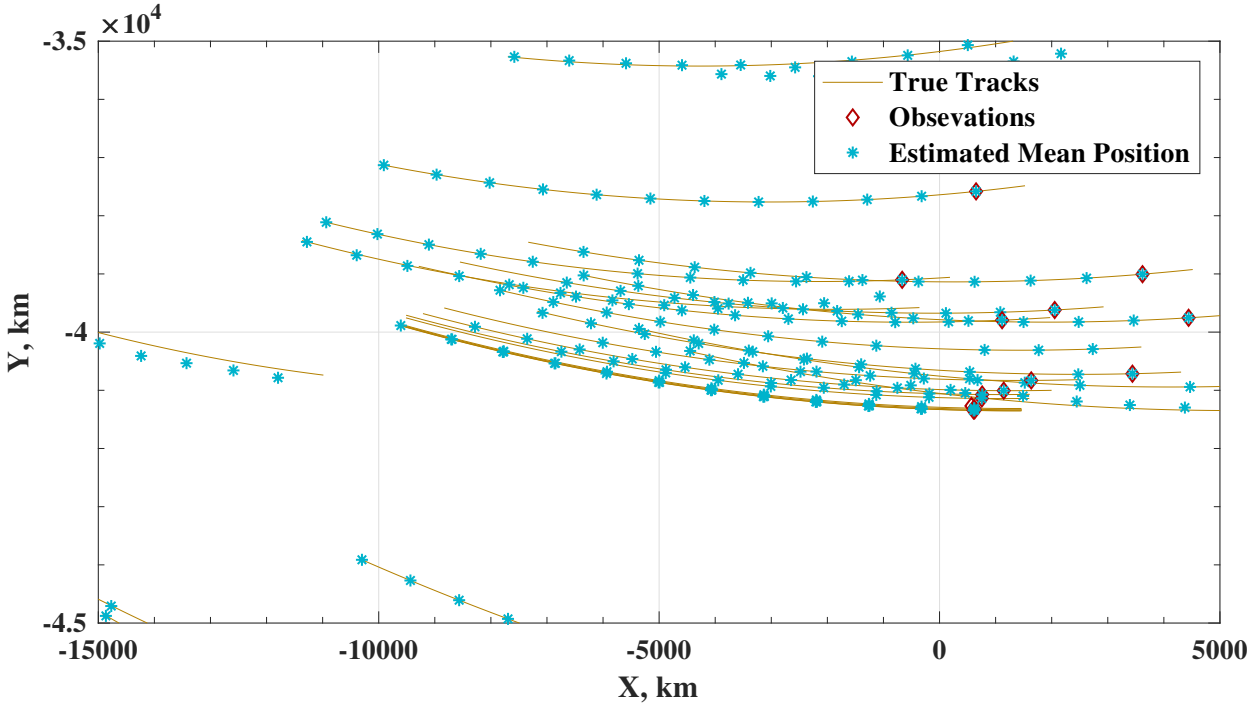


Figure 7.19: Estimated $x$,$y$ positions 1 hour minutes after breakup represented as blue stars. Estimated states are overlaid on top of true tracks.

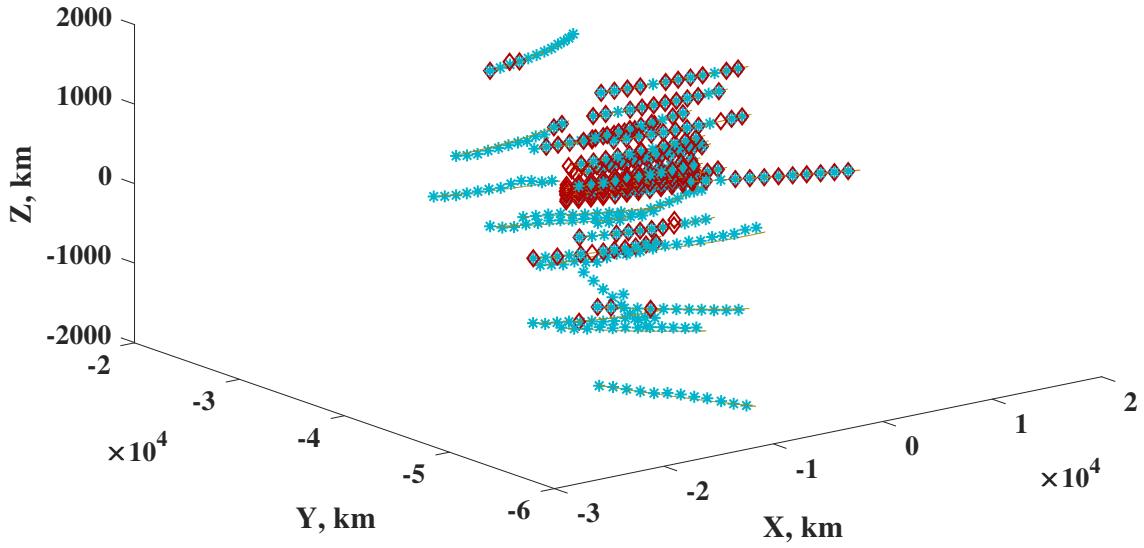


Figure 7.20: Estimated 3-space tracks (blue) and and observations (red diamond).

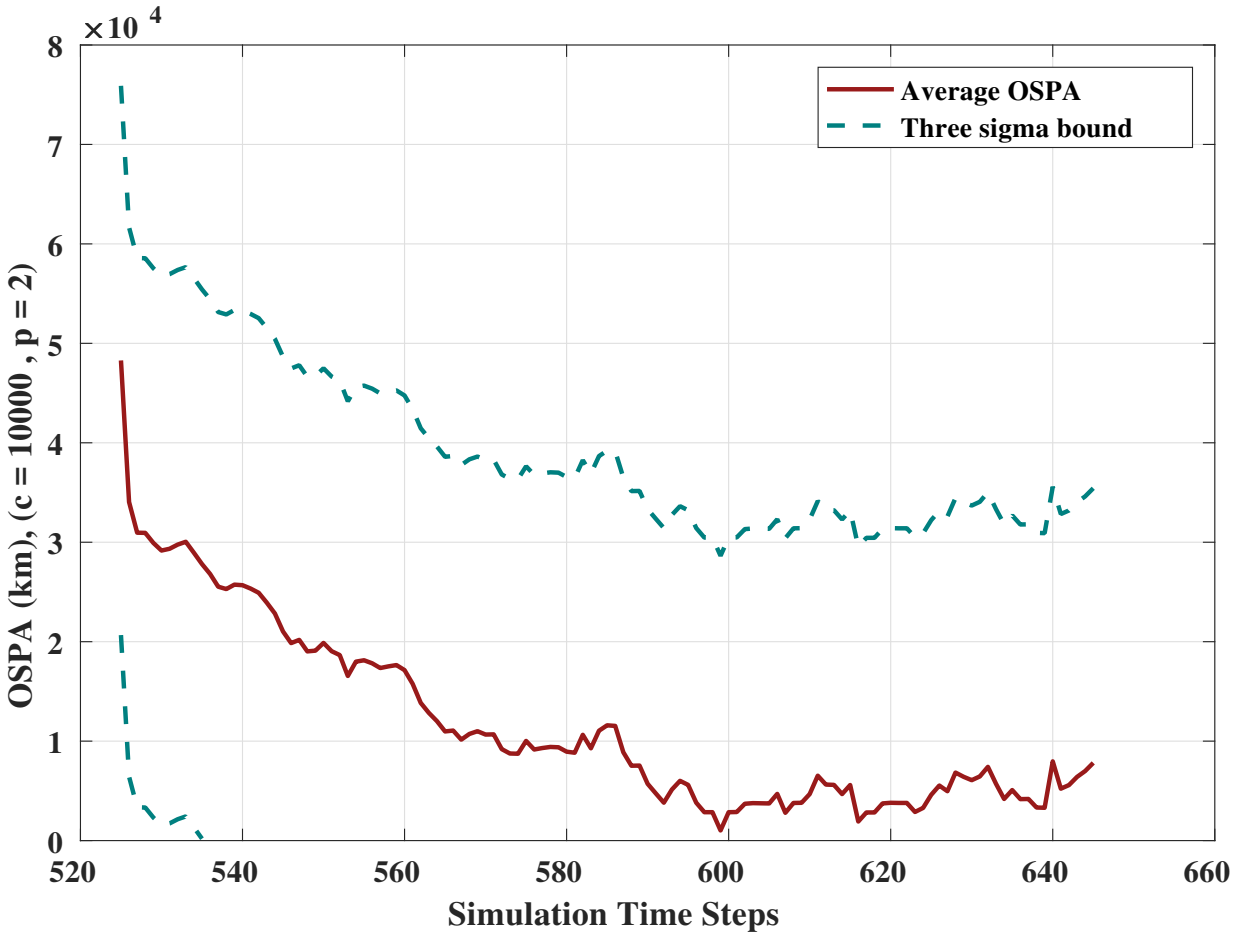


Figure 7.21: The "per-object" average OSPA distance versus time. Cut-off value, $c = 10000$ km to emphasize localization errors. (averaged over 55 Monte Carlo simulations).

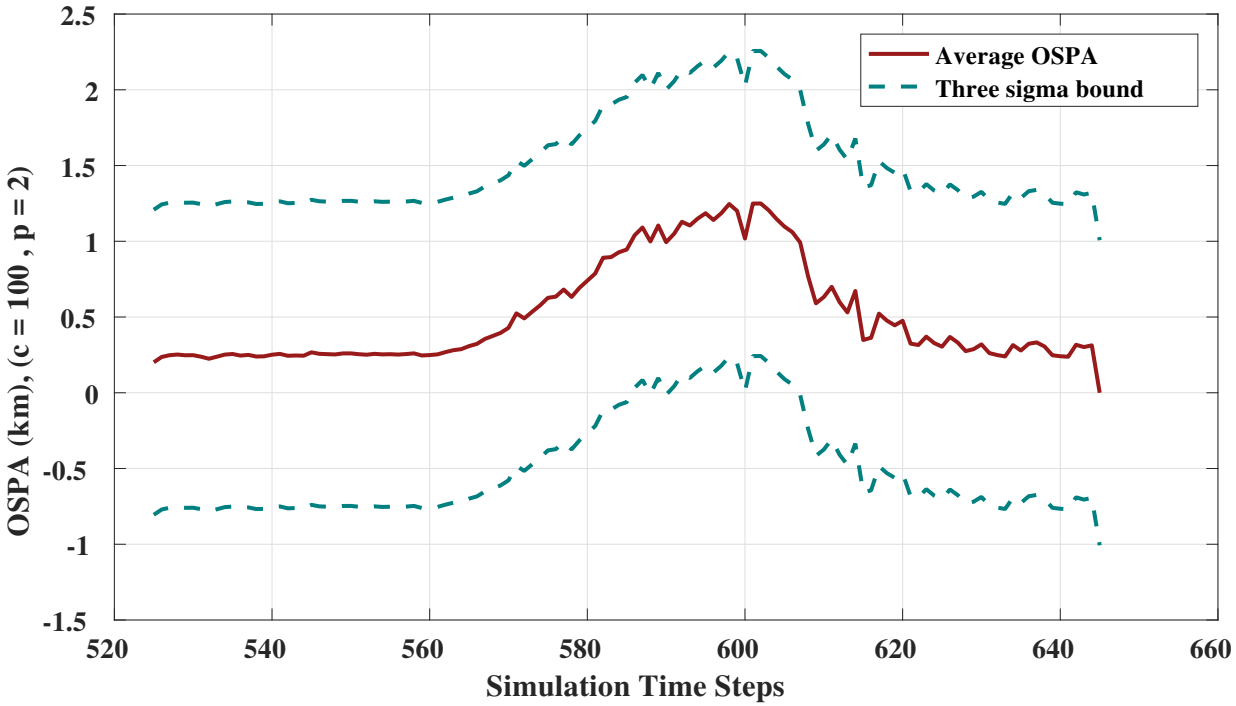


Figure 7.22: The "per-object" average OSPA distance versus time. Cut-off value, $c = 100$ km to emphasize localization errors (averaged over 55 Monte Carlo simulations).

- It is assumed that there is full coverage of the GEO population. Observations return only if proper line of sight conditions are met. Position measurements are provided with observation noise considered to be Normally distributed with standard deviation $\sigma_p = 100$m.
- Fragment PDFs are initialized assuming a full state measurement.
- Observations are received in $10$ minute intervals.
- R-FISST is initialized with a single hypothesis with Gaussian spatial beliefs on all of the initial GEO objects. Each spatial distribution initial mean equal to the RSO true initial position with $10$ km in position standard deviation and $0.1$ km/s standard deviation in velocity.
- Assumed model parameters $\lambda_B = 1, p_s = 0.9, \lambda_C = 1$, and $p_D = 0.9$.
- No fragmentation model was assumed in the motion model.

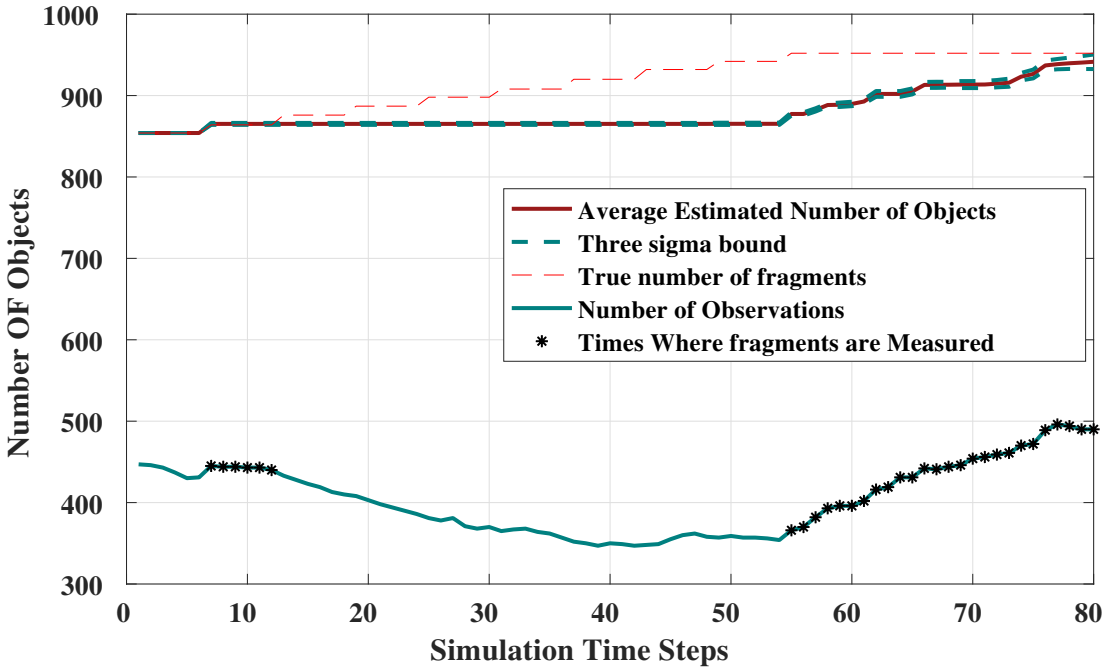


Figure 7.23: The number of estimated objects for the Collisional Cascading simulation with no missed detections or false alarms.

The goal of this simulation is to show that the R-FISST technique can maintain accurate tracking performance even in worst case scenarios like Collisional Cascading. For illustration, two cases are shown. Both cases are under the same assumptions. However, in case one, the simulated observations did not contain any missed detections or false alarms. The results for this case are shown in figures 7.23 and 7.24. In these figures, it can be seen that, as soon as measurements pertaining to the fragments are received, the estimated number of objects converges to the true number of objects. In the second case, missed detections are allowed and false alarms are received. In this case it takes much longer to converge to the true number of objects. This is illustrated in figure 7.25. Even though there is a delay all fragments are captured within 38 hours. R-FISST is capable of capturing these objects much faster than today's techniques because of it's ability to keep the problem computationally tractable.

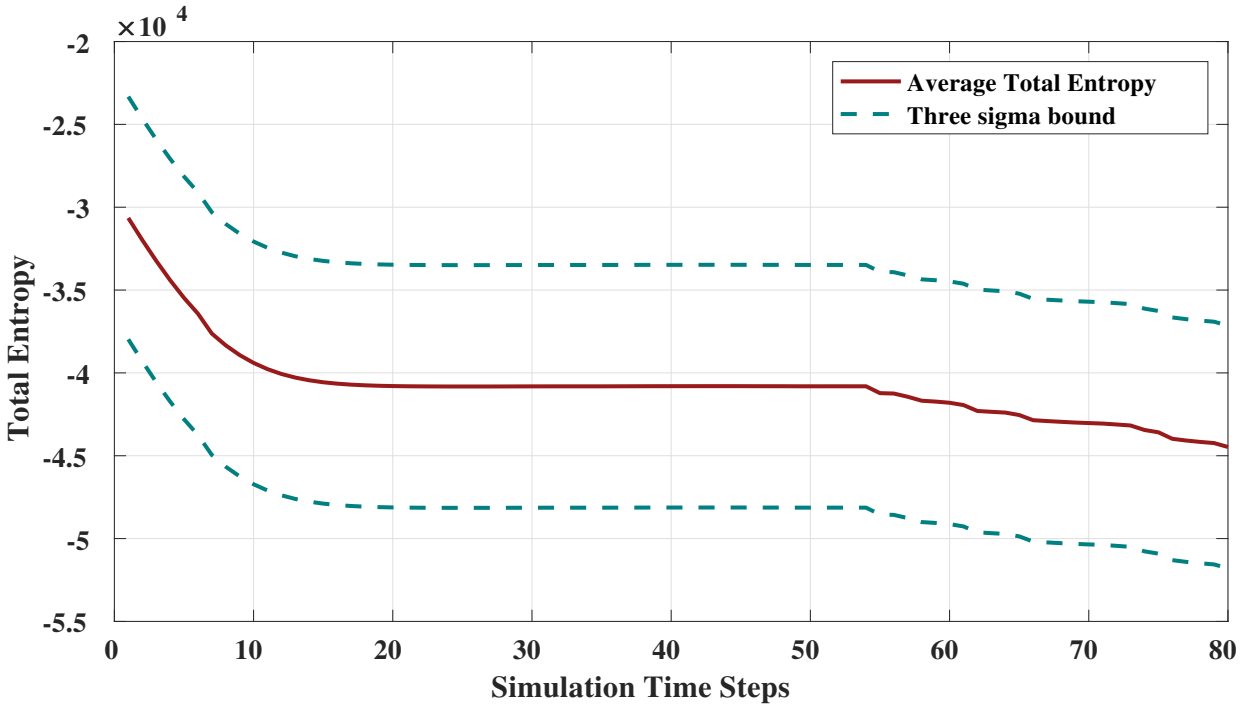


Figure 7.24: The total entropy throughout time for the Collisional Cascading simulation with no missed detections or false alarms.


Figure 7.25: The number of estimated objects for the Collisional Cascading simulation with missed detections and false alarms.

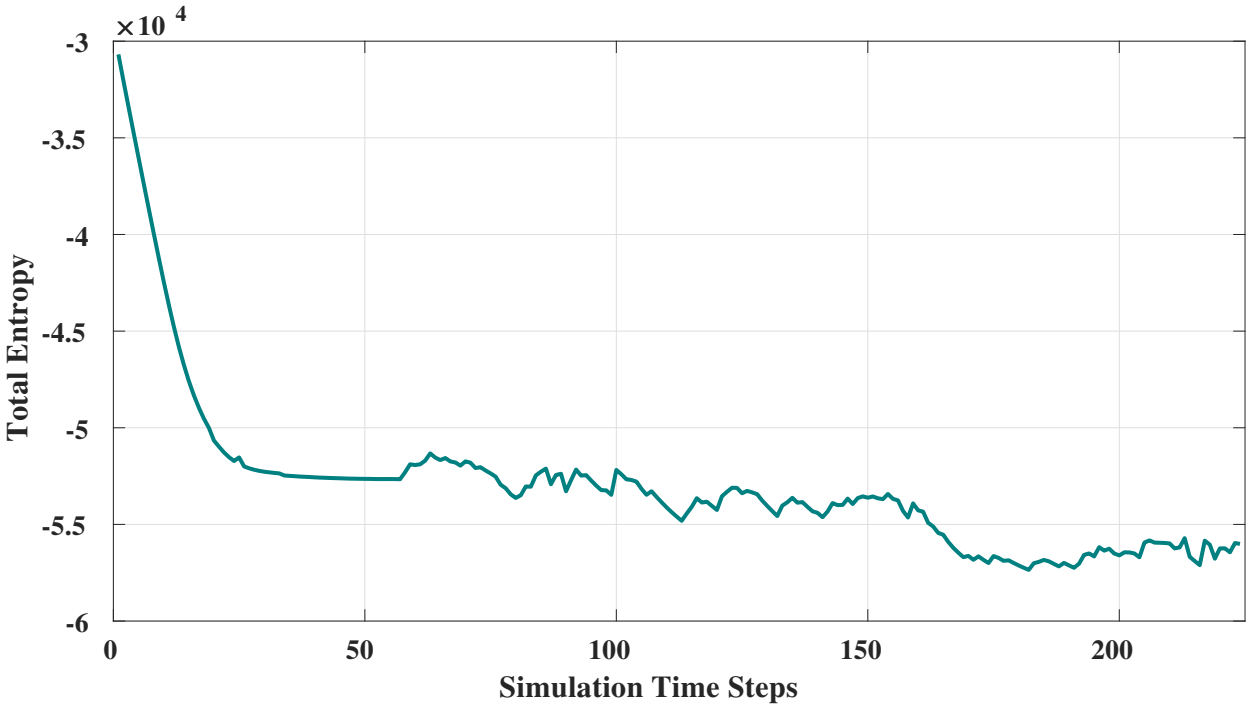


Figure 7.26: The total entropy throughout time for the Collisional Cascading simulation with missed detections and false alarms.

# 8. SUMMARY AND CONCLUSIONS

This dissertation addresses the topic of multiple object tracking as it pertains to SSA. More specifically, it answers the question of how to appropriately handle scenarios where the DAP becomes computationally intractable. The foundation of the derivation stands on three legs. The following sections describe each leg in detail.

## 8.1 The Hypothesis Representation Of The RFS Multi-Object PDF and The Relationship Between Classical and Modern Tracking Methods

To appropriately address the DAP inherent to multiple object tracking the solution must be founded off a statistically rigorous framework. Thus, a hypothesis perspective was derived from the statistically rigorous framework provided by the modern RFS based multi-object Bayes filter. In the derivation, Chapter 4, it is shown that the FISST based multi-object PDF can be represented using a hypothesis structure without loss of generality. Subsequently, a clear relationship can be drawn between the modern FISST based tracking methods and the classical Multiple Hypothesis methods such as HOMHT, as seen in Chapter 5. In summary, although the initial approaches of classical methods and modern methods are different,i.e. classical methods are in a sense more heuristic where as modern techniques are built upon clear mathematical development and statistical rigor, when viewed from the hypothesis perspective, Propositions 3 and 4. the following conclusions are drawn. Specifically, the hypothesis structure of the FISST multi-object PDF can be directly connected to HOMHT and in the case where there exist a fixed number of objects ,i.e. the motion model does not allow birth or death, the updates represent exactly the same underlying PDF and exactly the same weight. Due to it's foundation on statistical rigor, for the case where the number of objects is varying, the modern RFS based methods rightfully handle object birth as part of the prediction. This is as opposed to classical methods, such as HOMHT, that handle birth as part of the update. Thus, in this case, there are inconsistencies between the approaches. However, modulo the treatment of birth they draw the exact same conclusions. It can be shown

that, even with the inconsistencies, classical methods are a good approximation of the true update equation. It may also be argued that the classical heuristic of handling of birth in the update is actually advantages when it comes to computational cost. This is because carrying birth PDFs from prediction can be wasteful since it is logical that birth hypotheses without association to an observation are very unlikely. Carrying along predicted births that will never be hypothesized to generate an observations add zero information. In essence, the predicted birth that is not associated with a measurement is "dead weight".

## 8.2 Randomized Hypothesis Generation To Keep the DAP tractable

From the hypothesis perspective of Chapter 4, it can be seen each hypothesis have a corresponding weight. This weight is of particular interest because sampling from it ensures that one is sampling from the posterior distribution. Thus, in scenarios where the number of possible hypotheses is computationally intractable it is feasible to randomly sample a highly probable set of hypotheses without generating all possible hypotheses. In Chapter 6, standard hypothesis generation techniques are discussed along side with a newly proposed randomized hypothesis generation technique called SSMCMC. This method is used within the R-FISST technique to keep the DAP computationally tractable. SSMCMC is an MCMC based approach that creates a Markov Chain using possible hypotheses as states. It then uses a random walk to explore the chain favoring states with higher probability along the way. Once the burn in period is reached the remaining sampled states are taken as the set of highly probable hypotheses, $q*$. These hypotheses are taken to be accurate representation of $q$ and used to continue the Bayesian tracking recursions developed in Propositions 3 and 4. SSMCMC is different from other MCMC implementations because it utilizes a biased proposal distribution to help with convergence and is developed in a way that is compatible with other standard hypothesis generation techniques. 6 includes illustration on how to implement SSMCMC and a discussion on the advantages and caveats.

### 8.2.1 R-FISST: Applicability To Real World Problems

Chapter 7 and Appendix B show the application of the R-FISST technique to SSA multi-object tracking problems. These problems range from test cases that show proof of concept to examples of Collisional Cascading that shows the scalability of the technique. In all provided applications, R-FISST technique was able to keep the problem computationally and provide timely and accurate tracking date. This is of particular importance to the SSA community in order to protect assets and operations. Other tracking techniques techniques have to wait until data disambiguates before they can be applied [49], that is if it disambiguates at all. This point is reiterated through Chapter 7 where it is shown that, in highly ambiguous cases, exhaustively generating the hypotheses is intractable and GNN and heuristic gating techniques are insufficient. The R-FISST technique is particularly suited for such scenarios. The R-FISST technique has been tested and used in conjunction with many other techniques to show the applicability as realism is increased. This includes using different underlying pdf representations, different techniques for partial state initial orbit determination, and many different continuous filters for object pdf update. It has also been tested using different types of sensors with different measurement intervals as well as different dynamics models and state representations. In all cases, it has been shown to maintain accurate tracking data. However, performance is dependent on user defined parameters. In Section 7.2, a study is shown where birth parameters and models are varied. These variations have an effect on how quickly the estimated cardinality converges to the true cardinality. That being said, the more accurate that the model represents truth, the better the performance. Even when the birth models are not very accurate, the R-FISST technique will converge to true cardinality provided enough data.

### 8.2.2 Where To Next?

This dissertation has laid the foundation needed to increase current RSO tracking capabilities. There are surely many challenges and complications yet to be faced. Current efforts are in place to apply this research to real data. When considering other areas of future research, it is important to

consider the questions that were the driving force behind the current work, see Chapter 1. These questions continue to motivate the development of the research into areas that include but are not limited to the following:

- Take implementation to high performance computing platforms and GPUs.
- Expand the developments to include maneuver modeling and Interactive Multiple Model (IMM) like techniques.
- Further establish R-FISST capabilities within SSA and expanded applications to other types of multi-object tracking problems outside the realm of SSA.
- Continually incorporate new PDF representations, underlying filters, and initialization techniques as they are presented in literature.

# REFERENCES


[1] W. Faber, S. Chakravorty, and I. Hussein, "Multiple space object tracking with R-FISST," in *Proceedings of the AAS/AIAA Space Flight Mechanics Meeting Paper AAS 17-477*, (San Antonio Tx), February 5-9th 2017.

[2] W. Faber, M. Mercurio, W. Zaidi, I. Hussein, , C. W. T. Roscoe, M. P. Wilkins, and J. Paul W. Schumacher, "Application of multi-hypothesis sequential monte carlo for breakup analysis with the comparison of two probabilistic admissible region techniques," 2018. Space Flight Mechanics Meeting, AIAA SciTech Forum, Kissimmee, Florida Paper (AIAA 2018-2233).

[3] D. Reid, "An algorithm for tracking multiple targets," *IEEE Transactions on Automatic Control*, vol. 24, pp. 843–854, December 1979.

[4] Y. Bar-Shalom and X.-R. Li, *Multitarget-multisensor tracking: Principles and techniques*. Yaakov Bar-Shalom, 1995.

[5] S. S. Blackman and R. Popoli, *Design and Analysis of Modern Tracking Systems*. Norwood, MA: Artech House, 1999.

[6] T. Fortmann, Y. Bar-Shalom, and M. Scheffe, "Sonar tracking of multiple targets using joint probabilistic data association," *IEEE J. Oceanic Eng.*, pp. 173–184, 1983.

[7] A. Amditis, G. Thomaidis, P. Lytivis, and G. Karaseitandidis, "Multiple hypothesis tracking implementation," *Laser Scanner Technology*, 2012.

[8] Y. Bar-Shalom, S. S. Blackman, and R. Fitzgerald, "The dimensionless score function for measurement to track association," *IEEE Trans. Aerospace. Electronic Systems*, vol. 43, pp. 392–400, 2007.

[9] I. R. Goodman, R. P. S. Mahler, and H. T. Nguyen, *Mathematics of Data Fusion*. Kluwer Academic Publishers, 1997.

[10] R. P. Mahler, *Statistical Multisource-Multitarget Information Fusion*. Artech House, 2007.

[11] R. P. S. Mahler, "Multitarget bayes filtering via first-order multitarget moments," *IEEE Transactions on Aerospace and Electronic Systems*, vol. 39, pp. 1152–1178, Oct 2003.

[12] R. P. S. Mahler, "Phd filters of higher order in target number," *IEEE Transactions on Aerospace and Electronic Systems*, vol. 43, pp. 1523–1543, Oct 2003.

[13] B.-T. Vo, B.-N. Vo, and A. Cantoni, "The cardinality balanced multi-target multi-bernoulli filter and its implementations," *IEEE Transactions on Signal Processing*, vol. 57, pp. 409–423, February 2009.

[14] B.-T. Vo, B.-N. Vo, N. Pham, and D. Suter, "Joint detection and estimation of multiple objects from image observations," *IEEE Transactions on Signal Processing*, vol. 58, pp. 5129–5141, February 2009.

[15] S. Reutet, B.-T. Vo, B.-N. Vo, and K. Dietmayer, "Multi-object tracking using labeled multi-bernoulli random finite sets," (Salamanca, Spain), July 2014.

[16] R. P. S. Mahler, *Adnvances In Statistical Multisource-Multitarget Information Fusion*. Artec House, 20014.

[17] B. Vo *et al.*, "Sequential monte carlo methods for multi target filtering with random finite sets," *IEEE Tr. Aerosp. Electronic Systems*, vol. 4, pp. 1224–1245, 2005.

[18] H. Sidenbladh and S. Wirkander, "Tracking random sets of vehicles in terrain," in *Conference on Computer Vision and Pattern Recognition Workshop*, 2003.

[19] R. Mahler and T. Zajic, "A particle-systems implementation of the phd multitarget-tracking filter,," *Signal Processing, Sensor Fusion and Target Recognition XIII, SPIE*, vol. 5096, pp. 291–299, 2003.

[20] B. Vo and W. Ma, "The gaussian mixture probability hypothesis density filter," *IEEE Transactions On Signal Processing*, vol. 54, November 2006.

[21] I. Hussein, K. DeMars, C. Frueh, R. S. Erwin, and M. Jah, "An aegis-fisst algorithm for joint detection and tracking in space situational awareness," *AAS/AIAA Astrodynamics Specialist Conference*, August 2012.

[22] I. Hussein, K. DeMars, C. Frueh, R. S. Erwin, and M. Jah, "An aegis-fisst integrated detection and tracking approach to space situational awareness," *International Conference of Information Fusion*, July 2012.

[23] R. P. S. Mahler, "Multitarget markov motion models," *SPIE Conference on Signal Processing, Sensor Fusion, and Target Recognition*, vol. 3720, pp. 47–56, 1999.

[24] R. E. Kalman, "A new approach to linear filtering and prediction problems," *ASME Journal of Basic Engineering*, no. 82, 1960.

[25] R. E. Kalman and R. Bucy, "New results in linear filtering and prediction theory," *ASME Journal of Basic Engineering*, vol. 83, 1961.

[26] G. Smith, S. Schmidt, and L. McGee, "Application of statistical filter theory to the optimal estimation of position and velocity on board a circumlunar vehicle," Tech. Rep. NASA TR-135, NASA, Jan. 1962.

[27] S. J. Julier and J. K. Uhlmann, "A new method for the nonlinear transformation of means and covariances in nonlinear filters," *IEEE Transactions on Automatic Control*, vol. 44, pp. 477–482, March 2000.

[28] S. J. Julier and J. K. Uhlmann, "Unscented filtering and nonlinear estimation," *Proc. IEEE*, vol. 92, pp. 401–422, 2004.

[29] K. T. Alfriend and I. Park, "Covariance based track association," 2016.

[30] H. Sorenson and D. Alspach, "Recursive bayesian estimation using gaussian sums," *Automatica*, vol. 7, no. 34, p. 465âĂŞ479, 1971.

[31] D. S. N. Gordon and A. Smith, "A novel approach to nonlinear/non-gaussian bayesian state estimation," *IEEE Proceedings F, Radar and Signal Processing*, vol. 140, no. 2, pp. 107–113, 1993.

[32] H. Sorenson and D. Alspach, "Recursive bayesian estimation using gaussian sums," *Automatica*, vol. 7, no. 4, pp. 465–479, 1971.

[33] S. Arulampalam, S. Maskell, N. Gordon, and T. Clapp, "A tutorial on particle filters for online nonlinear/non-gaussian bayesian tracking," *IEEE Transactions on signal processing*, vol. 50, no. 2, pp. 174–188, 2001.

[34] G.Evensen, "Sequential data assimilation with a nonlinear quasigeostrophic model using monte carlo methods to forecast error statistics," *Journal of Geophysical Research: Oceans*, vol. 99, no. C5, pp. 10 143–10 162, 1994.

[35] G. Evensen, "Advanced data assimilation for strongly nonlinear dynamics," *Mon. weath. Rev.*, vol. 125, pp. 1342–1354, 1997.

[36] G. B. et. al., "Analysis scheme in th ensemble kalman filter," *Mon. Weath. Rev.*, vol. 126, pp. 1719–1724, 1998.

[37] G. Evensen and P. J. V. Leeuwen, "An ensemble kalman smoother for nonlinear dynamics," *Mon. Weather Rev.*, vol. 128, pp. 1852–1867, 2000.

[38] G. Evensen, "The ensemble kalman filter: theoretical formulation and practical implementation," *Ocean Dynamics*, vol. 53, pp. 343–367, 2003.

[39] D. Raihan and S. Chakravorty, "Particle gaussian mixture filterss," Tech. Rep. arXiv:1603.04510, arXiv, 2016.

[40] P. R. Escobal, *Methods of Orbit Determination*. New York, NY: John Wiley & Sons, 1965. (Reprint with corrections by Krieger Publishing Company, 1976).

[41] R. H. Gooding, "A new procedure for the solution of the classical problem of minimal orbit determination from three lines of sight," *Celestial Mechanics and Dynamical Astronomy*, vol. 66, no. 4, pp. 387–423, 1997.

[42] G. Tommei, A. Milani, and A. Rossi, "Orbit determination of space debris: Admissible regions," *Celestial Mechanics and Dynamical Astronomy*, vol. 97, pp. 289–304, 2007.

[43] A. Milani, G. F. Gronchi, M. de' Michieli Vitturi, and Z. Knežević, "Orbit determination with very short arcs: I. admissible regions," *Celestial Mechanics and Dynamical Astronomy*, vol. 90, pp. 59–87, September 2004.

[44] A. Milani and Z. Knežević, "From astrometry to celestial mechanics: Orbit determination with very short arcs," *Celestial Mechanics and Dynamical Astronomy*, vol. 92, no. 1–3, pp. 1–18, 2005.

[45] G. Tommei, A. Milani, D. Farnocchia, and A. Rossi, "Correlation of space debris observations by the virtual debris algorithm," in *Proceedings of the 5th European Conference on Space Debris*, (European Space Operations Center, Darmstadt, Germany), March 30–April 2 2009.

[46] A. Milani, G. Tommei, D. Farnocchia, A. Rossi, T. Schildknecht, and R. Jehn, "Correlation and orbit determination of space objects based on sparse optical data," *Monthly Notices of the Royal Astronomical Society*, vol. 417, no. 3, pp. 2094–2103, 2011.

[47] K. J. DeMars, M. K.Jah, and P. W. Schumacher, "Initial orbit determination using short-arc angle and angle rate data," *IEEE Transactions on Aerospace and Electronic Systems*, vol. 48, pp. 2628–2637, July 2012.

[48] K. J. DeMars and M. K. Jah, "Probabilistic initial orbit determination using gaussian mixture models," *Journal of Guidance, Control, and Dynamics*, vol. 36, no. 5, pp. 1324–1335, 2013.

[49] T. Kelecy, M. Shoemaker, and M. Jah, "Application of the constrained admissible region multiple hypothesis filter to initial orbit determination of a break-up," *Proceedings of the 6th European Conference on Space Debris Darmstadt, Germnay*, 08/2013.

[50] C. W. T. Roscoe, I. I. Hussein, M. P. Wilkins, and P. W. Schumacher, Jr., "The probabilistic admissible region with additional constraints," *Advances in the Astronautical Sciences*, vol. 156, pp. 117–130, 2015. (Proceedings of the AAS/AIAA Astrodynamics Specialist Conference, Vail, CO, August 9–13 2015, Paper AAS 15-577).

[51] I. I. Hussein, C. W. T. Roscoe, P. W. Schumacher, Jr., and M. P. Wilkins, "Probabilistic admissible region for short-arc angles-only observation," in *Proceedings of the Advanced Maui Optical and Space Surveillance Technologies Conference*, (Wailea, HI), September 9–12 2014.

[52] I. I. Hussein, C. W. T. Roscoe, P. W. Schumacher, Jr., and M. P. Wilkins, "Probabilistic admissibility in angles-only initial orbit determination," in *Proceedings of the 24th International Symposium on Space Flight Dynamics*, (Laurel, HI), May 5âĂŞ9 2014.

[53] Y. Bar-Shalom and T. Fortmann, *Tracking and Data Association*. New York: Academic Press, 1988.

[54] K. G. Murty, "An algorithm for ranking all assignments in order of increasing cost," *Operations Research*, vol. 16, no. 3, pp. 682–687, 1968.

[55] S. Oh, S. Russell, and S. Sastry, "Markov chain monte carlo data association for mutli-target tracking," *IEEE Transactions on Automatic Control*, vol. 54, no. 3, pp. 481–497, 2009.

[56] G. M. Yu and I. Cohen, "Multiple target tracking using spatio-temporal markov chain monte carlo data association," *In Proc. IEEE Int. Conf. on Computer Vision and Pattern Recognition*, pp. 1–8, 2007.

[57] W. Faber, S. Chakravorty, and I. Hussein, "A randomized sampling based approach to multi-object tracking with comparison to HOMHT," *Advances in the Astronautical Sciences*, vol. 156, 2015. (Proceedings of the AAS/AIAA Astrodynamics Specialist Conference, Vail, CO, August 9–13 2015, Paper AAS 15-745).

[58] W. Faber, S. Chakravorty, and I. Hussein, "R-FISST and the data association problem with applications to space situational awareness," in *Proceedings of the AIAA/AAS Astrodynamics Specialist Conference*, (Long Beach, CA), September 13-16 2016.

[59] W. Faber, S. Chakravorty, and I. Hussein, "A randomized sampling based approach to multi-object tracking," in *Proceedings of the 18th International Conference on Information Fusion*, (Piscataway, NJ), pp. 1307–1314, IEEE, 2015.

[60] W. Faber, W. Zaidi, I. Hussein, , C. W. T. Roscoe, M. P. Wilkins, and J. Paul W. Schumacher, "Application of multi-hypothesis sequential monte carlo for breakup analysis," 2017. (Proceedings of the AAS/AIAA Astrodynamics Specialist Conference, Stevenson, WA, Paper AAS 17-579).

[61] W. Faber, W. Zaidi, I. Hussein, , C. W. T. Roscoe, M. P. Wilkins, and J. Paul W. Schumacher, "Application of multi-hypothesis sequential monte carlo for breakup analysis," 2017. Proceedings of the Advanced Maui Optical and Space Surveillance Technologies Conference, Wailea, HI.

[62] R. P. S. Mahler, *Statistical Multisource-Multitarget Information Fusion*. Artec House, 2007.

[63] R. P. S. Mahler, "Measurement-to-track association and finite-set statistics," *Arxiv*, Jan 2017.

[64] J. Munkres, "Algorithms for the assignment and transportation problems," *Journal of the Society for Industrial and Applied Mathematics*, vol. 5, p. 32âĂŞ38, March 1957.

[65] H. W. Kuhn, "Variants of the hungarian method for assignment problems," *Naval Research Logistics Quarterly*, vol. 3, p. 253âĂŞ258, 1956.

[66] P. Bickel, B. Li, and T. Bengtsson, "The markov chain monte carlo method: an approach to approximate counting and integration," in *IMS Collections:Pushing the Limits of Contemporary Statistics: Contributions in Honor of Jayanta K Ghosh*, vol. 3, pp. 318–329, 2008.

[67] D. Kessler, "The kessler syndrome (as discussed by donald j. kessler),"

[68] N. L. Johnson, E. Stansbery, D. O. Whitlock, K. J. Abercromby, and D. Shoots, "History of on-orbit satellite fragmentations," *Advances in the Astronautical Sciences*, vol. 14th Edition, 2008. NASA's Orbital Debris Program Office.

[69] C. Henry, "Exoanalytic video shows telkom-1 satellite erupting debris," *SpaceNews*, 2017.

[70] N. L. Johnson, P. H. Krisko, J.-C. Lieu, and P. D. Am-Meador, "NASAâĂŹs new breakup model of evolve 4.0," *Adv. Space Res.*, vol. Vol. 28, No. 9, 2001. pp. 1377-1384.

[71] "Meo and leo rso catalogue https://www.space-track.org/." Web, 2017.

[72] B. Mahajan, S. R. Vadali, and K. T. Alfriend., "Analytic solution for satellite relactive motion: The complete zonal gravitational problem," *Advances in the Astronautical Sciences Spaceflight Mechanics*, vol. 158, 2016.

[73] D. Schuhmacher, B.-T. Vo, and B.-N. Vo, "A consistent metric for performance evaluation of multi-object filters," *IEEE Transactions On Signal Processing*, vol. 56 (8), pp. 3447–3457, 2008.

APPENDIX A

PROOF OF PROPOSITIONS

## A.1 Proof of Proposition 3

The proof of proposition 3 is provided below.

*Proof.* Let the FISST predicted multi-object pdf be given by:

$$P(X,n) = \sum_{q^{(n)}} \omega_{q^{(n)}} p^{q^{(n)}}(X). \tag{A.1}$$

The multi-object PDF in FISST is written as follows owing to the permutation of the arguments under the set representation:

$$p^{q^{(n)}}(X) = \sum_{\nu} \prod_{i} p^{q^{(n)},\nu_i}(x_i), \tag{A.2}$$

where the $\nu$ are all possible permutations of the indices $\{1, 2, \cdots n\}$, and $p^{q^{(n)},i}(.)$ represents the $i^{th}$ component of the product in the multi-object PDF. The FISST Bayesian update for the PDF given the measurement set $Z$ is:

$$p(X,n|Z) = \frac{p(Z|X,n) \sum_{q^{(n)}} \omega_{q^{(n)}} p^{q^{(n)}}(X)}{\sum_k \frac{1}{k!} \int p(Z/X,k) \sum_{r^{(k)}} \omega_{r^{(k)}} p^{r^{(k)}}(X')dX'}, \tag{A.3}$$

where the $k!$ factor is due to the interpretation of the denominator as a set integral. In the above expression, let us concentrate on the term:

$$T_{q^{(n)}}(X) = p(Z|x,n)\omega_{q^{(n)}} p^{q^{(n)}}(X)$$

$$= \omega_{q^{(n)}} \sum_{\sigma^{(n)}} p(\sigma^{(n)}|n) \sum_{\nu} p(Z|\sigma^{(n)}, X, n) \prod_{i} p^{q^{(n)},\nu_i}(x_i), \tag{A.4}$$

where $\sigma^{(n)}$ represents any $n$-object data associations possible given the measurement $Z$. It may be

seen that:

$$p(X,n|Z) = \frac{\sum_{q^{(n)}} T_{q^{(n)}}(X)}{\sum_k \frac{1}{k!} \sum_{r^{(k)}} \int T_{r^{(k)}}(X) dX}. \tag{A.5}$$

Let

$$\eta_{q^{(n)}} \equiv \frac{1}{n!} \int T_{q^{(n)}}(X) dX. \tag{A.6}$$

Let $\sigma^{(n)}$ be a particular data association that assigns exactly $k$ of the measurements to clutter, then:

$$p(Z|\sigma^{(n)}, X, n) = \frac{k!}{V^k} \prod_i p(z_{\sigma_i^{(n)}}|x_i). \tag{A.7}$$

Then given any other data association $\bar{\sigma^{(n)}}$ that assigns exactly $k$ measurements to clutter and a permutation $\nu'$, there always exists a unique k-clutter data association $\sigma^{(n)}$ and an associated permutation $\nu$ such that:

$$\prod_i p(z_{\bar{\sigma_i^{(n)}}}|x_i) p^{q^{(n)},\nu'_i}(x_i) = \prod_i p(z_{\sigma_i^{(n)}}|x_{\nu_i}) p^{q^{(n)},i}(x_{\nu_i}). \tag{A.8}$$

Therefore, using A.7, A.8 and A.4 in A.6:

$$\eta_{q^{(n)}} = \frac{1}{n!} \omega_{q^{(n)}} \sum_{\bar{\sigma^{(n)}}} p(\bar{\sigma^{(n)}}|n) \sum_{\nu'} \frac{k!}{V^k} \prod_i \int p(z_{\bar{\sigma_i^{(n)}}}|x_i) p^{q^{(n)},\nu'_i}(x_i) dx_i$$

$$= \frac{1}{n!} \omega_{q^{(n)}} \sum_{\sigma^{(n)}} p(\sigma^{(n)}|n) \sum_{\nu} \underbrace{\frac{k!}{V^k} \prod_i \int p(z_{\sigma_i^{(n)}}|x_{\nu_i}) p^{q^{(n)},i}(x_{\nu_i}) dx_{\nu_i}}_{= l_{q^{(n)}\sigma^{(n)}} \, \forall \, \nu}$$

$$= \sum_{\sigma^{(n)}} \omega_{q^{(n)}} p(\sigma^{(n)}|n) l_{q^{(n)}\sigma^{(n)}}.$$

The last line of the equation above follows from the fact that there are $n!$ permutations $\nu$.

Furthermore:

$$T_{q^{(n)}}(X) = \omega_{q^{(n)}} \sum_{\sigma^{(n)}} p(\sigma^{(n)}|n) \sum_{\nu} \frac{k!}{V^k} \prod_{i} p(z_{\sigma_i^{(n)}}|x_{\nu_i}) p^{q^{(n)},i}(x_{\nu_i})$$

$$= \omega_{q^{(n)}} \sum_{\sigma^{(n)}} p(\sigma^{(n)}|n) l_{q^{(n)}\sigma^{(n)}} \sum_{\nu} \prod_{i} p^{q^{(n)},\sigma^{(n)},i}(x_{\nu_i}),$$

$$p^{q^{(n)},\sigma^{(n)},i}(x_{\nu_i}) = \frac{p(z_{\sigma_i^{(n)}}|x_{\nu_i}) p^{q^{(n)},i}(x_{\nu_i})}{\int p(z_{\sigma_i^{(n)}}|x'_{\nu_i}) p^{q^{(n)},i}(x'_{\nu_i}) dx'_{\nu_i}}. \tag{A.9}$$

where $p^{q^{(n)},\sigma^{(n)},i}(.)$ is simply the $i^{th}$ PDF under $q^{(n)}$, $p^{q^{(n)},i}(.)$ updated by the measurement $z_{\sigma_i^{(n)}}$. Thus, it follows that:

$$p(X, n|Z) = \sum_{q^{(n)},\sigma^{(n)}} p^{q^{(n)},\sigma^{(n)}}(X) \frac{\omega_{q^{(n)}} p(\sigma^{(n)}|n) l_{q^{(n)}\sigma^{(n)}}}{\sum_k \sum_{r^{(k)}} \sum_{\delta^{(k)}} \omega_{r^{(k)}} p(\delta^{(k)}|k) l_{r^{(k)},\delta^{(k)}}},$$

$$p^{q^{(n)},\sigma^{(n)}}(X) = \sum_{\nu} \prod_{i} p^{q^{(n)},\sigma^{(n)},i}(X_{\nu_i}). \tag{A.10}$$

□

## A.2 Proof of Proposition 4

Below is the proof of proposition 4. For clarity a scenario with just birth is provided, which can be generalized to the birth and death case.

*Proof.* Let $X' = \{x'_1, ..., x'_n\}$ be an $n$ component multi-object state and let $X = \{x_1, \cdots x_r\}$ be an $r$ component multi-object state. Then, it is clear that:

$$p(X'|X, \sigma^b_{n-r}) = \sum_{\nu} \prod_{i=1}^{r} p(x'_{\nu_i}|x_i) \prod_{i=r+1}^{n} p^{\sigma^b}_{i-r}(x_{\nu_i}), \tag{A.11}$$

where $\sigma^b_{n-r}$ is any $n-r$ birth hypothesis. The primary task in proving Prop. 4 is to show Eq. 4.34 for any birth hypothesis $\sigma^b_{n-r}$. In the following, to simplify notation, the explicit reference to $n-r$

in the birth hypothesis is dropped.

$$p_{\sigma^b}^{q^{(r)},-}(X') = \frac{1}{r!}\int \sum_{\nu}\prod_{i=1}^{r} p(x'_{\nu_i}|x_i)\prod_{i=r+1}^{n} p_{i-r}^{\sigma^b}(x_{\nu_i})\sum_{\mu}\prod_{i=1}^{r} p^{q^{(r)},\mu_i}(x_i)dx_i,$$

$$= \frac{1}{r!}\sum_{\nu,\mu}\prod_{i=1}^{n-r} p_i^{\sigma^b}(x_{\nu_{r+i}})\prod_{i=1}^{r}\int p(x'_{\nu_i}|x_i)p^{q^{(r)},\mu_i}(x_i)dx_i,$$

$$= \sum_{\nu_{r+1}..\nu_n}\prod_{i=1}^{n-r} p_i^{\sigma^b}(x_{\nu_{r+i}})\frac{1}{r!}\sum_{\mu;\nu(r)}\int\prod_{i=1}^{r} p(X'_{\nu_i}|x_i)p^{q^{(r)},\mu_i}(x_i)dx_i,$$

where $\nu(r) = \{\nu_1, \nu_2, \cdots \nu_r\}$ represents the first $r$ elements of any n -permutation $\nu$. Given any $\nu(r)$ and $\bar{\nu}(r)$, there always exists a unique r-permutation $\bar{\mu}$ such that:

$$\int\prod_{i=1}^{r} p(x'_{\bar{\nu}_i}|x_i)p^{q^{(r)},\bar{\mu}_i}(x_i)dx_i = \prod_{i=1}^{r} p^{q^{(r)},i-}(x'_{\nu_i}). \tag{A.12}$$

Using Eq. A.12 to simplify the second sum on the last line of Eq. A.12,

$$\sum_{\mu;\nu(r)}\int\prod_{i=1}^{r} p(x'_{\nu_i}|x_i)p^{q^{(r)},\mu_i}(x_i)dx_i = r!\sum_{\nu(r)}\prod_{i=1}^{r} p^{q^{(r)},i-}(x'_{\nu_i}). \tag{A.13}$$

Hence, it follows that

$$p_{\sigma_{n-r}^b}^{q^{(r)}-}(x') = \sum_{\nu}\prod_{i=1}^{r} p^{q^{(r)},i-}(x'_{\nu_i})\prod_{i=r+1}^{n} p_{i-r}^{\sigma_{n-r}^b}(x'_{\nu_i}), \tag{A.14}$$

thereby proving the result. □

# APPENDIX B

# INCREASING REALISM AND ANALYSIS TOOLS

## B.1 Increased Realism

To show applicability to real world applications a number of improvements and techniques have been used to increase the realism in R-FISST simulations. The following sections detail some of these topics including, the modeling of fragmentation events, the incorporation of SMC techniques for object PDF representation, PAR approaches for SIOD, as well as the use of different filtering and propagation techniques.

### B.1.1 NASA Standard Breakup Model

In order to simulate fragmentation events as realistically as possible the NASA Standard breakup model [70] was used for a number of the simulations within this manuscript. This model characterizes the size distributions, area-to-mass and impact velocity assignments and distributions, and delta-velocity distributions where relevant for both colliding or exploding rocket body and spacecraft. Thus, for a spacecraft explosion in the GEO orbit regime, the number of debris fragments, distribution of area-to-mass, and the distribution of delta-velocities were developed directly from the NASA standard breakup model. An example of a GEO breakup event simulated using this model is provided in figures B.1 and B.2.

### B.1.2 Sequential Monte Carlo PDF Representation and Particle Gaussian Mixture Filter

Within the parent hypothesis the multi-object PDF constructed of $n$ independent object PDFs. Solving the recursive Bayesian filtering problem is easiest when the object PDF is approximated as a multivariate Gaussian distribution. This, coupled with normally distributed measurement noise, provides a normal joint distribution whose update can be expressed easily using many extensions of the common Kalman Filter. However, it is known that this assumption falls apart because the object PDF becomes non-Gaussian through propagation. This can lead to missed-associations and

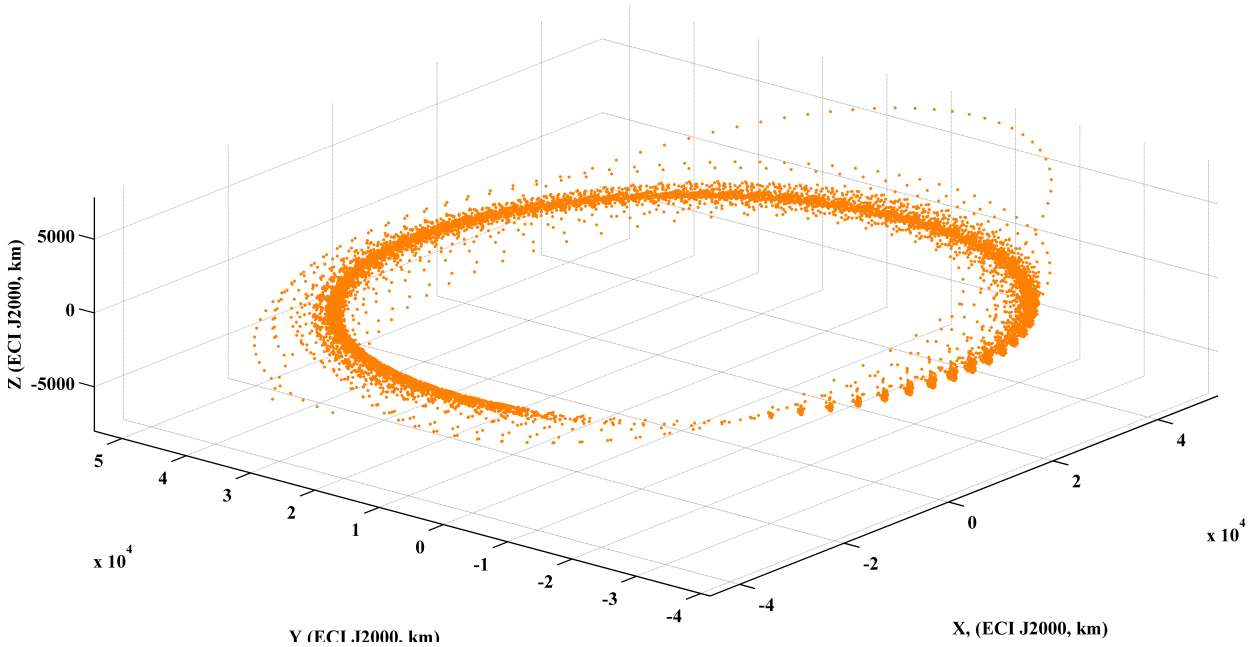


Figure B.1: Fragmentation event simulated using NASA's standard breakup model. Reprinted with permission from [2].

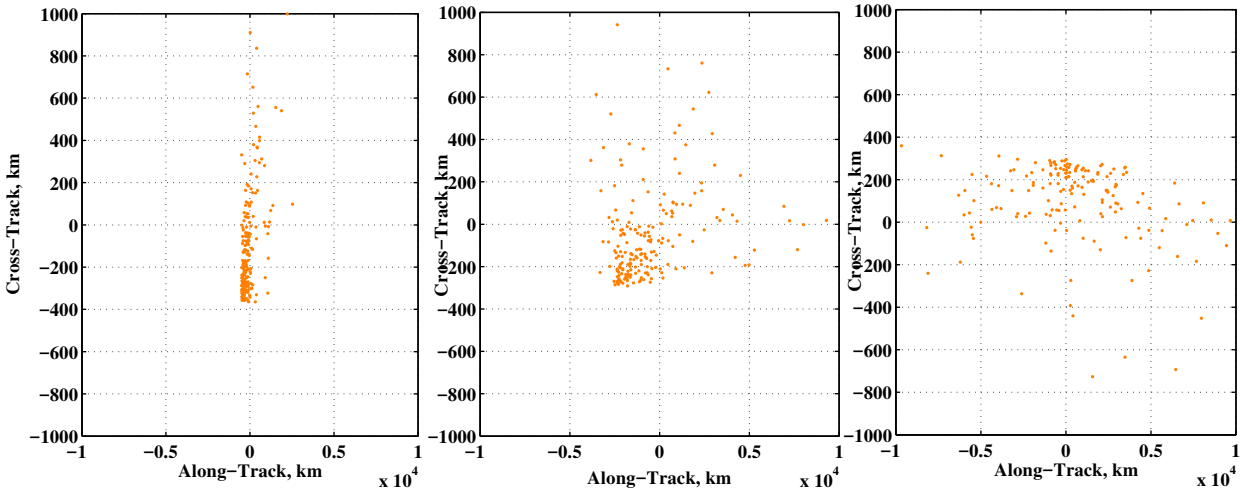


Figure B.2: Fragment positions plotted in track and cross plotted at one hour (left), twelve hour (middle), and twenty-four hours (right). Reprinted with permission from [2].

tracking inaccuracy. In the R-FISST framework, there are no assumptions about the underlying PDF; however, it may be computationally intractable to solve the prediction and update equations for some PDFs. Representing the object PDF using SMC techniques allows one to avoid making Gaussian assumptions. This has the benefit of properly representing the PDF through propagation at the added expense of computational burden. The expense is due to the requirement of propagating all particles instead of just propagating the mean and covariance of a PDF as in a Gaussian case.

The update of can be performed using any appropriate continuous filter. The choice of filter must be compatible with the representation of the RSO PDF. When representing the PDF using SMC techniques, a Particle Gaussian Mixture (PGM) filter can be used. The PGM filter able to update a particle representation without strictly forcing Gaussian assumptions. This filter was created to take advantage of the particle ensemble representation for propagation but alleviates the issues caused by particle updates such as particle depletion in the Particle Filter (PF). The PGM filter works in three steps. The first is to approximate the PDF represented by the particles using a Gaussian Mixture (GM). This is accomplished by clustering the particles into an optimal number of components using an optimal K-means algorithm. The second step is to update the GM representation using in our case a Unscented Kalman Filter update. The last step is performed by re-sampling the resulting posterior GMM. Figure B.3 is an example of a PGM filter update on a newly initialized PDF. The PGM filter is well suited to handle multi-modal PDFs, which makes it crucial for implementing PAR2D and PAR4D object PDF initialization discussed in the next section.

### B.1.3 Probabilistic Admissible Region

When predicting birth hypotheses the underlying spatial distribution can be initialized in many different fashions. One common birth spatial distribution is assumed to be uniform in the FOV. Due to the structure of the dynamic and measurement models in the SSA, a uniform spacial distribution is insufficient to characterize the object PDF. This can be overcome by incorporating information contained in associated observations. When considering birth from uncorrelated measurement re-

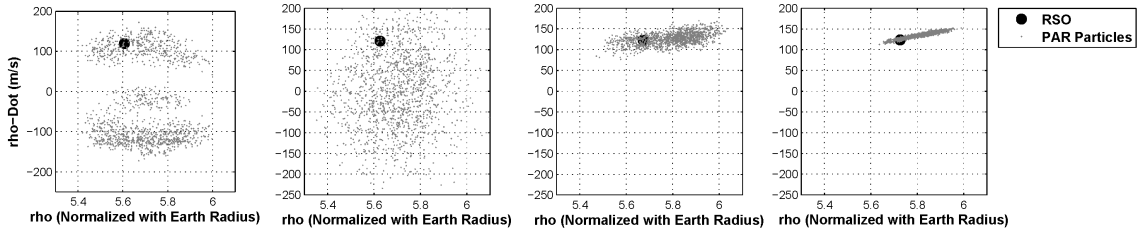


Figure B.3: Particle Ensemble from a PAR4D initialization updated over time using PGM. Reprinted with permission from [2].

turns spatial distributions can be initialized PAR approaches. The approach is described in detail and developed in a multiple hypothesis framework in Hussein et. al. [51]. Often the measurement model does not contain full state information. This forces one to initialize the birth PDF using partial state information. PAR can be performed using a number of different partial state measurement models. Figures B.4 and B.5 show initial birth PDF using the PAR2D and PAR4D technique respectively. The difference being that the PAR2D initializes object PDF using a four-dimensional measurement, in this case angle and angle rates. The PAR4D uses a two-dimensional observation, B.5 being observations containing angles-only data. The naming convention is not of the dimension of the observation but of the dimensions that the PAR technique has to extrapolate.

### B.1.4 Analysis Tools

This section describes tools used to analyze performance of the R-FISST techniques.

**Entropy** Entropy is used as a measure of the size of the uncertainty. It is useful to evaluate entropy to determine if the uncertainty is being reduced overtime. The entropy of a PDF can be expressed as follows,

$$S = \frac{1}{2}\log(|P|(2\pi e)^n), \tag{B.1}$$

where $P$ is the covariance of the PDF in $n$ dimensions. The total entropy for a particular hypothesis,

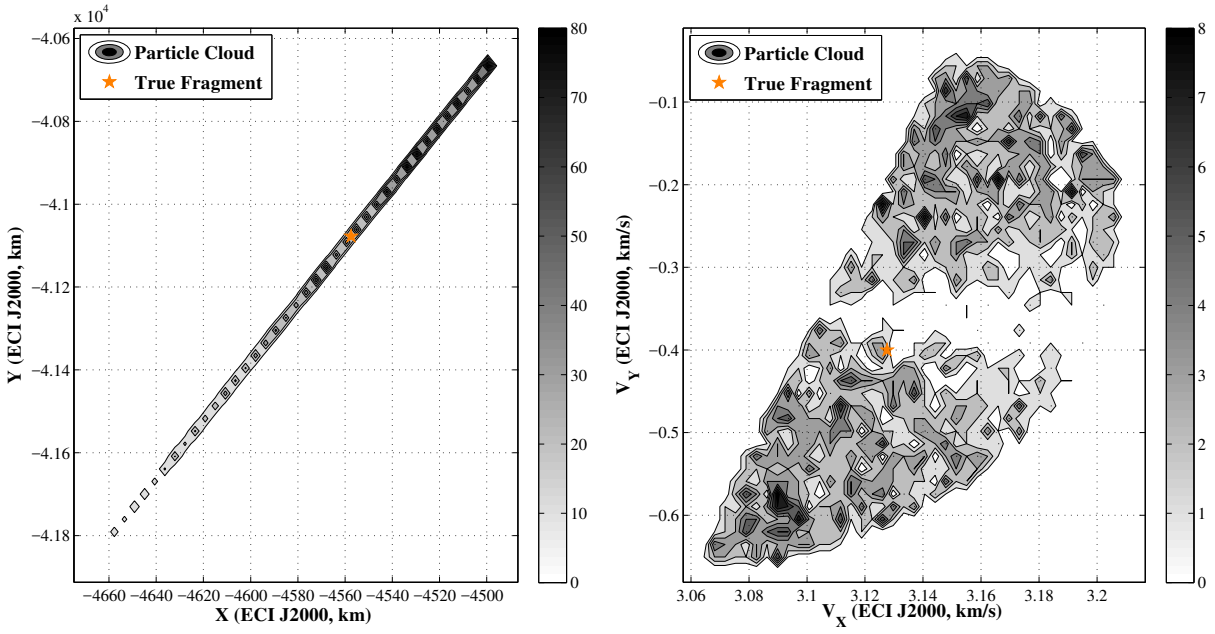


Figure B.4: Particle ensemble heat map as a result of initializing using PAR2D. Reprinted with permission from [2].

$S_{tot}$, is the sum of the entropy for all PDF within a hypothesis,

$$S_{tot} = \sum_i \frac{1}{/} 2 \log(|P_i|(2\pi e)^n), \tag{B.2}$$

Figures B.6 and B.7 are provided to illustrate the effects measurement updates have on the total entropy of a hypothesis. That is, as measurements are received the entropy reduces.

**Optimal Subpattern Assignment (OSPA) Metric** The OSPA metric, developed by Schuhmacher et. al. [73], is another tool that can be used to describe filter performance. It is used in Chapter 7 to provide an idea of the miss-distance between the set of mean states provided by the top hypothesis and the true states. The OSPA metric can handle scenarios where the cardinality of the estimated state set is not the same as the true cardinality. It also allows one to choose parameters $p$ and $c$ that control the order of the per-object error and the cut off distance. Within the applications Chapter 7, the cut of distance, $c$ is varied to provide insight on both localization errors and cardinality errors.

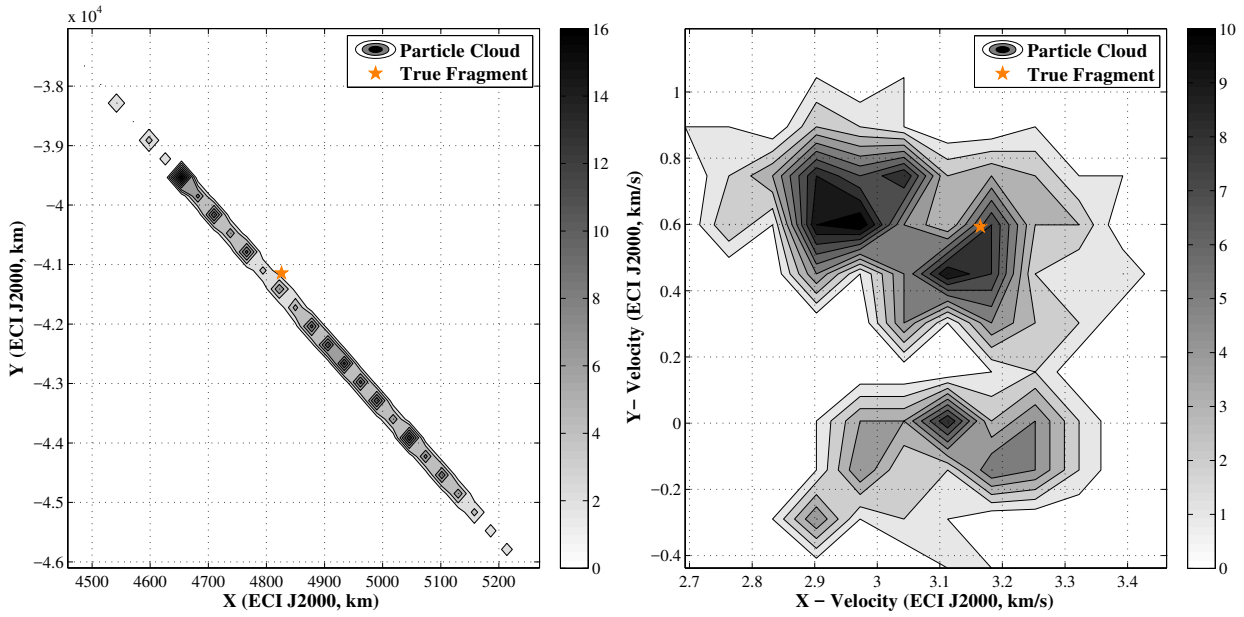


Figure B.5: Particle ensemble heat map as a result of initializing using PAR4D. Reprinted with permission from [2].

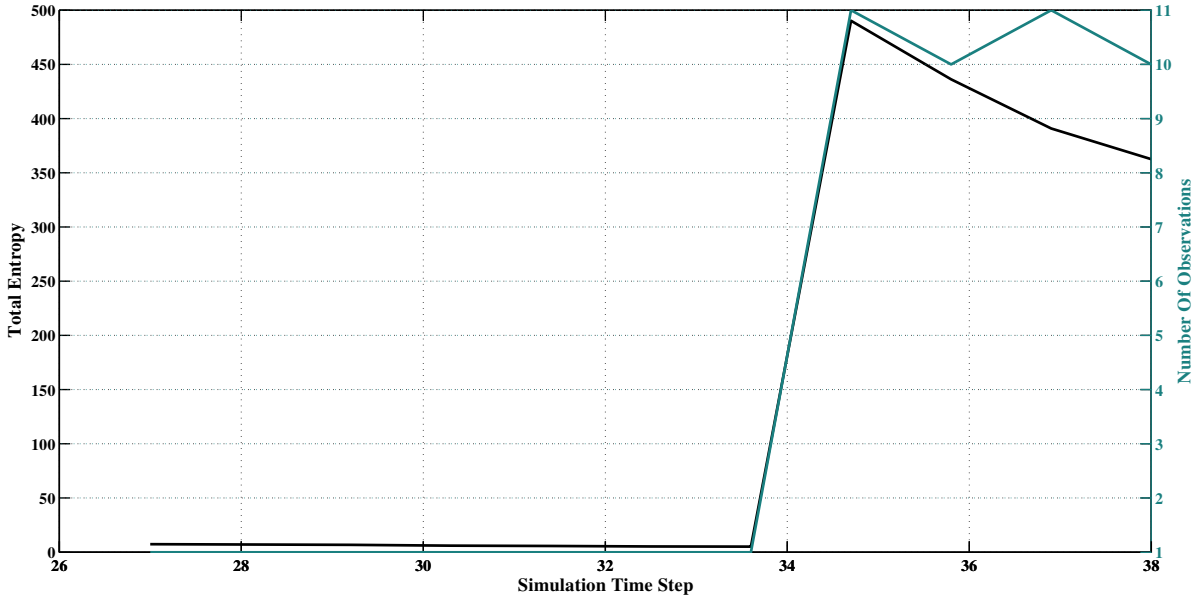


Figure B.6: Total entropy over time. Hypothesis contains fragment PDFs initialized using the PAR4D approach. Reprinted with permission from [2].

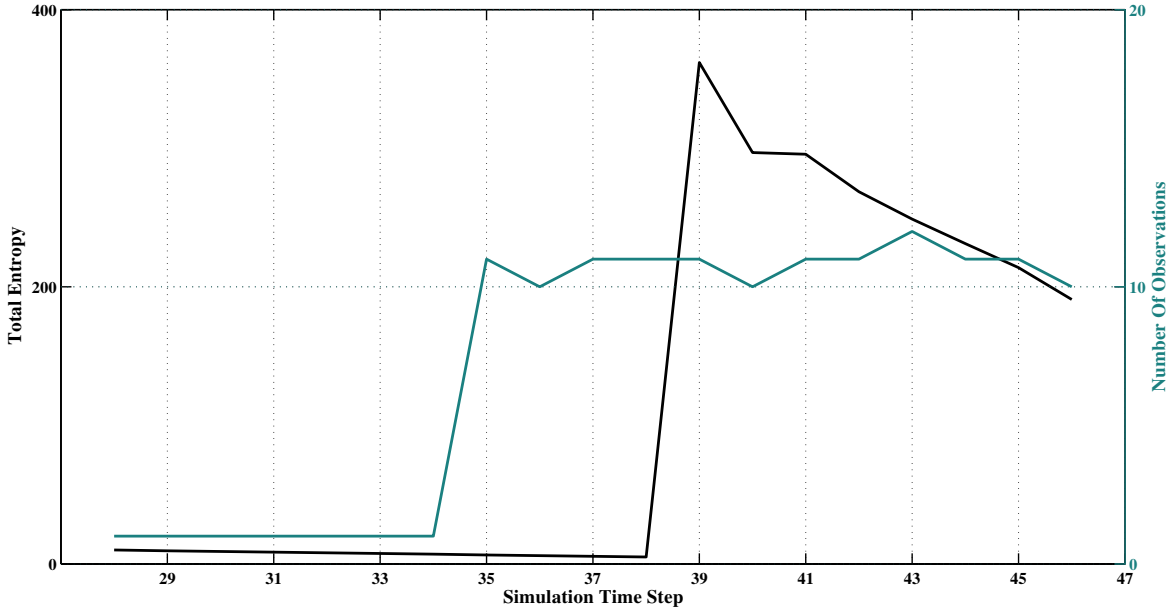


Figure B.7: Total entropy over time. Hypothesis contains fragment PDFs initialized using the PAR2D approach. Reprinted with permission from [2].

For more information on the OSPA metric see [73].